UNCLASSIFIED

AD ___492304___

DEFENSE DOCUMENTATION CENTER

FOR

SCIENTIFIC AND TECHNICAL INFORMATION

CAMERON STATION, ALEXANDRIA, VIRGINIA

UNCLASSIFIED

THE ANTI-ROLL STABILIZATION OF SHIPS
BY MEANS OF ACTIVATED TANKS

PART B
VERIFICATION OF BASIC THEORY BY MODEL SYSTEM STUDIES

BY
ALBERT J. MORRIS
JOSEPH H. CHADWICK

TECHNICAL REPORT NO. 15

DIVISION OF ENGINEERING MECHANICS
STANFORD UNIVERSITY
STANFORD, CALIFORNIA

JANUARY 1951

THE ANTI-ROLL STABILIZATION OF SHIPS
BY MEANS OF ACTIVATED TANKS.

PART B.

VERIFICATION OF BASIC THEORY BY MODEL SYSTEM STUDIES.

By.

Albert J. Morris
Joseph H. Chadwick
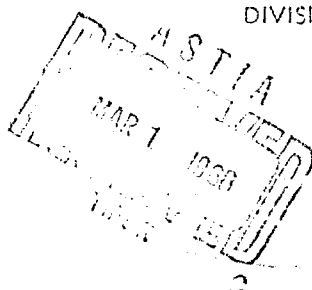
Technical Report No. 15

TR-15

Prepared under Contract N6-ONR-251 Task Order 2
(NR-041-943)

For

Office of Air Research

And

Office of Naval Research

Division of Engineering Mechanics
Stanford University
Stanford, California

January 1951

ABSTRACT

A five-ton model system used for the study of anti-roll stabilization of ships by activated tanks is described. ~~The system is used to compare~~ the basic theory of the problem is outlined in Part A (separately bound) of this report. Instrumentation problems and instruments developed in connection with the experimental program are discussed. Tests are conducted to determine actual system parameters and transfer characteristics. Theoretical and experimental data are compared. Excellent correlation is shown indicating that the linear theory is a useful tool in dealing with the problem. The effectiveness of this method of anti-roll stabilization is convincingly demonstrated. Weaknesses in the model system are pointed out along with recommended improvements.

TABLE OF CONTENTS

LIST OF FIGURES

LIST OF FIGURES Continued

I. INTRODUCTION

This is the second of four separately bound parts of a
technical report covering studies at Stanford University of
problems connected with "Anti-Roll Stabilization of Ships by
Activated Tanks". For the sake of completeness, the titles of
all four parts are repeated below:

Part A - Formulation of Problem and Basic Theory
Part B - Verification of Basic Theory by Model System
        Studies
Part C - Synthesis of High Performance Systems
Part D - Preliminary Considerations in the Design of
        Full Scale Systems

As indicated, this part of the report is concerned primarily
with verification of the basic theory developed in Part A. A
secondary purpose is to demonstrate the effectiveness of this
method of Anti-Roll Stabilization. A 5 ton dynamical model
system is utilized for this purpose.

Experimental verification of any theory is a highly de-
sirable goal. It is particularly desirable and important in
connection with "Activated-Tank Ship Stabilization". In Part A
the theory was developed on an entirely linear basis. The
writings of N. Minorsky, (1), (2), (3), (4), (5), (6),[+] are,
however, considerably different in approach. In these writings,
one gets the definite impression that non-linearities in the

[+] Numbers in parentheses refer to list of references which
appear at the end of the report.

system are of great importance in governing its behavior. The work of Minorsky in these references is certainly valid based on the assumptions he made concerning system behavior. It has not been entirely clear until now whether such assumptions are necessary or warranted. If it can be shown that linear theory is capable of adequately describing all important phases of system performance, then the powerful, well developed methods of linear servo theory can be brought to bear on the problem.

In Chapter II there is given a brief description of the model system. This is followed in Chapter III by a description of the problems involved in developing the instrumentation necessary for conducting the experimental program and a brief outline of the resulting test instruments. The experimental program is presented in three major parts, each with several subdivisions. Chapter IV covers static and dynamic tests of the ship-tank system. Chapter V covers tests of the controls, and Chapter VI covers tests of the complete system. In Chapter VII, the results of the tests are summarized and conclusions are drawn as to the usefulness of the linearized theory, and on the effectiveness of the stabilization system. In addition, some comments are made on areas of improvement in the control system and the way is pointed toward the subject matter of Part C of this report which is concerned with the synthesis of improved stabilization systems.

One thing should be noted in connection with this report.
It is written presupposing some knowledge of activated-tank roll
stabilization and in particular, some knowledge of pre-war and
post-war efforts by the U. S. Navy based on the Minorsky approach
to the problem. For a more detailed description of the model
system, the instrumentation used, and the experimental methods
and data, the reader is referred to (7).

II. DESCRIPTION OF MODEL SYSTEM

The model system which was used as the experimental tool
in the studies to be described is shown schematically on Figure
1[+] and pictorially on Figure 2 and Figure 3. Although this
system bears little apparent resemblance to an actual ship model,
its dynamic properties are such that its behavior can be taken as
a close approximation to that of a ship subjected to wave forces
causing rolling in only one degree of freedom. Approximations
do exist of course. These will be discussed in some detail in
Part D of this report. Here it is sufficient to note that the
equations developed in the first report are intended to closely
describe the behavior of the model system.

In describing the model, the same logical sequence will be
followed as in Part A. Specifically, the regulated element, the
regulating element, and the disturbing element will be treated as
separate entities.

A. Regulated Element : Ship-Tank System

The ship-tank system consists essentially of two coupled
pendula, one inside the other. The external pendulum, Figure
1.1[++], represents the ship. It is free to oscillate (roll) in

---

[+] All figures appear in back of text.
[++] First number means Figure 1. Second number refers to item
on Figure 1. Thus Figure 1.4 means item 4 of Figure 1.

one degree of freedom around a fixed center of rotation consisting of a shaft, Figure 1.2, mounted in fixed pillow block bearings. Keyed to one end of this shaft is a damping paddle immersed in an oil filled tank. The damping thus obtained represents the total external skin friction plus bilge keel damping of the ship. The internal pendulum consists of fluid caused to oscillate between two 2' x 2' x 3' tanks, Figure 1.10, 1.11, cross-connected by a 5" x 11" transfer duct, Figure 1.12. Under stabilization conditions, the oscillation of the fluid pendulum is forced by a variable-pitch propellor pump, Figure 1.13, located in one of the tanks. The pump is driven at constant speed by a motor, Figure 1.17, through an appropriate gear train. Variation of the pump blade angle in response to a control signal causes oscillation of the fluid pendulum. The problem is to so phase these oscillations as to always produce torque on the ship equal and opposite to the torque produced by wave forces.

B. Regulating Element : The Controls

The control system consists primarily of a roll sensing element, a voltage amplifier with adjustable phasing circuits, a servo-motor driving a hydraulic power amplifier, and a feed back selsyn which provides a signal for proportional control.

The roll sensing element is an accelerometer, Figure 1.16, mounted directly on the main pendulum shaft (see Figure 3). It responds only to angular acceleration. In Part A it was shown

- 5 -

that, for a system of this type, an accelerometer is the ideal
primary control element. To improve the low frequency response
of the system, it is possible to add position and velocity con-
trol elements to the acceleration control. The model system has,
however, only acceleration control. As it exists, it may there-
fore stabilize around an average angle other than zero. Since
the purpose of this program was not to redesign the model system,
no attempt was made to modify its controls in any fundamental way.
The effect of adding position and velocity control is, however,
covered in Part C. The accelerometer movable element has linked
to it a bucking coil system which moves in the field of a 200
cycle electromagnet when the movable element is displaced by ac-
celeration. With no acceleration, the bucking coils produce zero
net voltage. With acceleration, the coils produce a phase sensi-
tive modulated 200 cycle voltage which is fed to the amplifier in-
put.

The amplifier was designed and built by the Sperry Gyroscope
Co. before World War II. A block diagram of this amplifier is
shown on Figure 4. A schematic diagram is shown on Figure 5.
The primary function of the amplifier is to enable the basic con-
trol equation:

$$\mathcal{E} = m\ddot{\theta} - K\alpha$$

to be satisfied. In the actual amplifier, by provision of two
differentiating stages, the control equation becomes of the form:

$$\mathcal{E} = m\ddot{\theta} + n\dddot{\theta} + q\ddddot{\theta} - K\alpha$$

- 6 -

It is possible to independently control the amplitude of each of the derivatives. In practice, the $\dddot{\theta}$ factor is never used. Referring to Figure 4, it is seen that the accelerometer output signal is fed into two channels. One channel is a demodulator to allow for two differentiating steps at low frequency. The other consists of the amplifier stages. The differentiated signals are remodulated and then fed into the same amplifier stages. The $m\ddot{\theta} + n\dddot{\theta} + q\ddddot{\theta}$ signal is amplified and used to drive a 200 cycle servo motor. This motor is directly geared to the control valve which controls pump blade angle and also to a selsyn which feeds back to the input of the amplifier section a signal proportional to pump blade angle. Thus the net signal being amplified is:

$$\mathcal{E} = m\ddot{\theta} + n\dddot{\theta} + q\ddddot{\theta} - K\alpha$$

$$\text{where } \mathcal{E} \longrightarrow 0$$

This makes the blade angle proportional to acceleration plus derivatives. Reference to the schematic diagram on Figure 5 indicates that the demodulator and remodulator circuits are phase sensitive rectifiers. Differentiation is obtained by using audio trans-. formers at very low frequencies; in the region where they provide roughly 90° of phase advance. Amplification is performed primarily at the carrier frequency with straight forward transformer coupling used. Most important adjustments are to obtain maximum motor torque by proper phasing of the 200 cycle amplifier output and to properly phase the accelerometer and remodulator 200 cycle voltages so as to be exactly 180° out of phase with the feedback selsyn voltage in order to satisfy the control equation.

The servo-motor is a two phase, 200 cycle induction motor. One phase is fed directly by the 55 volt, 200 cycle line supply. The other is fed by the amplifier output. The motor shaft is geared to the hydraulic amplifier control valve.

A hydraulic power amplifier is used to control the pump blade angle. The piston of this amplifier is directly linked to the blade shifting mechanism so that motion of the piston produces a proportional motion of the blades. The hydraulic mechanism is located on the top of the tank system as shown on Figure 2. A sectionalized diagram of the piston and control valve mechanism along with the pump drive motor and mechanism is shown on Figure 6. A line diagram of the control oil system is shown on Figure 7. The amplifier is essentially a "unity follow-up" system. Linear motion of the control valve in response to a control signal through the servo-motor opens up ports in a cylinder fed by 100 psi oil. The ports, as designed, are opened in such a way as to provide an unbalanced pressure on the piston moving in the cylinder forcing it in the direction tending to close the ports. Thus, the piston always moves in the same direction and by the same amount as the valve (unity follow-up). Pressure for the system is provided by a separate motor driven gear pump, Figure 1.21, which uses the bilge keel damping oil tank as a sump. The pump feeds oil to an accumulator, Figure 1.20, which in turn feeds the high pressure cylinder.

C. Disturbing Element : Stevenson Link Mechanism (Wave Forces)

Wave forces are provided artificially by a Stevenson Link Mechanism shown best on the schematic diagram of Figure 1. The mechanism, as used in the tests to be described, had only one driving motor which restricts its output to simple harmonic motion. By varying the speed of this motor, a wide range of frequencies can be generated. Amplitude of motion is governed by mechanical adjustment of the linkage. Referring to Figure 1, a horizontal sliding rod connected to item 4 is driven in simple harmonic motion by the mechanism. This rod is linked to cross arm 22 causing to to rock back and forth. This arm is called the wave slope arm. It is connected through a set of parallel springs (Figure 1.3) to an identical arm keyed to the main shaft. Thus, motion of the wave slope arm creates a torque through spring action on the s :   .a causing the ship to roll. The angle from the vertical or the wave slope arm therefore becomes the effective wave slope acting on the ship model. Springs are, of course, necessary for coupling since under stabilization conditions the model system stands almost still with the springs alternately contracting and expanding to take care of the motion of the wave slope bar.

D. Concluding Remarks

It can be seen, even from this brief description, that the model system incorporates all of the essentials of an actual

ship installation. To complete the picture, a transfer function block diagram of the system is shown on Figure 8. The diagram is complete with the transfer function notation to be used throughout this part of the report. On this diagram, the system blocks A, B, C defined by Figure 6 of Part A are easily identified. From Part A, Figure 6, it is seen that A represents the control elements so that:

$$A = \frac{\alpha}{\theta} = \frac{e_1}{\theta} \cdot \frac{e_2}{e_1} \cdot \frac{X_1}{e_2} \cdot \frac{X_3}{X_1} \cdot \frac{\alpha}{X_3} = K_4 K_5 K_6 K_7 T_3 G_4(p) G_5(p) G_6(p) G_7(p)$$

Likewise, B of Part A, Figure 6, represents the active ship response; so that:

$$B = \frac{\theta_{out}}{\alpha} = \frac{\theta_{out}}{\dot{\phi}} \cdot \frac{\dot{\phi}}{\alpha} = K_2 K_3 G_2(p) G_3(p)$$

Also, C of Part A, Figure 6, represents the passive ship response; so that:

$$C = \frac{\theta_{in}}{\psi} = K_1 G_1(p)$$

In this notation, from Part A:

θ_{in} = Hypothetical motions due to waves alone

θ_{out} = Hypothetical motions due to stabilizer action alone

We now have some idea of the physical system to be studied. It is next necessary to consider the instrumentation needed to carry out the experimental program. The problems connected with the instrumentation and a brief description of the instruments used are covered in the following chapter.

III. INSTRUMENTATION

A. General Considerations

In order to carry out the experimental program, considerable instrumentation is of course necessary. It was early decided that the best way to properly determine relative phase and amplitude responses of at least six different elements of the system would be to record them simultaneously and on the same paper. In view of the fact that most frequencies of interest are less than 1 cycle/second, the Brush direct inking penmotor oscillograph appeared to be an ideal recording instrument. The frequency range of interest requires some clarification. Actually for steady state sinusoidal response measurements, the frequencies of interest lie well below 1 cycle/second. However, even under these conditions the water flow in the tanks will undoubtedly exhibit erratic motion due to closing of the duct as the blades go through zero. In addition, some chattering of the blades, valve, and motor may be expected along with backlash in the gear trains. In view of this, the instrumentation should be capable of fair reproduction of components up to at least 10 cycles/second, even though for phase measurements the design is for minimum instrumental phase lag below 1 cycle/second. Another important factor was that the fact that there existed twin channel model BL 201 Brush Recorders on the Stanford Campus and in addition one six channel Brush recorder. The choice of the recording instrument

- 11 -

dictated the necessity of deriving electrical signals to actuate the recorder. Also, it dictated the necessity of building DC amplifiers to drive the recorder channels. In view of the availability of the six channel recorder and the desirability of recording simultaneously several phenomena, a six channel DC power amplifier to drive the penmotors was built. Thus the fundamental instrumentation, common to all measurements, required multichannel recorders, multi-channel DC power amplifiers to drive the recorders, and an adequate stabilized power supply for the multiple amplifiers and other equipment to be used. Only a word need be said about the need for DC amplifiers as opposed to AC amplifiers. We are primarily concerned with frequencies from 0 to 1 cycle/second. No AC amplifiers exist which are useful in this range.

B. Recorders

These instruments are widely known and are almost ideal for the purpose of the tests to be described. They convert electrical voltages as a function of time into permanent records. In the frequency range covered by this report the pens respond with negligible time lag. Pertinent data are indicated below as a matter of general interest. Model EL 902 penmotors are used in each channel.

Frequency response - flat from 0-10 cycles/second, 1 db down at
                40 cycles/second

Sensitivity - 1.1 mm/volt.

Paper Speeds - 5 mm/sec, 25mm/sec, 125mm/sec.

Impedance - 1500 ohms (resistive)

For the purpose of these tests, great care must be taken that pens on all channels used simultaneously are properly aligned. If this is not so, we read an apparent (fictitious) phase shift linearly proportional to frequency and one which changes in steps as one changes paper speed. Equal sensitivity of pens in each channel is not so important as only relative amplitudes are needed.

C. DC Power Amplifiers

The DC power amplifiers used are shown schematically on Figure 9. The unit consists of six separate channels, five of which are essentially identical with the sixth (channel 5) having been modified from its original form like the other channels to act as a pre-amplifier in order to provide the possibility of greater voltage gain. The units (1, 2, 3, 4, 6) are designed to drive Brush recording penmotors. As such, they are essentially power amplifiers producing 15 volts across the 1500 ohm load of the penmotor windings. These channels have a voltage gain of only 7.5 but have a power gain of about 10,000.

The only difference between channels 1, 2, 3, and channels 4, 6 is the input arrangement. Channels 1, 2, 3 are designed to take inputs directly from helipots whereas channels 4, 6 are not. Channels 1, 2, 3 can, however, be used as straight forward amplifiers as well. When used with helipots, the voltages for the helipots are derived from the amplifier itself as indicated by the input arrangement for channels 1, 2, 3.

Each of the channels is provided with a switch which grounds the input grids to allow for balancing the amplifiers to zero with no signal in. A microammeter is used as the balance indicator. It can be switched across the two output cathode followers of each of stages 1, 2, 3, 4, 6 or the output to ground of channel 5 by the channel balance selector switch. In addition, each stage is provided with a 10:1 and 5:1 fixed attenuator as well as a gain control. The input impedance of each stage is sufficiently high (200K) to prevent loading of any signal of interest. The output of each stage, except 5, is taken from cathode followers and fed to the penmotor windings. Fifteen volts will produce maximum peak to peak pen deflection. The output stages, (except 5), are designed to overload if voltages much higher than 15 volts are produced. This characteristic serves to protect the penmotors from being over driven. This type of driving output circuit is now quite common. The only item not perfectly straight forward is the use of gas-tube coupling. The advantage of this type of coupling is that it provides DC coupling without signal attenuation. The gas tubes can operate at much lower current levels (10-20 microamps) than normally used in voltage regulator circuits and still perform satisfactorily. The use of gas tube coupling is discussed in detail in (8). As shown on Figure 9, channel 5 has been made into a voltage amplifier. Its input arrangement is the same as is in channels 4, 6. The voltage divider output of the first 6J5 is experimentally adjusted to give

- 14 -

zero or slightly negative DC volts on the grid of the second 6J5.
The output arrangement of the second 6J5 is the same as for the
first. It is zeroed by the use of the panel meter which is con-
nected between the output and ground. When biased to zero, the out-
put of channel 5 can be fed to the input of any of the other five
channels. It not only provides pre-voltage amplification if need-
ed but gives considerable additional bias control. The voltage
gain of channel 5 is 5.5.

D. DC Stabilized Power Supply

The schematic circuit of the DC Stabilized Power Supply is
shown on Figure 10. This is an entirely conventional supply and
incorporates only standard practices. In view of this it will
not be discussed in detail. The power supply is rated at 300V
and 400 m.a. In order to obtain this much current it was decided
to build the supply in two equal 200 m.a. sections. Control of
voltages to and from both sections is, however, accomplished by
common switches; so for practical purposes there is only one
supply to deal with. The large current requirements are dictated
by the necessity of providing power to the DC Power Amplifiers
and other equipments requiring stabilized voltage supply.

E. Sine Wave Generator

In order to determine transfer characteristics of the
system components, it is desirable to open the closed loops and
test the component parts of the system with artificial signals

derived from some source which replaces the signal originally obtained from the accelerometer. Also, in some cases, it is desirable to test the system at frequencies higher than those which are available from the Stevenson Link Mechanism. The form of the artificial signal must be that of a 200 cycle sinusoidal carrier, sinusoidally modulated at frequencies ranging from 0 to about 8 cycles/second.

The Sine Wave Generator used is shown diagramatically on Figure 11. It consists of a DC motor whose speed is varied by both field and armature control. The motor is geared down in two steps, 120:10.92:1. Two selsyn motors are used; one being coupled to the 120:10.92 shaft on the reduced speed side, and the other being coupled to the 120:1 shaft on the low speed side. Both selsyn motors were designed for 115/90V, 400 cycle input but are performing satisfactorily with the available 55V, 200 cycle input. Input power is fed to the selsyn motors and output is taken from the stators. Under these conditions the selsyn motors operate as variable transformers as desired. The frequency of modulation of the lowest speed selsyn can be varied from 0 to about 1.6 cycles/second and the higher speed selsyn can operate below 1.6 cycles/second up to 7.6 cycles/second. This gives a continuous range in available frequencies as high as desired for most purposes.

F. Test Demodulators

Two identical channels of demodulator circuits are provided
and are shown schematically on Figure 12. The purpose of the de-
modulators is to obtain the low frequency modulation component of
a modulated carrier to drive a pen recorder. In this case the
carrier frequency is always 200 cycles, and, depending on the
source, the modulation frequency has components of interest mostly
below 1 cycle/second. Sources of modulated carrier signals re-
quiring demodulation for purposes of these tests are the valve
selsyn for valve position, accelerometer output for accelerometer
response, the Sine Wave Generator for filter tests, amplifier
tests, etc. The circuit used is very standard and need not be
discussed in great detail. It is nothing more than a typical
phase sensitive rectifier.

In arriving at an appropriate time constant for the filter
section of the rectifier the following criteria must be satis-
fied.

    a. The resistance component must be small compared to the
        input resistance of the load. The load is the input
        grid of the DC power amplifiers which have 200K input
        resistance.

    b. The time constant must be as small as possible in order
        to minimize phase shift in the frequency range of in-
        terest.

c. The time constant must be large enough to effectively filter the 200 cycle carrier.

A time constant of 0.1 seconds was originally designed for. This was reduced to .056 seconds after experimental check of the demodulator performance indicated that RC = 0.056 seconds gave a tolerable ripple, indicated by a slight thickening of the recorded trace.

G. Test Panel

For almost every measurement it was necessary to derive voltages from several far removed places. In view of this, it was decided to bring the majority of the signals and power supply voltages that would be needed to one place and simply plug into an appropriate socket to derive the desired voltage. The voltages available are shown on Figure 13. This test panel installation has paid itself back many times.

H. Electromagnetic Induction Flowmeter

All of the instrumentation previously described represents well known servomechanism practice and is the type of instrumentation required for almost any experimental program dealing with servo devices. However, among the most important factors to be determined experimentally in this program are those connected with the dynamic characteristics of the flow in the tanks as a function of blade angle, time and frequency. Of primary interest is the relation between $\dot{\phi}$, the flow rate, and α the pump blade

angle. It is necessary therefore to measure $\dot{\phi}$ and compare its instantaneous value with that of $\propto$ and other system components. Since the flow measuring instrument must give an accurate indication of both phase and amplitude of flow, the requirements to be met are quite severe. These requirements are:

    a. The instrument must measure fluid velocities absolutely linearly in the velocity range $(+18)-0-(-18)$ feet/sec.

    b. The data obtained should be recorded simultaneously with information on pump blade angle, tank position, etc., to enable measurement of time and/or phase lags.

    c. The measuring instrument must in no way disturb or distort the flow.

    d. The instrument must respond <u>only</u> to fluid velocity and must not be sensitive to static or kinetic pressure forces.

    e. The instrument should have instantaneous response and not introduce any time lag of its own.

Two main factors are involved which greatly restrict the choice of instruments. First, the flow covers a wide range of Reynolds numbers so that devices such as paddles, current meters, and Pitot tubes operating on (velocity)^2 are ruled out due to inherent non-linearity as well as non-constancy of the Reynolds number over the range of interest. Second, the fluid is not always moving at a constant velocity but is usually accelerating.

In addition, the tanks and duct in which it moves are also
usually accelerating, and at the same frequency. Therefore, any
instrument sensitive to pressure not only responds to the level
of the liquid in the tanks and to the velocity head but is also
effected by the change in pressure caused by two separate ac-
celerating forces between which it would be almost impossible to
distinguish. A current metering device would seem to offer
promise but the duct size is small and almost any such device
inserted into the stream would distort the flow. Also there is
no guarantee of its linearity over the entire range of interest.
Thus we seem to have ruled out all instruments upon which the
fluid acts directly with a force. Photographic methods seemed
highly undesirable. For one thing it would be necessary to inter-
pret and transcribe the information from the film after a trouble-
some developing and printing process. For another, although it
would help us visualize the flow, it would be extremely difficult
to obtain a continuous measure of fluid velocity without tracing
individual particles in the stream. The photographic method was
used for tank level metering by Minorsky (1), (2) but was un-
satisfactory for the reason stated above as well due to turbulence
of the fluid level and necessity of interpolating true level due
to tilt of tanks. There remained an electromagnetic induction
method which was chosen for use since it appeared to satisfy all
of the above requirements very nicely. This method is described
in some detail in (7) and (9). It will be described only very
briefly here.

The method is based on Faraday's law of induction. A voltage is induced in a conductor moving at right angles to a static magnetic field. At any point along the conductor this voltage is proportional to the magnetic field strength, the velocity of the conductor and the incremental length of conductor under consideration. Theoretically, a conductor is not necessary. A voltage will be induced independent of the conductivity of the moving material. In practice, however, it is desired to measure this voltage. For this purpose it helps to have a high conductivity material such as water so that the amplifying means will not load the voltage generating system. Refer to Figure 14 showing a picture of the actual flowmeter installation. Oscillating flow takes place in the 5" x 11" transfer duct connecting the two tanks. The two radar magnetron type permanent magnets create a magnetic field through the lucite section of the duct at right angles to the flow. Thus, when flow occurs, a voltage is induced in the moving elements of water. This voltage is picked up at two electrodes located in the sides of the duct. Figure 15 shows a schematic diagram of the equipment associated with the flowmeter. The signal voltage is superimposed on a polarization bias voltage which is canceled out of the system. The a-c noise on the signal is taken out by a low-pass filter. A chopper type d-c amplifier provides the pre-amplification needed to drive a d-c power amplifier which in turn drives the recorder.

I. Concluding Remarks

The instrumentation briefly described in the preceding sections was all carefully calibrated to determine the phase and amplitude distortion introduced by the instrumentation itself. This information is not presented here but exists in detail in (7). Suffice to say that the experimental curves presented in the following sections have all been corrected when necessary for instrumentation distortion.

We now know something about the system to be investigated. In addition, the tools are now available with which to conduct the investigations. The next step is to actually get into the problem. This is done in succeeding chapters.

IV. STUDY CF SHIP-TANK SYSTEM : THE REGULATED ELEMENT

A. Notation and Basic Equations

It is intended to present the theoretical and experimental results in dimensionless form in order to maintain generality and prepare the way for later extrapolation of model system studies to full scale studies. The analytical treatment of the ship-tank system presented in Part A has given us the expected "form" of the characteristic functions and will enable us to determine from the experimental results the various system parameters. The equations of motion of the ship tank system derived in Part A are repeated below so that the meaning of the parameters to be obtained is clear:

For the Ship (equation 14 of Part A)

$$(p^2 J_s + pB_s + K_s)\theta + (p^2 J_{st} + K_t)\phi = K_{ss}\psi \qquad (1)$$

For the tank water (equation 15 of Part A)

$$(p^2 J_{st} + K_t)\theta + (p^2 J_t + p B_t + K_t)\phi = K_p\alpha \qquad (2)$$

where:

(All definitions are such that the parameter times its associated angle or its derivatives results in a torque on the ship)

θ = Angle of ships' mast from vertical

ϕ = Angle formed by line drawn between the centers of the fluid surfaces in each tank relative to a horizontal line through ship

- 23 -

B_s = Skin friction parameter of ship to waves

K_s = Righting parameter of ship with water in tanks but duct blocked

J_t = Moment of inertia of water in tanks

B_t = Skin friction parameter of water in tanks plus dynamic head-loss coefficient of the pump

K_t = Torque on ship due to a head of displaced water in tanks

J_{st}= Inertia coupling parameter between tank water and ship

K_p = Pump static head parameter

K_{ss}= Sea-ship torque parameter

$p = j\omega$ Assuming steady state sinusoidal behavior

Before setting down the equations in dimensionless form, it seems desirable to again define certain dimensionless parameters already defined in Part A.

Let:

$$P = \frac{j\omega}{\omega_s}$$

where ω_s represents the resonant frequency of the ship. Then let us define another dimensionless ratio as:

$$\Omega_r = \frac{\omega_r}{\omega_s}$$ where ω_r represents resonant frequency of system element being considered.

When considering the tank water for instance:

$$\Omega_r = \Omega_t = \frac{\omega_t}{\omega_s}$$

It will be noted that P gives an insight into what happens when the natural frequency of the ship is changed. The use of Ω_r gives an insight into the effect of changing the natural frequency of the ship as well as the natural frequency of the system component under consideration.

Now for specific dimensionless parameters:

SHIP TERMS

$$Q_s = \frac{\omega_s J_s}{B_s} = \text{resonance factor of ship}$$

$$\Omega_s = \frac{\omega_s}{\omega_s} = 1$$

$$\omega_s = \sqrt{\frac{K_s}{J_s}}$$

TANK TERMS

$$\lambda_t = \frac{K_t}{K_s} = \text{normalized static torque parameter of tanks}$$

$$\Omega_t = \frac{\omega_t}{\omega_s} = \frac{\text{tank natural frequency}}{\text{ship natural frequency}} = \frac{\text{normalized natural frequency of tanks}}{\text{quency of tanks}}$$

$$Q_t = \frac{\omega_t K_t}{B_t} = \text{resonance factor of tanks}$$

$$\omega_t = \sqrt{\frac{K_t}{J_t}} = \text{resonant frequency of tank water system}$$

MUTUAL TERMS

$$\Omega_{st} = \frac{\omega_{st}}{\omega_s} = \frac{\text{"secondary resonance" frequency}}{\text{ship natural frequency}} = \frac{\text{normalized secondary resonance frequency}}{}$$

$$\omega_{st} = \sqrt{\frac{K_t}{J_{st}}} = \text{secondary resonance frequency}$$

FORCING TERMS

$$\lambda_{ss} = \frac{K_{ss}}{K_s} = \text{normalized wave slope torque parameter}$$

$$\lambda_p = \frac{K_p}{K_s} = \text{normalized pump torque parameter}$$

With notation well in hand, the next step is to put equations 1 and 2 into normalized form. This is a simple matter of algebraic manipulation. The result is:

$$(P^2 + \frac{1}{Q_s} P + 1)\epsilon + \lambda_t [(\frac{P}{\Omega_{st}})^2 + 1] \phi = \lambda_{ss} \psi \qquad (1')$$

$$\lambda_t [(\frac{P}{\Omega_{st}})^2 + 1]\theta - \lambda_t [(\frac{P}{\Omega_t})^2 + \frac{1}{Q_t} (\frac{P}{\Omega_t}) + 1] \phi = \lambda_p \alpha \qquad (2')$$

The first step in experimentation will be to determine the static and dynamic parameters of the system as defined above. Having determined these parameters, we can compute the transfer responses of different elements of the system and compare these responses to the experimentally determined transfer responses. This comparison will provide a check on the validity of the assumption of linearity made in Part A. The transfer responses of interest in this chapter are those intimately tied in with the regulated element (ship-tank system). These are defined on Figure 8 as:

$$K_1G_1(p) = \theta_{in}/\psi = \text{Passive Ship Response}$$

$$K_2G_2(p) = \theta_{out}/\dot{\phi} = \text{Ship-Water Response}$$

$$K_3G_3(p) = \dot{\phi}/\alpha = \text{Pump Response}$$

There is much justification for considering the pump, due to its size, weight and cost, as part of the regulated element rather than as part of the control elements which are in general small, light and relatively inexpensive. In view of this we call:

$$K_2K_3G_2(p)G_3(p) = \theta_{out}/\alpha = \text{Active Ship Response}$$

To obtain θ_{in}/ψ we set $\alpha = 0$ in equation (2'). This leaves a direct relation between θ and ϕ. Eliminating ϕ gives:

$$\frac{\theta_{in}}{\psi} = \frac{\lambda_{ss}[(\frac{P}{\Omega_t})^2 + \frac{1}{Q_t}(\frac{P}{\Omega_t}) + 1]}{(P^2 + \frac{1}{Q_s}P + 1)[(\frac{P}{\Omega_t})^2 + \frac{1}{Q_t}(\frac{P}{\Omega_t}) + 1] - \lambda_t[(\frac{P}{\Omega_{st}})^2 + 1]^2} \quad (3)$$

To obtain θ_{out}/α we set $\psi = 0$ in equation (1'). This gives:

$$\frac{\theta_{out}}{\alpha} = \frac{\lambda_p[(\frac{P}{\Omega_{st}})^2 + 1]}{\lambda_t[(\frac{P}{\Omega_{st}})^2 + 1]^2 - (P^2 + \frac{1}{Q_s}P + 1)[(\frac{P}{\Omega_t})^2 + \frac{1}{Q_t}(\frac{P}{\Omega_t}) + 1]} \quad (4)$$

We now have the "passive" ship response and the "active" ship response. It remains to determine the transfer functions $K_2G_2(p)$ and $K_3G_3(p)$ indicated above. To obtain $K_2G_2(p) = \theta_{out}/\dot{\phi}$, we need only set $\psi = 0$ again in equation (1'). This gives, from equation (1') alone:

$$\frac{\theta_{out}}{\phi} = \frac{-\lambda_t \left[(\frac{P}{\Omega_{st}})^2 + 1 \right]}{(P^2 + \frac{1}{Q_s} P + 1)} \tag{5}$$

but $\dot{\phi} = p\phi$ so:

$$\frac{\theta_{out}}{\dot{\phi}} = \frac{-\lambda_t \left[(\frac{P}{\Omega_{st}})^2 + 1 \right]}{\omega_s P(P^2 + \frac{1}{Q_s} P + 1)} \tag{6}$$

The derivation of $K_3 G_3(p) = \dot{\phi}/\alpha$ (pump response) is a little tricky. Actually, if we set $\psi = 0$ we can determine two distinctly different functions, both properly called $\dot{\phi}/\alpha$. One is obtained by blocking the ship ($\theta = 0$). This is the unilateral transfer response of the pump alone. If we leave the ship unblocked, then the existence of a value for $\dot{\phi}$ means a corresponding torque on the ship causing it to roll. This rolling modifies the $\dot{\phi}$ produced by the pump alone. That this is so can be seen from the fact that, even with the pump not running, we can produce a $\dot{\phi}$ by rolling the ship. Thus $\dot{\phi}$ obtained with an unblocked ship is _not_ unilateral. In other words, the "output" is reacting back on the "input". We will still find the relation $\dot{\phi}/\alpha$ with ship unblocked an important relation in checking our linear theory. It will therefore be derived for both cases.

For the ship blocked case ($\theta = 0$, $\psi = 0$)

Equation (2') reduces to:

$$\frac{\phi}{\alpha} = \frac{\lambda_p}{\lambda_t \left[(\frac{P}{\Omega_t})^2 + \frac{1}{Q_t}(\frac{P}{\Omega_t}) + 1 \right]}$$

$$\frac{\dot{\phi}}{\alpha} = \frac{\omega_s P \lambda_p}{\lambda_t [(\frac{P}{\Omega_t})^2 + \frac{1}{Q_t}(\frac{P}{\Omega_t}) + 1]} \tag{7}$$

For ship unblocked case ($\Theta \neq 0$, $\psi = 0$)

Equation (1') gives a relation between Θ and ϕ which, when substituted in equation (2') and remembering that $\dot{\phi} = p\phi$ gives:

$$\frac{\dot{\phi}}{\alpha} = \frac{\lambda_p \omega_s P(P^2 + \frac{1}{Q_s}P + 1)}{\lambda_t(P^2 + \frac{1}{Q_s}P + 1)[(\frac{P}{\Omega_t})^2 + \frac{1}{Q_t}) + 1] - \lambda_t^2[(\frac{P}{\Omega_{st}})^2 + 1]^2} \tag{7'}$$

The ship-tank system parameters are now all defined. We have derived the theoretical linearized transfer functions of the ship-tank system based on the linear theory developed in Part A. Our next step is the experimental determination of these parameters and of the transfer responses. In special cases, the experimental values for the parameters will be checked against theoretically calculated values. These cases will be confined to the tank water parameters such as K_t and ω_t, and to the mutual parameter J_{st}; since, it is assumed that the primary problem is to install stabilization systems on existing ships or, in any case, where ship parameters are known in advance. If this is so, in designing a system, it is only necessary to calculate the parameters of the "added" system and how these parameters change the unmodified ship parameters. In all cases, theoretical and experimental transfer responses will be compared.

B. Determination of Static Parameters

Referring to equations (1) and (2), there are four static parameters which must be determined. These are:

K_s = Righting parameter of ship with water in tanks but duct blocked

K_t = Force on ship due to head of displaced water in tanks

K_{ss} = Sea-Ship torque parameter

K_p = Pump static head parameter

For experimental determination of the static parameters it is useful to look at the static equations of the ship-water system as obtained from equations (1) and (2).

For Ship

"Torque" + $K_s \theta + K_t \phi = K_{ss} \psi$

For Water

$K_t \theta + K_t \phi = K_p \propto$

"Torque" refers to some known force applied for purposes of calibration. By holding appropriate angles constant, it is simple to separate the effects of the individual parameters.

The test set-up involved applying a known force by means of a spring scale and pulley arrangement at a fixed distance from the ships center of rotation.

1. Determination of K_s - Experimental

K_s, being a ship parameter, has not been determined theoretically. It is not determined directly experimentally. It is possible, however, to determine K_s-K_t directly and K_t

directly. From these, K_s can be determined indirectly. Here the experimental determination of $K_s - K_t$ will be described.

If the duct is left open and ψ is constant, then $\phi = -\theta$ at zero frequency if pump is off. Then the ship equation reduces to:

$$(K_s - K_t)\triangle\theta = \triangle\text{Torque}$$

This means that all we need do is apply known torques to the ship and cause it to tilt to different angles to determine $K_s - K_t$.[+] From these tests, the average value of $K_s - K_t$ is:

$$(K_s - K_t) = 4.20 \times 10^3 \frac{\text{lb. ft}}{\text{radian}} = \text{average torque/radian}$$

The value of K_t obtained in the following section is

$$K_t = 1.25 \times 10^3 \frac{\text{lb. ft}}{\text{radian}} = \text{average torque/radian of } \phi$$

so $K_s = 4.20 \times 10^3 + 1.25 \times 10^3 = 5.45 \times 10^3 \frac{\text{lb. ft}}{\text{radian}}$

2. Determination of K_t

a. Theoretical

In Part A, the theoretical equation for K_t is given as:

$$K_t = 2\rho A_o L^2$$

where A = area of tanks = 1.92 ft.^{2}

L = distance from center of rotation to center of tank = 2.29 ft.

ρ = density of water = 62.4 lbs/ft^3

[+] As previously indicated, those readers interested in specific data must refer to (7). The loan of this document can be arranged.

so $K_t = 2 \times 62.4 \times 1.92 \times (2.29)^2$

$= 1.25 \times 10^3$ lb.ft/radian

    b. Experimental

For this test θ and ψ are held constant and torque and ϕ are varied. The ship equation reduces to:

$$K_t \triangle \phi = \triangle \text{Torque}$$

Procedure was to pump water to different levels in the tanks and measure the torque required to restore the ship to its reference position. Experimental data give an average value for K_t of:

$$K_t = 1.25 \times 10^3 \frac{\text{lb. ft}}{\text{radian}} = \text{average torque/radian of } \phi$$

3. Determination of K_{ss} - Experimental

For this tests θ and ϕ are held constant while "torque" and ψ are varied. The ship equation reduces to:

$$K_{ss} \triangle \psi = \triangle \text{torque}$$

The procedure was to measure the force required to restore the ship to a known position after varying the wave slope angle ψ. Experimental data give an average value for K_{ss} of:

$$K_{ss} = 1.32 \times 10^3 \frac{\text{lb. ft}}{\text{radian}} = \text{average torque/radian of } \psi .$$

4. Determination of K_p Experimental

For this test, θ and ψ are held constant and ϕ is measured as a function of $\propto$, the pump blade angle. The tank water equation reduces to:

$$K_t \triangle \phi = K_p \triangle \propto$$

so
$$\frac{K_p}{K_t} = \frac{\triangle \phi}{\triangle \propto}$$

In order to get sufficient range for ϕ, the ship was tilted initially and all subsequent measurements were corrected for this tilt. The procedure was to vary the pump blade angle $\propto$ and measure the corresponding level of the water in the tanks. Experimental data are plotted on Figure 16. As can be observed from this plot, K_p/K_t is not very constant except for blade angles from roughly 0 to $\pm$ 2 degrees. Under stabilization conditions, the pump blade is varying between the limits $\pm$ 5 degrees on the average, depending on the frequency. In view of this, a fairly arbitrary average slope at $\propto = 5°$ was drawn and this was used to determine:

$$K_p/K_t = 5.6$$

From this we get:

$$K_p = 5.6 \ K_t = 7 \times 10^3 \ \frac{lb. \ ft}{radian}$$

5. Summary and Discussion of Results on Static Parameters

	Theoretical	Experimental	
K_s	None	5.45×10^3	
K_t	1.25×10^3	1.25×10^3	all results in $\frac{lb.ft.}{radian}$
K_{ss}	None	1.32×10^3	
K_p	None	7×10^3	

Using the experimental values, we get for the dimensionless parameters:

$$\lambda_s = K_s/K_s = 1$$
$$\lambda_t = K_t/K_s = 1.25/5.45 = 0.23$$
$$\lambda_{ss} = K_{ss}/K_s = 1.32/5.45 = 0.242$$
$$\lambda_p = K_p/K_s = 7.0/5.45 = 1.28$$

It will be noted that the theoretical and experimental values for K_t agree exactly. Close agreement should be expected since this calculation involves little approximations. The value of λ_p above involves a considerable approximation, since obviously it is only an estimated "average" value. It will turn out, however, that the nature of the dynamic pump characteristic is such that this approximation, which now might appear excessive, does not seriously effect the final results.

C. Determination of Dynamic Parameters

Referring again to equations (1) and (2), there are two dynamic self parameters in the ship equation, two in the water equation, and one mutual parameter, the same one, in each equation. It is possible to determine these parameters, first by isolating the ship and water system and treating them as separate entities, and second by operating as a coupled system. In what follows, it is first assumed that the experimentally determined transfer response has the same functional form as that predicted by the linear theory. If this is so, by a process of curve

fitting we can determine the system parameters. Using these parameters in the theoretical equations, we may plot the theoretical response of the system. This is then compared to the experimental response on the same graph to give an indication of the validity of our assumption of proper "form".

1. Single Degree of Freedom Tests

The isolated system experiments come under the heading of single degree of freedom tests. By blocking the duct, we eliminate water motion, and by blocking the ship, we eliminate ship motion.

a. The Ship System

The isolated ship system is essentially a simple pendulum with viscous damping rotating at small angles around a fixed center. Therefore, its response is well known.

i. Theory (Steady State)

With the duct blocked the ship equation 1 reduces to:

$$\frac{\theta}{\psi} = \frac{\lambda_{ss}}{P^2 + \frac{1}{Q_s} P + 1}$$

Therefore, if we determine ω_s by experiment we will have J_s since we have already determined K_s by experiment. We can determine Q_s by experiment. This together with ω_s and J_s will give the value of B_s. From the experimental results of the following section, the values of the parameters are:

$$Q_s = 25$$

$$\omega_s = 1.39 \text{ radians/sec.}$$

$$J_s = 2.83 \times 10^3 \ \frac{\text{lb.ft.sec}^2}{\text{radian}}$$

$$B_s = 157 \ \frac{\text{lb.ft.sec}}{\text{radian}}$$

Substituting these values into the above theoretical equation gives:

$$\frac{\theta}{\psi} = \frac{\lambda_{ss}}{1 - (\frac{f}{.222})^2 + \frac{jf}{5.55}}$$

Theoretical values of θ/ψ as a function of frequency, determined from the above equation, are plotted on Figure 17 as a solid line. Points shown on this figure represent experimentally determined values.

Before proceeding to the determination of the dynamic parameters used in the theoretical equation and of the experimental response for θ/ψ , we will consider the transient theory of the single degree of freedom system.

1. Theory (Transient)

With the duct blocked, the ship system is analogous to a L-R-C series electrical circuit. In view of this, the treatment in Ramo-Whinnery (10) in defining the system Q, η [+] and δ will be followed:

[+] The attenuation constant is designated as η here instead of α as in (10) to avoid confusion with the blade angle designated as α in other sections of this report.

The angle of roll at any time will be given by

$$\theta = \theta_o \, e^{-\eta t} \cos (\omega_s \, t)$$

where θ_o is the initial angle of tilt

η is the attenuation constant

The energy in the system is:

$$U = \frac{1}{2} J_s \, \theta_o^2 \, e^{-2\eta t}$$

For small damping, the negative rate of change of this stored energy over several cycles is the average energy dissipated/second:

$$-\frac{dU}{dt} = W_L = -2\eta \, U$$

so $\quad \eta = \dfrac{W_L}{2U}$

Now define the system Q_s (quality factor) as:

$$Q_s = \omega_s \, \frac{(\text{energy stored})}{(\text{energy dissipated/second})} = \frac{\omega_s U}{W_L}$$

then $\eta = \dfrac{\omega_s}{2Q_s}$

The damping can be described in terms of a damping decrement defined as:

$$\delta = 1 - e^{-\eta T_s} \cong \eta T_s \quad \text{if } \eta T_s << 1$$

then $\delta = \dfrac{\omega_s}{2Q_s} \, T_s = \dfrac{2\pi f_s}{2Q_s} \cdot \dfrac{1}{f_s} = \dfrac{\pi}{Q_s}$

showing the simple relation between δ and Q_s.

In terms of the system constants, solution of the single degree of freedom ship equation gives:

$$\eta = \frac{B_s}{2J_s} = \frac{\omega_s}{2Q_s} \quad \text{from before}$$

and $\omega'_s = \omega_s \sqrt{1 - (\frac{1}{2Q_s})^2}$ = resonant frequency of damped ship system

$$\omega_s = \sqrt{\frac{K_s}{J_s}} = \text{undamped natural frequency of ship system}$$

The tools are now available for experimental determination of the single degree of freedom system parameters and the transfer response.

ii. Experiment

Two experiments were run to determine the response of the tank system with the duct blocked. The first experiment consisted of driving the tank system sinusoidally by means of the Stevenson Link mechanism through a range of frequencies below and above resonance and recording the amplitude of rolling in response to the forcing wave. The second experiment, one which yields essentially the same information but which provides a good check on results, consisted of simply tilting the tank system and recording the resulting damped sinusoidal oscillation. Both measurements give a measure of the natural frequency of the tank system with and without damping, the damping decrement, and the Q of the tank system.

Steady State Response

From the steady state response plotted on Figure 17 it is seen that the resonance occurs at:

$$T_s = 4.5 \text{ seconds}$$

This is a very sharp resonance and the value of $f_s = \frac{1}{T_s} = 0.222$ cycles/second can be relied on. To obtain the corresponding value of Q_s, the most effective method is to match the experimental data with the theoretical data for different values of Q. By this method we obtain a value of:

$$Q_s = 25$$

Transient Response

From the upper damped oscillation curve of Figure 18 the following constants are determined:

$$T_s = 4.50 \text{ seconds (average)}$$

so $\omega'_s = \frac{2\pi}{T_s} = 1.39$

$$\delta = \frac{27.9 - 25.0}{27.9} = 0.104$$

and $Q_s = \frac{\pi}{\delta} = \frac{\pi}{0.104} = 30$

also $\omega_s = \dfrac{\omega'_s}{\sqrt{1 - (\frac{1}{25})}} = \omega'_s = 1.39$ within experimental error

iii. Results

From section B-1 we found experimentally:

$$K_s = 5.45 \times 10^3 \text{ ft. lb./radian}$$

From section C-1 we have:

$$\omega_s = 1.39$$
$$Q_s = 25$$

Using these values we get:

$$J_s = \frac{K_s}{\omega_s^2} = \frac{5.45 \times 10^3}{(1.39)^2} = 2.83 \times 10^3 \ \frac{lb.ft.sec.^2}{radian}$$

$$B_s = \frac{\omega_s J_s}{Q_s}$$

$$= \frac{1.39 \times 2.83 \times 10^3}{25} = 157 \ \frac{lb.ft.sec.}{radian}$$

It will be noted that the check between transient and steady state tests of the natural frequency of the system is quite good as expected. The value of Q_s obtained from steady state tests is used since it is the value which matches most closely with theory. This is borne out in other experiments as well. Study of the transient rolling record clearly indicates that, in this system, B_s is a non-constant coefficient. This will probably be equally true for full scale ships. Fortunately, for high Q systems such as this or an actual ship, variation in B_s has negligible effect on stabilization performance. In fact, the work of Part C of this report is greatly simplified by assuming $Q_s = \infty$. That this simplification has considerable justification can be easily seen by putting appropriate numbers in the $\frac{\theta_{in}}{\psi}\Big|_{\phi = 0}$ equation.

b. The Water System

If we assume linearity, the water system is also closely analagous to a simple pendulum. Its response will also be of the same well known form.

- 40 -

1. Theory

With the ship blocked, the water equation becomes:

$$(p^2 J_t + pB_t + K_t)\, \phi = K_p \alpha$$

This reduces to:

$$\left.\frac{\dot{\phi}}{\alpha}\right|_{\psi = 0} = \frac{\lambda_R}{\lambda_t} \cdot \frac{\omega_s P}{(\frac{P}{\Omega_t})^2 + \frac{1}{Q_t}(\frac{P}{\Omega_t}) + 1}$$

This equation indicates that if we study the steady state $\dot{\phi}/\alpha$ response we can ascertain the value of $\omega_p = \omega_t$ and $Q_p = Q_t$. For a low Q system such as this we can expect more accurate values for resonant frequency from transient tests of tank water oscillations.

From the experimental results of the following sections, the values of the parameters are:

$\omega_t = 1.27$ radians/sec

$J_t = 0.77 \times 10^3$ lb. ft. sec.^{2}/radian

$B_t = 5.05 \times 10^3$ lb. ft. sec./radian

$Q_t = 0.19$

substituting these values into the above equation gives:

$$\frac{\dot{\phi}}{\alpha} = 0.309\ \frac{if/.203}{1 - (f/.203)^2 + j5.16\,(f/.203)}$$

Theoretical values of $\frac{\dot{\phi}}{\alpha}$ are plotted as a function of frequency on Figure 19 as a solid line. Points shown on this figure represent experimentally determined values.

J_t is a parameter which depends on the "form" of the tank water system. In Part A it is shown that

$$T_t = 2\pi \sqrt{\frac{S'}{2g}} \qquad \text{Where } T_t = \frac{2\pi}{\omega_t} = \frac{2\pi}{\sqrt{K_t/J_t}}$$

$$\text{ans } S' = \int_0^S \frac{AQ}{As} \; ds$$

Since we already know K_t, if we calculate T_t we are effectively calculating J_t. The calculation of S' is given in Appendix I. From this we get $S' = 36.4$ ft. so:

$$T_t = 2\pi \sqrt{\frac{36.4}{64.4}} = 4.72 \text{ seconds}$$

ii. Experiment

Steady State Tests

The ship was blocked and the water oscillated by driving the pump blades with a signal derived from the sine wave generator. Values of $\dot{\phi}$ and α as a function of frequency are plotted on Figure 19. It can be seen that, due to the extremely high dynamic-head-loss coefficient of the blades, the value of Q_t is very low. From this test the apparent frequency of maximum oscillation amplitude is:

$$f_t = 0.25 \text{ cycles/sec.}$$

The system is so highly damped that it is useless to try to deduce the "true" value of f_t from this data. We will rely on the transient tests for this.

The value of Q_t is obtained by using the value for ω_t obtained from transient tests and then looking for a value of Q_t which best matches the experimental data. A value of: $Q_t = 0.19$ appears to be the best match. It gives about the minimum integrated error over the range of frequencies covered.

Transient Tests

In the first test, the pump was run at large blade angles and then stopped as rapidly as possible by braking the pump motor flywheel. Under this condition, the water undergoes a damped oscillation which can be recorded on a Brush tape by means of the flowmeter. This information gives the natural frequency of the water system and gives a good indication of the damping of the tanks alone, without pump action. The data tabulated below were obtained from a series of such transient tests at different blade angles:

Experimental Data For Variation of Q'_t With Blade Angle(Ship Blocked)

α (degrees)	(damping) (decrement)	T'_t (sec)	T_t (sec)	Q'_t
30	0.046	4.9	4.9	11.0
25.2	0.068	4.9	4.9	7.3
19.6	0.077	4.94	4.92	6.5
14.0	0.01	5.01	4.97	5.0

so average $T_t = 4.92$ seconds

or $f_t = 0.203$ cycles/sec.

Note the variation in Q'_t (without pump action), with blade angle due to increased throttling of the flow. Apparently, the value of Q'_t for the tank system without pump installed would be something greater than 11.0, but probably not much. The great amount of increased "effective" damping created by the dynamic head loss of the blades when they are moving is apparent from comparison of the Q's determined here as compared with a Q_t of 0.19 from the steady state tests. Attempts to determine, by transient test, the damping with pump blades rotating were unsuccessful. We must rely on the Q_t obtained in the preceding section to get the value of B_t.

iii. Results

$$\omega_t = 1.27 \text{ radians/sec}$$

$$J_t = K_t/\omega_t{}^2 = \frac{1.25 \times 10^3}{(1.27)^2} = 771 \ \frac{\text{lb.ft.sec.}^2}{\text{radian}}$$

$$B_t = \frac{\omega_t J_t}{Q_t} = \frac{1.27 \times 771}{0.194} = 5.05 \times 10^3 \ \frac{\text{lb.ft.sec.}}{\text{radian}}$$

$$Q_t = 0.19$$

It will be noted that the following values have been obtained for T_t:

Theoretical $T_t = 4.7$ sec.

Experimental $T_t = \frac{2\pi}{\omega_t} = 4.9$ sec.

These values check quite well considering that the theoretical value of T_t was obtained by an approximation method.

Inspection of Figure 19 makes it quite clear that the values indicated above for Q_t and B_t are only approximate and represent an "average" of a sort. The lower frequency portion of the experimental curve indicates a higher effective "Q". This is to be expected since, at the lower frequencies, it was necessary to drive the pump blades to higher angles. Thus, on the average, the duct was wider open for greater periods, resulting in a higher apparent "Q". It is apparent that this is not a constant resistance pump since B_t depends on blade angle. What will be of interest is, taking an average $Q_t = 0.19$, can we still predict system performance? This remains to be shown.

2. Two Degree of Freedom Tests

Two degree of freedom tests consist of operating as a coupled system with both the ship and the water free to oscillate with mutual interaction.

The mutual coupling parameter J_{st} is the last dynamic parameter left to determine. It can be obtained by measuring the so-called coupled system "secondary resonance" frequency to be discussed below:

a. Theory

Equation (1) for the ship becomes:

$$(p^2 J_s + p B_s + K_s) \, \theta = - (p^2 J_{st} - K_t) \, \phi$$

where $\psi = 0$, (i.e. self-rolling in still water.)

The right side of the above equation reduces to:

$$-K_t \left(- \frac{\omega^2}{\omega_{st}^2} + 1 \right)$$

- 45 -

where $\omega_{st}^2 = K_t/J_{st}$

Note that at a frequency $\omega = \omega_{st}$, the net force on the ship is zero. This condition is referred to as "secondary resonance". As can be seen from the equation, it occurs when the torque on the ship due to a static head of water is exactly cancelled by the torque on the ship created by the kinetic couple resulting from acceleration of the water.

From the results of Part A, it is possible to calculate ω_{st} from:

$$T_{st} = 2\pi \sqrt{\frac{S''}{2g}} \quad \text{where } S'' = \int_0^S \frac{D_s}{L} \, ds$$

The calculation of S'' is given in Appendix I. For the result we have:

$$S'' = 11.14 \text{ ft.}$$
$$\text{so} \quad T_{st} = 2\pi \sqrt{\frac{11.14}{64.4}} = 2.61 \text{ sec.}$$

b. Experiment

To determine ω_{st}, the first step was to establish a standard water level (about half way up tanks). The ship was then caused to roll by driving the pump with a signal derived from the sine-wave generator. As the frequency of pump drive was raised, a point was reached where the static force of the water was counteracted exactly by its kinetic force which, in the model system, at low frequencies, acts in the opposite sense. At this frequency (secondary resonance) the water is oscillating vigorously in the tanks but there is no detectable rolling. Actual

determination of ω_{st} was made by observing the output of the accelerometer which is a much more sensitive indication. From this test:

$$T_{st} = 2.6 \text{ seconds}$$

so $\quad \omega_{st} = \dfrac{2\pi}{T_{st}} = 2.41 \text{ radians/sec.}$

$$= \sqrt{K_t/J_{st}}$$

and $\quad J_{st} = \dfrac{K_t}{\omega_{st}^2} = \dfrac{1.25 \times 10^3}{(2.41)^2} = 0.216 \times 10^3 \ \dfrac{\text{lb.ft.sec.}^2}{\text{radians}}$

The value of T_{st} obtained experimentally agrees very well with the theoretical result.

3. Summary and Discussion of Results on Dynamic Parameters

Final experimental values of system dynamic parameters are listed below. These values will be used in calculating theoretical transfer responses of the system in following chapters.

$$\underline{\text{Ship}} \ J_s = 2830 \ \frac{\text{lb.ft.sec.}^2}{\text{radians}}$$

$$B_s = 157 \ \frac{\text{lb.ft.sec.}^2}{\text{radian}}$$

$$Q_s = 25$$

$$\omega_s = 1.39 \ \frac{\text{radians}}{\text{sec}}$$

$$\Omega_s = 1$$

$$\text{Water } J_t = 771 \ \frac{\text{lb.ft.sec}^2}{\text{radian}}$$

$$B_t = 5050 \ \frac{\text{lb.ft.sec.}}{\text{radian}}$$

$$Q_t = 0.19$$

$$\omega_t = 1.27 \ \frac{\text{radians}}{\text{sec.}}$$

$$\Omega_t = 0.92$$

Mutual

$$J_{st} = 216 \ \frac{\text{lb.ft.sec.}^2}{\text{radian}}$$

$$\omega_{st} = 2.41 \ \frac{\text{radians}}{\text{sec.}}$$

$$\Omega_{st} = 1.73$$

Determination of the ship dynamic parameters was simple,
as the ship, (with duct blocked), is a simple pendulum. Although
the damping parameter B_s is not constant, it is sufficiently un-
important to the final results so that its variation can be ne-
glected.

Determination of the water parameters was a much more
difficult problem. It is clear from the results that the skin
friction damping of the tanks and duct is negligible compared to
the dynamic head loss of the pump. The parameter B_t is not
constant but varies with blade angle. Fortunately, the "effective"
damping of the water system is so high due to pump action that
the variations in B_t also become unimportant. That is to say
that, in this system, B_t does not vary over a sufficient range to
effect the final result. The effect of variation of B_t is clearly

shown in Part C. Also, to some extent, the variation of B_t is compensated by the variation in K_p. This can be seen by studying the $\dot{\phi}/\alpha$ transfer function.

Determination of ω_{st} was the simplest test of all. Considering the confusion which has existed in the past about the "Kinetic Reaction" phenomenon and "secondary resonance", it was most gratifying to observe the water oscillating vigorously in the tanks and being able to detect no motion of the tank system at the "secondary resonance" frequency.

D. System Response Studies - (Controls Off)

Now that we have determined the parameters of the ship-water system, the next step is to determine the transfer responses indicated in section A of this chapter. Three experiments are included under this heading. The first is determination of the ship-water response, $\dfrac{\theta_{out}}{\phi}$, with $\psi = 0$. The second is the determination of the active ship response, $\dfrac{\theta_{out}}{\alpha}$ with $\psi = 0$. The third is the determination of the passive ship response $\dfrac{\theta_{in}}{\psi}$, with $\alpha = 30°$ and pump not running; representing maximum Frahm damping.

1. Theory

The equations for each of these cases have already been worked out and presented in dimensionless form at the beginning of this chapter. Using these equations and the experimentally determined parameters we get for the transfer functions involved in these three tests:

$$\left.\frac{\theta_{out}}{\phi}\right|_{\psi=0} = K_2 G_2(p) = \frac{-0.036}{f} \cdot \frac{[1 - (\frac{f}{.384})^2]}{1 - (\frac{f}{.222})^2 + j0.04(\frac{f}{.222})} \quad (8)$$

Equation (8), as a function of frequency is plotted as the solid lines on Figure 20.

$$\left.\frac{\theta_{out}}{\alpha}\right|_{\psi=0} = K_2 K_3 G_2(\rho) G_3(p) =$$

$$1.28 \cdot \frac{[1 - (\frac{f}{.384})^2]}{[1-(\frac{f}{.222})^2+j(\frac{f}{5.53})][1-(\frac{f}{.203})^2+j\frac{f}{.039}]-0.23[1-(\frac{f}{.384})^2]^2} \quad (9)$$

Equation (9), as a function of frequency, is plotted as solid lines on Figure 21.

$$\left.\frac{\theta_{in}}{\psi}\right|_{\alpha=30°} = K_1 G_1(p) =$$

$$0.242 \cdot \frac{[1 - (\frac{f}{.203})^2 + j\frac{f}{.61}]}{[1-(\frac{f}{.222})^2+j\frac{f}{6.66}][1-(\frac{f}{.203})^2+j\frac{f}{.61}]-0.23[1-(\frac{f}{.384})^2]^2} \quad (10)$$

Equation (10), as a function of frequency, is plotted as the solid lines on Figure 22. It should be noted that in equation (10) the value of $Q_t = 3$ is used, not the value of $Q_t = 0.19$ as in other tests. The reason is because the pump blades are open and not rotating. This value of $Q_t = 3$ gives the best check with the experimental data. In addition, the value of $Q_s = 30$ instead of $Q_s = 25$ is used. The experiment corresponding to equation (10) was run during the warm summer months. As a result,

- 50 -

the ship damping was decreased resulting in a Q_s higher than that for previous tests.

2. Experiment

To obtain the ship-water response $\theta_{out}/\dot{\phi}$, the ship was driven by oscillating the pump water by means of a signal derived from the sine-wave generator. The wave slope bar was fixed at $\psi = 0$. Experimental points are plotted on Figure 20.

To obtain the active ship response $\theta/_{out}\, \alpha$, the same procedure was followed but we measured α instead of $\dot{\phi}$. These points are plotted on Figure 21.

To obtain $\dfrac{\theta_{in}}{\psi}$, the system is driven by the Stevenson Link mechanism with the pump blades fixed in the wide open position. Experimental points are plotted on Figure 22.

3. Discussion of Results

Inspection of Figure 20 indicates excellent correlation between theoretical and experimental data for $\left.\dfrac{\theta_{out}}{\dot{\phi}}\right|_{\psi=0}$. We would expect good correlation here since reference to equation (6) shows that this ratio depends on constants which are known with some precision and also on the ratio of mutual terms to ship terms, both of which depend primarily on inertia and form, and should be reliable.

Inspection of Figure 21 indicates what was unexpectedly close agreement between theory and experiment for $\left.\dfrac{\dot{\theta}_{out}}{\alpha}\right|_{\psi=0}$. Reference to equation (4) might lead one to expect considerable

difficulty in correlation in view of the non-constant pump para-
meters which appear in this equation. However, the ship charac-
teristics override the tank characteristics in this system so
that non-linearity in the pump has little net effect on system
operation.

Inspection of Figure 22, showing $\frac{\Theta_{in}}{\psi}$, again reveals unex-
pectedly close correlation between theory and experiment. In
this case of Frahm damping, the system is highly sensitive to the
ratio $\Omega_t = \frac{\omega_t}{\omega_s}$ so that some of the discrepancy observed may re-
sult from that.

In general, the results of these system tests, (controls off)
show unexpectedly good correlation between experiment and linear
theory and lead one to hope that actual stabilization results
may likewise be predictable. This we shall investigate in
Chapter VI.

E. Concluding Remarks

We have established notation and derived the transfer func-
tions of the ship-tank system. Experimental determination of static
and dynamic system parameters as well as transfer characteristics
in all cases agreed well with linear theory. The crucial test of
the theory will come when we operate with the regulated element as
part of the closed servo loop. However, before we can check over-
all performance it is necessary to have the equations governing
the regulating elements in hand. This is done in the following
chapter.

V. STUDY OF CONTROLS: THE REGULATING ELEMENT

Referring back to the treatment of ship-stabilization as a servo problem in Chapter III of Part A, it is seen that in the preceding chapter we have evaluated the factors:

$$\underline{B} = \frac{\theta_{out}}{\alpha} = \text{Active Ship Response}$$

$$\underline{C} = \frac{\theta_{in}}{\psi} = \text{Passive Ship Response}$$

It is apparent that, in order to proceed to the case of stabilization, it is necessary to evaluate:

$$\underline{A} = \frac{\alpha}{\theta} = \text{Controller Response}$$

Once $\underline{A}$ is determined, the evaluation of overall stabilization follows immediately:

$$\text{Overall stabilization} = \frac{\theta}{\psi} = \frac{\theta_{in}}{\psi} \cdot \frac{\theta}{\theta_{in}} = \underline{C} \cdot \frac{1}{1-\underline{A}\,\underline{B}}$$

The elements which comprise $\underline{A}$ are shown on Fig. 8 and listed on Page 12. All of these elements are well understood devices so that their theoretical treatment will be kept to a minimum. The primary interest here is to determine what $\underline{A}$ actually is in this system so that we can proceed to check the validity of the linearized theory. At the same time, the performance of the system is also of interest. As previously indicated, while certain necessary improvements have been made, no attempt was made to optimize the characteristics of $\underline{A}$. Thus, what follows is a brief theoretical treatment of each element

along with experimental determination of the element parameters
and transfer response. Comments are made on how each of the
elements could be improved.

We will be particularly interested in the _distribution_ of
control lags among the various links in the control chain. As
indicated in Chapter V of Part A, the elements which must pro-
vide the strongest force should produce the greatest lags. If
this is not so, one should become immediately suspicious of the
correctness of the system design. It will be shown in this chap-
ter that this rule-of-thumb is grossly violated in the model
system set-up. A similar situation may well have caused the
difficulties in the pre-war installation on the U.S.S. Hamilton.

A. Roll Sensing Element - The Accelerometer

The desirability of using an accelerometer as the primary
control signal source is discussed in detail in Part C of this
report. An angular accelerometer is used here. Instruments of
this type are well understood.

1. Theory

The equation of motion of the angular accelerometer is:

$$\ddot{\Theta} = \frac{1}{2mr^2} \left(J_{ac} \ddot{\gamma} + B_{ac} \dot{\gamma} + K_{ac} \gamma \right)$$

where

J_{ac} = moment of inertia of weights

K_{ac} = constant or restoring springs

B_{ac} = viscous damping constant

γ = angular displacement of weight relative to ground

ω_{ac} = $\sqrt{K_{ac}/J_{ac}}$ = natural frequency of the accel-erometer

θ = angle of ship's roll (as before)

From above:

$$\ddot{\theta} = \frac{1}{2mr^2} (p^2 J_{ac} + p\, B_{ac} + K_{ac})\, \gamma$$

so

$$\frac{\gamma}{\ddot{\theta}} = \frac{2mr^2}{p^2 J_{ac} + p\, B_{ac} + K_{ac}} = \frac{2mr^2}{K_{ac}} \cdot \frac{1}{(\frac{P}{\Omega_{ac}})^2 + \frac{1}{Q_{ac}} (\frac{P}{\Omega_{ac}}) + 1}$$

where $\Omega_{ac} = \omega_{ac}/\omega_s$

$$Q_{ac} = \frac{\omega_{ac} J_{ac}}{B_{ac}}$$

$$2mr^2 = J_{ac}$$

then:

$$\frac{e_1}{\ddot{\theta}} = \frac{V_1}{\omega^2_{ac}} \cdot \frac{1}{(\frac{P}{\Omega_{ac}})^2 + \frac{1}{Q_{ac}} (\frac{P}{\Omega_{ac}}) + 1} \qquad (11)$$

where: V_1 = volts/radian/sec^2.

In this application it is often desirable to use the transfer function e_1/θ instead of $e_1/\ddot{\theta}$. For this we get:

$$\frac{e_1}{\theta} = \frac{V_1 (\frac{P}{\Omega_{ac}})^2}{(\frac{P}{\Omega_{ac}})^2 + \frac{1}{Q_{ac}} (\frac{P}{\Omega_{ac}}) + 1} = K_4 G_4(p) \qquad (12)$$

From the experimental data in the following section we have:

$$K_4 = 5.5 \text{ volts/degree}$$
$$\omega_{ac} = 6.28 \text{ radians/sec}$$
$$Q_{ac} = 0.6$$

putting these values into equation 11 gives:

$$e_1/\hat{\theta} = \frac{5.5}{39.7} \times \frac{1}{1-f^2 + \frac{jf}{0.6}}$$

The theoretical response of $e_1/\hat{\theta}$ as a function of frequency is plotted as the solid curves on Fig. 23.

2. Experiment

A series of several tests were run on the accelerometer. In the test set-up, any motion of either the tanks which are keyed to the main shaft, or of the accelerometer movable element, results in a modulated 200 cycle signal being fed to a demodulator, amplified, and recorded.

a. Transient Tests

The purpose of the first test was to ascertain the natural frequency of the accelerometer. ($f_{ac} = \omega_{ac}/2\pi$). To do this, it is only necessary to remove the damping oil dashpots, deflect the movable element, and then release it and let it oscillate. A record of this motion is shown on R-3 on Fig. 23. The natural period is obtained by measuring the time between corresponding zeros. Since each horizontal division on R-3 represents 1 second, it can easily be seen

- 56 -

that T_{ac} = 1 second so f_{ac} = 1 cycle/sec. The damping observed
is friction damping in the mechanism.

The purpose of the second test was to adjust and measure
the total damping with oil dashpots. Damping is adjustable by
varying the viscosity of the oil in the damping dashpots or by
varying the openings in the ports in the damping paddles.
Several combinations were tried with typical results indicated
on records R-4, R-5, and R-6 on Figure 23. It can be seen that
with orifices closed and SAE 50 oil, the accelerometer is highly
overdamped. With SAE 30 and ports half closed it is somewhat
underdamped. With SAE 50 and the ports open the damping is
about 85% of critical. This accelerometer is unsatisfactory
in its present form since its damping does not remain constant.
However, it is simple to readjust and this was done before con-
ducting any tests to verify regions of instability. The damping
was checked by simply deflecting the movable element, releasing
it, and observing its overshoot. The result was then compared
with normalized transient curves in (11) to deduce the damping
factor.

b. Steady State Tests

The third test was designed to determine the ampli-
tude and phase response of the accelerometer with the damping
factor set at 0.84. Unfortunately, no means were available to
test this instrument much beyond one-half of its natural fre-
quency. However, the accelerometer is such a well-known
instrument that only a few points need be determined.

The data for a typical test run are plotted as experimental points on Figure 24. It is clear that, for the test shown, the damping corresponds to about 84% of critical damping. The amplitude data is quite poor since it is very difficult to obtain smooth drive. The slightest deviations from sinusoidality in the rolling is greatly exaggerated by the p^2 multiplier of θ resulting in considerable distortion of the recorded wave forms.

The final test made was to determine the accelerometer transfer function constant V_1. V_1 should be large for high sensitivity, i.e., large voltage output for small accelerations. The procedure was to roll the system with the Stevenson Link Mechanism, recording amplitude and frequency of roll and the corresponding voltage output of the accelerometer's moving coil system. As a check, this experiment was run at three different frequencies. Prior to making the steady state tests, the value of the damping factor was redetermined from step function tests and found to be 0.6. Thus $Q_{ac} = 1/1.2$ for the following calculations. The transfer function of the accelerometer is given in equation 12. V_1 is a _real_ constant which we wish to determine. From equation 12:

$$V_1 = \frac{e_1}{\theta} \cdot \frac{(\frac{p}{\Omega_{ac}})^2 + \frac{1}{Q_{ac}}(\frac{p}{\Omega_{ac}}) + 1}{(\frac{p}{\Omega_{ac}})^2}$$

Therefore, if we know Q_{ac}, ω_{ac}, θ, and e_1 at a given frequency we can obtain V_1. The data for this test are tabulated below:

Frequency (cyc/sec)	$\frac{1}{Q_{ac}}$	$\frac{1}{\theta}$	f^2	$\left\| -f^2 + \frac{jf}{Q_{ac}} + 1 \right\|$	$\frac{V_1}{\text{Volts}}$ $\frac{}{\text{Degree}}$
.183	1.2	.187	.0335	.978	5.45
.1515	1.2	.130	.0230	.985	5.56
.220	1.2	.242	.0485	.968	4.83

- Note that $p/\omega_{ac} = \frac{j2\pi \, f}{2\pi \times 1} = jf$ since $f_{ac} = 1$ cycle/second

It will be noted that at a frequency of 0.22 cycles/second, corresponding to $\ddot{\theta} = 20.75$ degrees/sec^2 of the ship, the value of V_1 is below its lower frequency values. This indicates limiting in the bucking coil system due to moving too far out of the magnet poles. From this we can estimate that the accelerometer voltage output is linear with acceleration up to $\ddot{\theta} \cong 20$ degrees/sec^2, above which limiting occurs in the moving coil system.

Final data on the accelerometer characteristics are indicated below:

<u>Natural frequency</u> $= 1$ cycle/second

<u>Damping factor</u> $= \frac{1}{2 \, Q_{ac}} = 0.84$

<u>Q_{ac}</u> $= 0.6$

<u>Phase Lag</u> $= 100°$/cycle/sec/up to 1/2 cycles/sec. (nearly linear)

<u>V_1</u> $= 5.5$ volts/degree (average)

The most obvious deficiency in this accelerometer is its
lack of constant damping. This condition need not and should
not be tolerated in future installations. Both the choice of
natural frequency and damping will determine the phase lag
introduced by the accelerometer. Theoretically, one is con-
cerned with obtaining minimum phase lag commensurate with ade-
quate sensitivity. Practical considerations of mounting an
accelerometer on a ship's hull must be carefully considered.
Compromises may be necessary to maintain acceptable signal to
noise ratios from the accelerometer output. For instance, on
the U.S.S.Peregrine, linear accelerometers were used. These
were separated by almost the entire ship's beam to get increased
sensitivity. Unfortunately, the hull vibrations at opposite
sides of the ship were not of equal amplitude; neither were
they in phase. This resulted in an unbalanced "noise" signal
from the accelerometers. Instruments of this type should be
designed with the particular application in mind. A vital
point should be kept firmly in mind for any further work with
model systems. It is <u>necessary</u> to scale the parameters of
the control elements as well as those of the ship and tanks
to obtain useful answers on stability and performance.

B. The Servo-Amplifier

In this system, the control amplifier is an electronic
device. As such, it is probably the least expensive and most

flexible of many possible amplifying devices. It suffers from the poor inherent reliability of most existing electronics systems and therefore is not necessarily an ideal choice for this purpose.

1. Theory

The low frequency response characteristics of the servo-amplifier are entirely determined by the differentiating circuits. Only the differentiator $\ddot{\theta} \longrightarrow \dddot{\theta}$ is ever used. If $\ddot{\theta}$ alone is used, the response of the system is a constant depending on the gain settings only. Regardless of how much of the derivative control is used, the frequency characteristic of the last stages of the amplifier operating around the 200 cycle carrier is also a constant independent of the setting of the gain controls. Therefore, the only transfer function which need be developed analytically is that of the differentiating transformer. Of interest is $\dfrac{e_{out}}{e_{in}}$, the ratio of output voltage to input voltage as a function of frequency.

Referring to the schematic diagram on Figure 25, the differential equations for a differentiating transformer circuit are:

$$R_1 i_1 + p\, L_1 i_1 - p\, M i_2 = e_{in}$$

$$R_2 i_2 + p\, L_2 i_2 - p\, M i_1 = 0$$

By algebraic manipulation we get:

$$\frac{e_{out}}{e_{in}} = \frac{R_2 p M}{R_1 R_1 - p\,(R_1 L_2 + R_2 L_1) + p^2\,(L_1 L_2 - M^2)}$$

- 61 -

from this we get:

$$\frac{e_{out}}{e_{in}} = \frac{R_2}{\frac{R_2 R_1/M}{p} + \frac{R_1 L_2 + R_2 L_1}{M} + p\frac{(L_1 L_2 - M^2)}{M}}$$

Now observe that this equation has the identical functional form of the ratio of voltage output across a resistor in a series circuit consisting of R's, L's, C's to an input voltage. In such a series circuit we get:

$$\frac{e_{out}}{e_{in}} = const. \quad \frac{1}{R + pL + \frac{1}{pC}}$$

by analogy:

$$C = M/R_1 R_2$$

$$L = \frac{L_1 L_2 - M^2}{M}$$

$$R = \frac{R_1 L_2 + R_2 L_1}{M}$$

so

$$\omega_L = \frac{1}{\sqrt{LC}} = \sqrt{\frac{R_1 R_2}{L_1 L_2 - M^2}}$$

$$Q_L = \frac{\omega_L L}{R} = \sqrt{\frac{R_1 R_2 (L_1 L_2 - M^2)}{R_1 L_2 + R_2 L_1}}$$

using these relations we get:

$$\frac{e_{out}}{e_{in}} = K_9 \cdot \frac{\frac{p}{\Omega_L}}{(\frac{p}{\Omega_L})^2 + \frac{1}{Q_L}(\frac{p}{\Omega_L}) + 1} = K_9 G_5'(p) \qquad (13)$$

$$\text{where } \Omega_L = \frac{\omega_L}{\omega_s}$$

- 62 -

Therefore, the actual amplifier transfer function is:

$$\frac{e_2}{e_1} = K_5 G_5(p) = K_8 + K_9 \cdot \frac{\frac{P}{\Omega_L}}{(\frac{P}{\Omega_L})^2 + \frac{1}{Q_L}(\frac{P}{\Omega_L}) + 1} \tag{14}$$

It should be noted that at very low frequencies and large values of M, the transfer function $\frac{e_{out}}{e_{in}}$ is identical in form to that obtained from the simple R-L equivalent circuit shown on Figure 25. The R-L circuit is a well-known differentiator so the action of the transformer coupling at low frequencies should be identical.

Terman, in his 3rd edition of "Radio Engineering", p. 246, shows the expected gain variation and phase shift of such a coupled circuit. This plot is reproduced schematically on Figure 25. It indicates that at the low frequency end of the spectrum the amplitude ratio varies at 6db/octave and the phase lead approaches 90°.

2. Experiment

Both K_8 and K_9 are variable gain controls. K_8 governs the magnitude of the $\dot{\theta}$ signal. K_9 governs the magnitude of the $\ddot{\theta}$ signal. It is necessary to know the gain corresponding to each setting of these controls. For K_8 this is done by simply measuring output/input ratios for different values of the $\ddot{\theta}$ control. Results of this test are plotted on Figure 26. It can be seen that the variation of K_8 is essentially linear. For future use, $K_8 = 0.095 \times \dot{\theta}$ gain control setting.

From the previous section, with the $\ddot{\theta}$ control set at zero:

$$K_9 = \frac{e_2}{e_1} \cdot \frac{(\frac{P}{\Omega_L})^2 + \frac{1}{Q_L}(\frac{P}{\Omega_L}) + 1}{\frac{P}{\Omega_L}}$$

It is therefore necessary to modify the voltage ratios measured by the frequency characteristic of the differentiators before arriving at a true value for K_9. Actually, in addition to the frequency characteristic of the differentiator circuit, there is a frequency characteristic introduced by the input demodulator filter which is not negligible. These corrections are obtained from data presented in the following paragraphs. The test runs were made at two different frequencies for check purposes. The data used to make the corrections are:

$$f_L = 4.3 \text{ cycles/sec.}$$
$$Q_L = 0.35$$

$$\epsilon\Big|_{0.5} = 0.82 = \text{factor by which } K_9 \text{ must be reduced due to demodulator filter response at 0.5 cycles/sec.}$$

$$\epsilon\Big|_{0.82} = 0.98 = \text{factor by which } K_9 \text{ must be reduced due to demodulator filter response at 0.82 cycles/sec.}$$

So K_9 (0.5 cycles/sec) $= \dfrac{e_2}{e_1} \times 0.82 \times \dfrac{\left|1-(\frac{\omega}{\omega_L})^2 + j\frac{\omega}{\omega_L}\right|}{j\frac{\omega}{\omega_L}} = 8.86\,\dfrac{e_2}{e_1}$

K_9 (0.82 cycles/sec) $= \dfrac{e_2}{e_1} \times 0.98 \times \dfrac{\left|1-(\frac{\omega}{\omega_L})^2 + j\frac{\omega}{\omega_L}\right|}{j\frac{\omega}{\omega_L}} = 3.54\,\dfrac{e_2}{e_1}$

- 64 -

These were the multiplying factors used in determining the values of K_9, plotted on Figure 27.

Inspection of Figure 27 indicates that the K_9 variations determined at two different frequencies are essentially parallel and linear but with a fixed separation. This discrepancy can be attributed to the difficulty of measuring the e_2/e_1 ratio due to noise signals in the amplifier distorting the wave forms and making reading difficult. An average between the two sets of points represents a reasonable indication of actual performance and this will be used in future work. From this average we get:

$K_9 = 0.865 \times \ddot{\theta}$ gain control setting

We now have the gain constants K_8 and K_9, both of which depend on variable front panel gain control. The gain constant K_{10} of the section of the amplifier which operates at the 200 cycle level is fixed once certain internal gain controls have been adjusted properly. This constant will, however, vary depending on whether the additional amplifier stage shown on Figure 5 is switched in or out.

The average value of K_{10} is:

$K_{10} = 66$ with extra amplifier out

The gain of the extra amplifier is 4.4. Therefore:

$K_{10} = 66 \times 4.4 = 290$ with extra amplifier in.

Now all that remains is to determine the response of the differentiating transformer and the input demodulator low-pass filter and from this determine Q_L and ω_L.

The response of the input demodulator filter is plotted on Figure 28. In order to obtain this response it was necessary to compare its action with that of the test demodulators described previously in this report and then correct for the known response of the test demodulators.

The overall response from amplifier input through the first differentiator was next obtained. The data are plotted on Figure 29. In order to obtain the actual differentiator response it is necessary to correct for the action of the input demodulator filter. These corrections are obtained from Figure 28. The resulting response of the differentiator alone is also shown on Figure 29. Therefore, from the data on the differentiator alone, we determine

$$f_L = 4.3 \text{ cycles/second}$$

The value of Q_L is estimated at 0.35 from comparing the curve of amplitude response of the differentiator to normalized data in Terman's "Radio Engineer's Handbook," page 140.

Thus the final data on the servo-amplifier are:

$\omega_L = 2\pi f_L = 27$ radians/sec. $K_9 = 0.865 \times \dddot{\theta}$ gain control setting

$Q_L = 0.35$ $K_{10} = 66$ without extra amplifier

$K_8 = .095 \times \ddot{\theta}$ gain control setting $K_{10} = 290$ with extra amplifier

A few more words will be said about the servo amplifier.
The use of differentiators to advance phase of control to compensate for system phase lags is no longer widespread. What is actually wanted is an equalizer-amplifier in which the response as a function of frequency is controlled in a prescribed manner based on the known characteristics of the other control elements, and of the ship-tank system. Furthermore, it is certainly possible to construct an amplifier which is not as troubled by extraneous signals or as difficult to adjust.

C. Servo-Motor

1. Theory

The motor is a two-phase induction motor with a high resistance rotor. If we assume that its output torque is a linear function of its input voltage, then:

$$\text{Torque} = J_m \ddot{\beta} + B_m \dot{\beta}$$

where J_m = total inertia of motor including gear train

B_m = total friction resistance on motor shaft

β = angle of rotation of rotor

now $\beta = (x_1 \cdot \text{const.})$ since, due to gearing, the vertical displacement of the valve rack is directly proportional to β.

Also   Torque = const. (e_3') (since torque is proportional to volts)

so $x_1/e_3' = \dfrac{\text{constant}}{p^2 J_m + p B_m}$

now define $\omega_0 = B_m/J_m$ and $\Omega_0 = \dfrac{\omega_0}{\omega_s}$

then $x_1/e_3' = \dfrac{J_m K/B_m^2}{(\frac{p}{\Omega_0})^2 + (\frac{p}{\Omega_0})} = K_6' G_6'(p)$ (15)

- 67 -

In order to obtain the closed loop transfer function $K_6 G_6(p)$ we need only apply the standard feed back amplifier approach, i.e.:

$$e_3 = e_2 - V_2 X_1$$

$$X_1/e_3 = K_{10} K_6' G_6'(p)$$

then

$$\frac{X_1}{e_2 - V_2 X_1} = K_{10} K_6' G_6'(p)$$

so

$$\frac{X_1}{e_2} = \frac{K_{10} K_6' G_6'(p)}{1 + V_2 K_{10} K_6' G_6'(p)}$$

$$= \frac{K_{10} K_6'}{\frac{1}{G_6'(p)} + V_2 K_{10} K_6'} = \frac{K_{10} K_6'}{(\frac{P}{\Omega_o})^2 + (\frac{P}{\Omega_o}) + K_{10} K_6'}$$

$$= \frac{1/V_2}{\left(\frac{P/\Omega_o}{\sqrt{V_2 K_{10} K_6'}}\right)^2 + \frac{1}{\sqrt{V_2 K_{10} K_6'}} \left(\frac{P/\Omega_o}{\sqrt{V_2 K_{10} K_6'}}\right) + 1}$$

$$= \frac{1/V_2}{(\frac{P}{\Omega_m})^2 + \frac{1}{Q_m} (\frac{P}{\Omega_m}) + 1} = K_6 G_6(p) \qquad (16)$$

where

$$Q_m = \sqrt{V_2 K_{10} K_6'} \qquad\qquad K_6 = 1/V_2$$

$$\Omega_m = \frac{1}{\Omega_o \sqrt{V_2 K_{10} K_6'}}$$

$$\omega_m = Q_m \omega_o$$

- 68 -

From the form of equation (16), it is clear that the Q of the closed motor loop depends on the loop gain as expected. Also the "natural" frequency of the motor is multiplied by a factor dependent on gain which determines the actual resonance.

2. Experiment

The Servo-motor was the object of considerable attention because of instability on the closed loop defined by $K_6 G_6(p)$. The resulting oscillations were particularly troublesome when attempts were made to check transfer characteristics of valve versus piston, blade angle versus water, and all other tests which depended on a smooth sinusoidal valve drive. The instability was removed by the addition of an eddy current damping wheel on the motor shaft.

i. Open Loop Transient Tests

A typical open loop step function response of position vs. time for the modified motor is shown on the lower record of Figure 30. The upper record shows the same response for the unmodified servo-motor. It is apparent that the motor time constant, T_o, has been reduced from its original value, meaning that $\omega_o = 1/T_o$ has increased. Since $\omega_o = B_m/J_m$, this means the motor damping was increased more than its inertia. The data for the open loop determination of T_o derived from Figure 30 are plotted on Figure 31. From this plot, a good value of the "true" unsaturated time constant is:

$$T_o = 0.07 \text{ seconds.}$$

This value is _not_ however obtained in actual present practice due to _very rapid_ saturation of the servo-motor. This effect shows up vividly in the following test.

ii. Closed Loop Transient Tests

Another way of determining the time constant of the motor is to perform closed loop step function transient tests. From the data obtained in these tests it is possible, by comparing actual curves to curves in (11), to obtain a fair value of the motor time constant. Typical data of this type are shown on the lower five records of Figure 32. These records were each obtained in exactly the same way but with _one signifi-cant difference_. The deflection of the valve from zero is different in each case. Note the corresponding difference in time constants obtained as indicated below each record. With large valve deflections and correspondingly large voltage output from the feed back selsyn, the motor is _much_ over-saturated, i.e. torque $\neq$ (const. x volts). With small deflections, the motor is less saturated and the time constant approaches its open loop unsaturated value. It is important to note that even for valve motions less than 0.1 inches the motor is saturated. This indicates that in operation, this particular motor is almost _always_ saturated.

iii. Closed Loop Steady-State Tests

The next step was to perform closed loop tests of the servo motor to determine its overall response.

Data from a series of three typical tests are plotted on Figure 33. From the data shown on Figure 33, depending on amplitude of valve motion, values of T_o obtained differ by over 50%. Thus again we see the effect of saturation due to large valve motions. The oil pressure seems to introduce a negative capacity loading. This is evidenced by the fact that with no voltage on the motor, the valve tends to accelerate in the direction of an initial displacement. The loop can be stable with oil pressure off but becomes unstable with it on.

iv. Open Loop Steady-State Tests

It is necessary to try to pin things down a little more at this point. In this connection an open loop steady-state test was run on the motor. Data from this test are plotted on Figure 34. For this test the amplifier was in, oil pressure off and the selsyn was out of the loop. The motor time constant is obtained by determining the frequency corresponding to 135° phase lag. At this point $\omega = \omega_o$. So, from Figure 34:

$$\omega_o = 2\pi \times 0.9 = 5.65 \text{ radians/sec}$$
$$\text{so} \quad T_o = \frac{1}{5.65} \quad = 0.177 \text{ seconds}$$

This figure agrees pretty well with those obtained in closed loop transient tests. The main interest is the functional form of the open loop response. An "ideal" servo of this type would never exceed 180° phase lag. This servo is up to 202° lag at 4 cycles/sec. The additional phase lag due to either

- 71 -

sticking, back lash, or some other non-linear phenomenon is
what caused the motor to oscillate in the first place. Evi-
dently, the eddy current damper has done some good. However,
it is obvious that this servo-motor is not adequate for the
designed purpose. Either a new motor or some other device
performing the same function would be needed.

v. Determination of Selsyn Constant, V_2

The valve feed back selsyn constant, V_2 (volts/inch),
was obtained by feeding a constant signal into the amplifier
producing a constant voltage into the closed loop described
by $K_6 G_6(p)$. Due to this signal, the valve was deflected by an
amount proportional to the setting of the valve gain control.
The variation of valve position versus valve control setting for
a given input signal was determined. These data are plotted on
Figure 35. From Figure 35 we get:

$$V_2 = 1 \cdot 0.69 \times \text{Valve gain control setting}$$

vi. Final Results

From the above section we know the value of V_2
unequivocally. Similarly, from amplifier tests we know the
value of K_{10} both with the extra amplifier in and with it out.
There are two constants of the motor ω_o and K_6', which have not
yet been determined in a clear-cut fashion. We can obtain K_6'
from the closed loop steady state tests from the relation:

$$K_6' = \frac{Q_m^2}{K_{10} V_2} = 1.29 \times 10^{-4}$$

- 72 -

The amplifier gain was reduced to improve stability since the data plotted on Figure 33 were taken. With present parameters:

$$f_m = 0.455 \text{ cycles/sec (amplifier in - valve gain setting at 4)}$$

$$f_m = 0.280 \text{ cycles/sec (amplifier out - valve gain setting at 4)}$$

so

$$V_2 = 1 + .69(4) = 3.76 \text{ volts/inch}$$

and

$$Q_m = 0.376 \text{ (amplifier in)}$$

$$= 0.179 \text{ (amplifier out)}$$

then

$$\omega_o = \frac{2\pi f_m}{Q_m} = 6.28 \times \frac{0.455}{0.376} = 7.6 \text{ radians/sec (amplifier in)}$$

$$= 6.28 \times \frac{0.286}{0.179} = 10 \text{ radians/sec (amplifier out)}$$

It is apparent that the motor is still saturating, although not as much as before. For simplicity, we will assume an average $\omega_o = 8$ radians/sec in future calculations. This should not make the calculated results far from reality.

Below are the final values used for the servo motor:

$$\omega_o = 8 \text{ radians/sec.}$$

$$K_6' = 1.29 \times 10^{-4}$$

$$V_2 = 1 + 0.69 \times \text{valve gain control setting (volts/inch)}$$

$$Q_m = \sqrt{0.0374 \times V_2} \text{ with extra amplifier in}$$

$$= \sqrt{0.0085 \times V_2} \text{ with extra amplifier out}$$

$$\omega_m = Q_m \, \omega_o$$

$$K_6 = 1/V_2 \text{ inches/volt}$$

$$K_{10} = 290 \text{ with extra amplifier in}$$

$$= 66 \text{ with extra amplifier out}$$

Due to saturation, the motor is the weakest link in this control system. It introduces phase lags far in excess of what could be expected from such a device for the frequency range and power level covered. Because of this saturation, it is difficult to pin down the motor parameters to values that can be fully trusted. Fortunately, the final results do check fairly well indicating that the values of the parameters listed above are not too far off. Certainly, however, some of the discrepancy in the final results is due to the above approximations. Going ahead a bit to Chapter VI, it is seen that this servo-motor is providing most of the phase lag of the system. Clearly then it is violating the concept of "control difficulty factor" outlined in Chapter V of Part A.

D. Hydraulic Amplifier

The positioning motor used in the model system is a hydraulic device. One would expect that this system component would, due to its mass, introduce the greatest phase lags into the system. As will be seen, in the model system, such is not the case.

1. Theory

In this hydraulic oil system, the linear motion of a valve opens high pressure ports causing pressure to be put on a piston driving it in such a direction as to tend to close the ports. For this particular system, it can be assumed

that the velocity of the piston is proportional to the displacement of the valve, i.e. the amount of valve opening. Thus we can say that:

$$\dot{X}_3 = X_2 \times \text{const.} \quad \text{(Refer to Figure 8)}$$

but $\quad X_2 = X_1 - X_3$

so $\quad \dot{X}_3 = (X_1 - X_3) \, \text{const.}$

and $\quad (p + \text{const.}) \, X_3 = X_1 \cdot \text{Const.}$

so $\quad X_3/X_1 = \dfrac{\text{const.}}{p + \text{const.}} = K_7 G_7(p)$ \hfill (17)

Note that if the constant is large (very high pressure) this response function will be quite flat to appreciable frequencies.

Since the hydraulic amplifier is <u>not</u> a resonant system, there is not much to be gained in normalizing its frequency scale.

From the experiments discussed in the next section we get:

$$K_7 = 78.8 \text{ radians/sec}$$

Substituting this in the above equation gives:

$$X_3/X_1 = \frac{78.8}{78.8 + j\omega}$$

Values for X_3/X_1 as a function of frequency are plotted as the solid curve on Figure 36. The points shown on Figure 36 were determined by experiment.

2. Experiment

Determination of K_7 in effect determines the entire transfer characteristic of the hydraulic amplifier. It turns

out, however, that this constant is so large that at the highest frequency at which we can drive the system, the ratio X_3/X_1 has dropped only about 10%. In order to determine K_7 <u>accurately</u> it would have been desirable to reach at least the point at which $|p| = K_7$. However, the estimate below should be useful anyway.

In making this test, the valve is driven sinusoidally by the servo-amplifier which is fed by the sine wave generator. The output of the feed-back selsyn geared to the valve gives valve position. The output of a selsyn linked to the blade angle shifting shaft gives hydraulic piston position. Both signals are fed to the Brush recorder and the relative amplitudes and phases are determined. The resultant data are plotted as experimental points on Figure 36.

In order to estimate K_7 from the data we have:

$$\left| \frac{X_3}{X_1} \right| = M = \left| \frac{K_7}{K_7 - j\omega} \right| = \frac{K_7}{\sqrt{K_7^2 + \omega^2}} \quad \text{so } K_7 = \frac{M\omega}{\sqrt{1 - M^2}}$$

Using this relation at the three highest frequencies we get:

$$K_7 = \frac{(.901)^2 \ (2\pi \times 7.2)}{\sqrt{1 - (.901)^2}} = 84.0 \text{ at } 7.2 \text{ cycles/sec.}$$

similarly $K_7 = 75.2$ radians/sec at 6.1 cycles/sec.

$\qquad\qquad K_7 = 77.4$ radians/sec at 4.33 cycles/sec.

so $\qquad K_7 = 78.8$ radians/sec. (average)

With this high value of K_7 we can certainly assume that the $K_7 \Omega_7(p)$ response is constant over the entire range of

frequencies at which the ship rolls to appreciable angles (all below 0.5 cycles/second). The phase data for the amplifier is not plotted for two reasons: First, the phase lag is essentially zero well above the highest frequency of ship rolling. Second, the amplitude of valve motion due to the driving motor response dropping off at high frequencies is so small, that data are extremely difficult to get. It is estimated that at the highest frequencies used (7.2 cycles/sec.) the maximum phase lag is 10° ± 5°.

From these data alone it is apparent that the hydraulic blade control, from the frequency response viewpoint, is actually the strongest link in the chain of servo-components. Two things are not in its favor however. The first is that at high frequencies and large valve motions the oil pressure drops radically with a resultant decrease in performance. This is actually due, however, to an inadequate pump and should not rightly be charged against the hydraulic amplifier. Provision of a pump with greater capacity would eliminate this undesirable characteristic. There is a second effect in connection with the hydraulic amplifier which is not predicted by the theory outlined but which definitely effects the system operation. It has been observed that if the rack linking the control valve to the control motor is removed, leaving the valve uncoupled to anything but the hydraulic piston, the valve undergoes a relaxation type of oscillation, i.e., the valve falls slowly

due to its own weight and then some unbalanced pressure snaps
it back up again. With the valve rack in place and the system
together again, this oscillation is not observed due to the
heavy load of the gearing, motor and selsyn on the rack. That
this oscillation effects system performance is evidenced by the
closed loop response tests of the motor, with and without oil
pressure on, plotted in the previous section. The cause of the
effect is undoubtedly some unbalance in the hydraulic system.
This was not investigated since it represented but one of many
interesting side effects not directly related to the primary
purpose of the program.

It should be noted that the units of K_7 are in radians/sec.
From its average value of 78.8 it can be estimated that the
hydraulic amplifier response will be down 3 db at a frequency:

$$f = \frac{78.8}{6.28} = 12.55 \text{ cycles/sec.}$$

From the data obtained this seems to be a reasonable figure.

The hydraulic power amplifier frequency response charac-
teristic is worth a second look. It is the control element
which is providing the major source of control energy to the
system and yet it introduces negligible phase lag. It is
true that the particular hydraulic amplifier used with the
model system does introduce problems. On the other hand, it
should be clear that a main power element can be obtained
with similar frequency response characteristics but without
the associated difficulties encountered with this particular
device.

- 78 -

E. Concluding Remarks

We have determined what we set out to do; namely the parameters and the frequency response characteristics of the control elements. No attempt was made to improve on these elements, although in each case major areas of improvements were obvious. It was ascertained that the main power producing element, the hydraulic amplifier, introduced considerably less control lag than either the accelerometer or the servo motor. This state of affairs obviously represents poor design, since, in the ordinary case, one would expect to be able to design a system in which most of the lag was concentrated in the element doing the most work. In Chapter V of Part A, in the section on "Difficulty Factor", it is stated that in a ship stabilization system, due to the low frequencies involved, the burden on the controls should not be especially great. This is clearly borne out in these model control tests, since the main control power element introduces negligible phase lag in the system. With proper design, the other control elements would introduce even less.

Two important practical conclusions can be drawn from the experimental results of this chapter. First, it should be possible to obtain a control system for even full scale ships which will introduce small, if not negligible control lags. Second, hydraulic power amplifiers are strong contenders for the role of the main positioning element.

VI. STUDY OF OVERALL SYSTEM

The preceding two chapters have been concerned with a study of the regulated element and the regulating elements by themselves. It is now time to link the two together into a unified system and investigate overall system behavior. In connection with system behavior, we are primarily concerned with two things:

> A - Performance
>
> B - Stability

Both of these items will be covered in succeeding sections.

A. Performance

1. Steady State Theory

The stabilized rolling response of the system to an input wave slope ψ can be derived from equations 1 and 2 plus a known relation between the pump blade angle α and the roll acceleration $\ddot{\theta}$. We will treat the ideal zero time lag case where: $\lambda \ddot{\theta} = K_p \alpha$. λ is a gain parameter only and is not a function of frequency. This relation indicates that the pump blade angle varies directly as the control signal as though there were a perfect amplifier in between.

For this case we get:

$$\frac{\theta}{\psi} = \frac{\lambda_{ss}\left[\left(\frac{P}{\Omega_t}\right)^2 + \frac{1}{Q_t}\left(\frac{P}{\Omega_t}\right) + 1\right]}{\left(P^2+\frac{1}{Q_s}P+1\right)\left[\left(\frac{P}{\Omega_t}\right)^2+\frac{1}{Q_t}\left(\frac{P}{\Omega_t}\right)+1\right] - \lambda_t\left[\left(\frac{P}{\Omega_{st}}\right)^2+1\right]^2 +P^2 K\left[\left(\frac{P}{\Omega_{st}}\right)^2+1\right]} \quad (18)$$

where $K = \lambda/J_s$

The values of all parameters but λ have been previously determined. To obtain $\dot\lambda$ we must go ahead a bit to the experimental data and choose an experimental value for $|\theta/\psi|$ which fits well with surrounding data. Using $|\theta/\psi| = 0.162$ at $f = 0.2$ cycles/sec. we solve for λ and get:

$$\lambda = 35,400 \ \frac{\text{lb.ft.sec.}^2}{\text{radian}}$$

This value of λ is used to calculate the zero time lag approximation from the following equation:

$$\frac{\theta}{\psi} =$$

$$\frac{0.242\left[1-\left(\frac{f}{.203}\right)^2 + \frac{jf}{.0394}\right]}{\left[1-\left(\frac{f}{.222}\right)^2+j\frac{f}{5.55}\right]\left[1-\left(\frac{f}{.203}\right)^2+j\frac{f}{.0394}\right] - .23\left[1-\left(\frac{f}{.384}\right)^2\right]^2 -257f^2\left[1-\left(\frac{f}{.384}\right)^2\right]}$$

Results of this calculation are plotted as a solid line on Figure 37.

It is already known that there is lag in the control loop. Between the actual $\ddot{\theta}$ signal and $\propto$ there is the accelerometer, the servo-amplifier, the servo-motor and the hydraulic amplifier. Since the experiment which is being used to check the results used only $\ddot{\theta}$ control and no $\ddot{\theta}$ control, the servo-amplifier introduces no frequency characteristic. Also, we have seen that the hydraulic amplifier has a response which is essentially constant over the range of rolling frequencies. Therefore, we need only allow for corrections introduced by the transfer functions $K_4 G_4(p)$ and $K_6 G_6(p)$ of accelerometer and servomotor respectively.

It will be noted from equation (18) that the stabilization term is:

$$p^2 \, K \, [(\frac{p}{\Omega_{st}})^2 + 1]$$

Now in order to take into account the control lags, this term becomes:

$$p^2 \, K[K_4 G_4(p)][K_6 G_6(p)][(\frac{p}{\Omega_{st}})^2 + 1]$$

$$\text{where } K_4 G_4(p) = -5.5 \, \frac{f^2}{1-f^2 + j1.3f}$$

$$\text{and } \quad K_6 G_6(p) = \frac{0.266}{1-(\frac{f}{.286})^2 + j \, \frac{f}{0.0511}}$$

It is necessary to recompute λ by the same process as before. For this we get:

$$\lambda = 30850 \ \frac{\text{lb.ft.sec.}^2}{\text{radian}}$$

The modified data including actual control lags are also plotted as a solid line on Figure 37.

2. Steady State Experiments

The system was driven over a range of frequencies with $\ddot{\theta} = 20$, $\dddot{\theta} = 0$. The stabilized ratio θ/ψ was measured. These data are plotted as experimental points on Figure 37.

Following this test, at each frequency, the $\ddot{\theta}$ and $\dddot{\theta}$ controls were varied to minimize the rolling. The results of this experiment show that, over the entire range of driving frequencies, (0.1 to 0.31 cycles/sec) it was possible at each frequency to reduce the roll to a minimum of approximately:

$$\left| \theta/\psi \right| = 0.162$$

3. Transient Tests

A series of transient stabilization and de-stabilization tests were run on the system to get some idea of how quickly the tanks could take hold. Records of a representative group of these tests are shown on Figure 38 for different combinations of $\ddot{\theta}$ and $\dddot{\theta}$ control amplifier settings. For the de-stabilization tests, the phase of the control was simply reversed 180° by a switch and a slight motion imparted to the system. The rapid build up in system oscillation is shown on the upper two records of Figure 38. For the stabilization tests, the system was driven by hand to large amplitude

oscillations with the controls switched on suddenly at the time noted. The results are apparent. An unstabilized damping decrement record is included for comparison purposes. In addition, on Figure 38, an indication is given of the effect of Frahm action alone in damping the system's free oscillation.

4. Results

The results of these tests are very gratifying. First, to give a better perspective of steady state performance, Figure 39 shows in one place the rolling of the unstabilized ship (blocked duct), the rolling with Frahm action (pump blades open, pump motor off), the stabilized rolling for one fixed setting of the $\dot{\theta}$ and $\ddot{\theta}$ controls, and the stabilized rolling resulting from optimizing $\dot{\theta}$ and $\ddot{\theta}$ controls at each frequency. It is clear, that with stabilization, for this particular system, it is possible to reduce the undamped rolling to about 16% of the forcing wave slope. For this particular system with a $Q_s = 25$, the rolling at resonance is reduced to about 2.4% of its unstabilized value. It should be clear that the percentage reduction in rolling at resonance is a poor criterion for stabilization performance. Actually, this percentage is directly proportional to Q_s which may vary over a considerable range, even for a given ship, depending on sea, weather, and loading conditions. The ratio θ/ψ (stabilized) is relatively insensitive to changes in Q_s. This ratio therefore has greater significance in the specification of performance. Now, getting

back to Figure 37, it should first be noted that the amplitude
scale is much expanded over that shown on Figure 39 so that
what looks like a high peak of roll amplitude is still actually
quite small. Figure 37 clearly indicates that the control lags
are relatively unimportant up to 0.2 cycles/second but that above
that frequency they adversely effect stabilization performance.
Considering the many factors which might tend to cause experi-
ment to deviate from theory, the correlation is quite close.
This is particularly true when it is remembered that the theo-
retical transfer responses (only experimental parameters used)
are being used to determine control lags, not actual transfer
responses determined by experiment. It is clear from Figure
37 that it is possible, with the phase adjustments on the
control amplifier, to compensate, at each frequency, for the
control lags which are deleterious to system performance.
Adjustment of the controls at each frequency, enabled us to
provide sufficient phase lead to compensate for these delet-
erious lags so that, as expected, the experimental points
followed the zero phase lag theoretical curve more closely.

Not much need be said of the transient rolling records
of Figure 39. It is apparent that the setting of the $\ddot{\theta}$ and
$\ddot{\theta}$ controls has an important effect on system performance. It
should be noted that the goal of an efficient stabilization
system is not necessarily dead beat damping of a ship which
has been forced to roll at its natural frequency. Although
this could probably be obtained, it would be at the price of

greatly excessive weight of stabilizing fluid. Of greater int-
erest may be a system which will reduce the usual range of
rolling at sea to a minimum. This can be done with much less
weight of stabilizing fluid, and while it may be incapable of
handling all possible wave conditions, it will represent a
much more efficiently used system. This question has been dis-
cussed somewhat in Chapter V of Part A and will be discussed
further in Part D.

B. Stability

Referring to Figure 8 which shows a transfer function
block diagram of the system, it is possible to calculate the
open loop response of the system and determine theoretically
the regions of stability and instability as a function of the
different control gain settings. This open loop response is
obtained by multiplying the following transfer ratios as
indicated:

$$\frac{e_1}{\theta} \cdot \frac{e_2}{e_1} \cdot \frac{x_1}{e_2} \cdot \frac{x_3}{x_1} \cdot \frac{\theta_{out}}{x_3} = \frac{\theta_{out}}{\theta}$$

The calculations to determine $\frac{\theta_{out}}{\theta}$ for important combina-
tions of the useful ranges of all gain controls have been
made. Since these represent a huge mass of data, no attempt
will be made to reproduce the data in this report nor will all
of the resulting performance curves be shown. Instead, three
representative Nyquist diagram plots showing the effect of

- 86 -

variation of the different control gain parameters are included.

Figure 40 shows the effect of varying the valve (feed back selsyn) gain control for fixed values of other gain parameters. It can be seen that with the valve control set at 2 the system will be unstable since the -1.0 point is encircled. At valve control settings of 6 and 10 the system is stable but would be highly oscillatory.

Figure 41 shows the effect of switching in the extra amplifier stage in the servo-amplifier for fixed setting of all other controls. The effect here is mostly one of increased gain but the phasing is also changed somewhat.

Figure 42 shows the effect of different combinations of $\ddot{\theta}$ and $\dddot{\theta}$ controls. It is apparent that addition of $\ddot{\theta}$ control makes the system more stable by reducing the phase lag in the closed control loop.

Due to shortage of time, it was not possible to run open loop tests of the system to obtain experimental points on some of the theoretical Nyquist diagram plots. It was possible to observe qualitatively, from closed loop performance, that for certain settings of the $\tilde{\theta}$ and $\bar{\theta}$ controls, reducing the valve control to lower numerical values reduced the system's stability and could introduce self oscillation. Likewise, increasing the $\ddot{\theta}$ control could restore the system from an unstable oscillation to stable control.

The importance of such Nyquist diagrams lies in connection with the design of future systems. Diagrams such as these, or Bode diagrams, or any phase/amplitude versus frequency plot which indicates the behavior of the system and its components will enable a rational approach to design of a stable system.

C. Concluding Remarks

In this chapter we have considered the problems of performance and stability. It was shown that the performance indicated rather remarkable agreement between experiment and linear theory.

The word remarkable is appropriate when one considers the number of parameters whose values had to be "approximated". This indicates that the parameter values which are non-constant, such as B_s, B_t, K_p, are not "critical". This is borne out further in Part C. Those parameters, such as ω_{st}, ω_s, ω_t, etc., which do have appreciable effect on performance when changed, fortunately all tend to remain fairly constant in actual practice.

Perhaps as remarkable is the overall roll reduction vs. frequency performance of the system. It is certainly clear that in almost every aspect the system could be considerably improved. From the results of this chapter it is evident that control lags are the worst enemies of the stabilization process. These should be avoided by all means.

Stability considerations are a must in any servo problem. This is no exception. It was stability which ruined the pre-war efforts of Minorsky at the very point of fruition. In 1940, the tools to study this problem were either not available or unknown. Today they are available and are known. No servo system can be used if it is unstable. Therefore, stability is our first criterion. Stability is necessary in any servo, alone it is not sufficient. Stability and high performance together are both necessary and sufficient.

VII. SUMMARY AND CONCLUSIONS

The primary purpose of this study was to check the validity
of a linearized theory for the behavior of a ship system stabil-
ized against rolling by activated tanks of the Minorsky type,
where activation is effected by a variable-pitch propellor
pump. To check this theory, there was available a 5-ton model
system which, neglecting coupling to other degrees of freedom,
was essentially equivalent to a ship rolling in waves.

It was necessary to develop special instrumentation to
conduct the required experiments. This was done, and the final
correlation obtained between theory and experiment have made
the time and effort expended on instrumentation problems well
worth while.

The parameters of the ship-tank coupled system were care-
fully determined. The ship parameters, with the exception of
B_s, are constants as expected. B_s shows some dependence on
roll angle. However, this variation of B_s is negligible since
B_s is small and is a relatively unimportant parameter in the
stabilization process. The tank water static parameter K_t is
straight forward as is the dynamic parameter, J_t. Both depend
on geometry and mass alone. As expected, B_t is not a constant
coefficient. The contribution to B_t by skin friction in the
tanks was shown to be negligible compared to the contribution
of the pump dynamic head loss coefficient. Thus, B_t varies
rapidly with blade angle. From this, one might be led to

expect significantly non-linear transfer response action. This, fortunately, does not turn out to be the case. Referring to equations 7 and 7', it is seen that, since Q_t is small, we may expect ϕ/α to be proportional to the ratio of $\frac{K_p}{B_t}$ except at very low or very high frequencies. Both quantities vary with blade angle and in the same direction. That is, as K_p increases so does B_t and vice versa. Thus, variations in K_p and B_t tend to cancel each other.

Experimental transfer responses of individual isolated elements of the ship-tank system checked quite well with the responses calculated from the linear theory. In particular, the pump blade angle to tank water angle response was considerably closer to the theoretical response than was expected.

Tests were made of the system both without and with controls. The close agreement obtained between experiment and linear theory was entirely welcome. There are probably several reasons for this. One good reason is that the tank water system is such a low Q (highly damped) system that even relatively large variation of B_t and K_p still results in a relatively flat amplitude/frequency characteristic. Such a low Q tank system means inherently tighter coupling between tank water and ship. Going ahead a bit to Part C, the effect of variation of Q_t is illustrated there. Quite low values of Q_t are shown to be optimum for activated tank damping. This is an important design criterion in any future installation of

a system of this type. Another reason for the overall linearity observed is that a closed loop servo system of this type is essentially a feed back amplifier with 100% negative feed back. In any negative feed back amplifier, the effect of variation of system parameters is greatly reduced.

The performance of the model system is adequately described by the linear theory developed in Part A. Performance can now be predicted; something which could not be done before. There seems to be no reason why the same theory could not be applied, with perhaps some modifications, to full scale ships. It will of course be necessary to review the assumptions made in Part A, such as coupling to other degrees of freedom, etc.

It must be clear that the system used for these studies represents a fixed set of parameters and parameter ratios. The next step is to determine what combinations of parameters produces optimum stabilization. This is a process of synthesis, one which is carried out in Part C of this report.

Getting back to the model system, it would be well to look at it briefly as an actual system. It is gratifying, knowing how many things about the system can be improved, how effective a job of stabilization it actually does.

Design of the accelerometer leaves much to be desired. Phase lag can be considerably reduced by raising the natural frequency. Damping should be properly adjusted and kept constant by using silicone oils, for example, and sensitivity

can certainly be increased. Above all, the present instrument
has a relatively crude voltage pick-off which has been a source
of much trouble. Accelerometers can easily be built which are
entirely adequate for ship-stabilization control. They need
not be a weak link in the control system.

Further, any modern servo-system would use equalizing
networks rather than differentiators in the amplifier; such
networks being designed after all other elements of the system
have been chosen so that proper compensation can be obtained
over a wide range of frequencies. The amplifier will be the
cheapest, smallest, lightest and most flexible element in the
entire closed loop. It should be tailored to the system, not
the system to it. Again, there is no reason why the amplifier
should be a weak link in the system.

The present servo-motor tends to saturate, representing
the weakest link in the existing control system. Certainly,
this undesirable condition can be avoided. With proper design,
there is no reason why this element of the system need intro-
duce difficulty.

Significantly, the hydraulic amplifier is the strongest
link in the model control system. This was much damned in
pre-war tests; but, by all available evidence, this damning was
based on insufficient data. Certainly hydraulic power amplifiers
should not be arbitrarily discarded from consideration. It can
be concluded that if the element with the greatest inertia,

the one doing the most work, can be designed to produce acceptable control lags, it should be easily possible to get even better performance from the lower power level devices.

Finally, the model system used only accelerometer control, with acceleration and rate of change of acceleration as control signals. Such things as integrated position control, position control and velocity control could all be added to the system. Combinations of some of these controls are considered in Part C. There is also the possibility of incorporating feed-ahead control to get still further improvement in roll reduction. This also is discussed in Part C.

All in all, it is evident that activated tank stabilization, even in the relatively crude form that exists on the model system studied can be very effective. It is true, that even before the war it was effective in model tests of the U.S.S. Hamilton but couldn't even be tried in full scale ship tests due to instability in the system. The possibility of such difficulties arising can be understood by considerations such as covered in this report. For instance, in the full scale installation, additional amplification was added to drive two pump control motors. The motors were different. The hydraulic amplifier was different and the accelerometer was the same. It is almost certain that the control lags in the full scale installation loop were much different than those in the model loop. This possibility was not considered so it is not

surprising that difficulty was encountered with loop stability. The unfortunate thing was that insufficient time was available to really pin down the source of trouble. Had this been done, it is almost certain that an effective full scale system would have existed before World War II. The dynamic design of the tank-pump system on the U.S.S. Hamilton would have resulted in acceptable performance with good controls.

The applicability of the linear theory has been demonstrated. The effectiveness of a "first try" system is encouraging. The next logical step is to understand the effect of variation of system parameters. This is done in Part C. In Part D, the information outlined in Parts A, B, C is tied together and used to attack a hypothetical problem of a full scale ship installation. With the information contained in all parts of this report, the way is clear for a successful program of stabilization of actual full scale ships by means of activated tanks.

CALCULATION OF TANK FORM FACTORS FOR THE MODEL

The two most important form factors of the tank system are:

$$S' = \int_0^S \left(\frac{A_0}{A_s}\right) ds$$

and

$$S'' = \int_0^S \left(\frac{D_s}{L}\right) ds$$

The first, S', characterizes the natural frequency of the U-tube tanks and the second, S'', characterizes the frequency of secondary resonance. Thus,

$$\omega_t = \text{natural frequency of tanks} = \sqrt{\frac{2g}{S'}}$$

$$\omega_{st} = \text{frequency of secondary resonance} = \sqrt{\frac{2g}{S''}}$$

As defined in Part A, these form factors depend on the path traced out by the centerline of the tank system taken relative to the "virtual" center of rotation of the ship. In the model this center of rotation is fixed and known, while in an actual ship its determination is a more difficult matter. This determination will be discussed in Part D.

Being given the center of rotation and the placement and shape of the tanks, it is a relatively simple matter to proceed with the calculation of S' and S''. Figure A shows a cross-

section of the tanks, the trajectory of their centerline, and the center of rotation for the model. As is indicated, the trajectory is divided into eight parts. The factors are then integrated numerically using an eight-point Simpson's Rule.

A. **Calculation of S'**

From Simpson's Rule,

$$S' = \frac{s}{12} \left[\frac{y_0}{2} + 2y_1 + y_2 + 2y_3 + y_4 + 2y_5 + y_6 + 2y_7 + \frac{y_8}{2} \right]$$

where
$$y_0 = \frac{A_0}{A_0}$$

$$y_1 = \frac{A_0}{A_1} \qquad \text{etc.}$$

Now from Figure A, we may determine a table of area ratios:

$$y_0 = \frac{A_0}{A_0} = \frac{1.92 \text{ sq. ft.}}{1.92 \text{ sq. ft.}} = 1.00 = y_8$$

$$y_1 = \frac{A_0}{A_1} = \frac{1.92}{1.47} \qquad = 1.30$$

$$y_2 = \frac{A_0}{A_2} = \frac{1.92}{.560} \qquad = 3.43$$

$$y_3 = \frac{A_0}{A_3} = \frac{1.92}{.331} \qquad = 5.80$$

$$y_4 = \frac{A_0}{A_4} = \frac{1.92}{.331} \qquad = 5.80$$

$$y_5 = \frac{A_0}{A_5} = \frac{1.92}{.331} \qquad = 5.80$$

$$y_6 = \frac{A_o}{A_6} = \frac{1.92}{.384} \qquad = 5.00$$

$$y_7 = \frac{A_o}{A_7} = \frac{1.92}{1.47} \qquad = 1.30$$

Using these values,

$$S' = \frac{S}{12} \ (43.63)$$

And as $\quad$ S $\ = 10$ feet

$$S' = \frac{10}{12} \ (43.63) = \underline{36.4 \ ft.}$$

B. Calculation of S"

From Simpson's Rule,

$$S'' = \frac{S}{12} \ [\frac{X_o}{2} + 2X_1 + X_2 + 2X_3 + X_4 + 2X_5 + X_6 + 2X_7 + \frac{X_8}{2} \ ]$$

Where $\qquad X_o = \frac{D_o}{L}$

$$X_1 = \frac{D_1}{L} \qquad \text{etc.}$$

Now from Figure A, we may determine a table of these length ratios:

$$X_o = \frac{D_o}{L} = \frac{2.29 \ ft.}{2.29 \ ft.} \ = 1.00 = X_8$$

$$X_1 = \frac{D_1}{L} = \frac{2.29}{2.29} \qquad = 1.00$$

$$X_2 = \frac{D_2}{L} = \frac{2.33}{2.29} \qquad = 1.02$$

- 98 -

$$X_3 = \frac{D_3}{L} = \frac{2.84}{2.29} \qquad = 1.24$$

$$X_4 = \frac{D_4}{L} = \frac{2.84}{2.29} \qquad = 1.24$$

$$X_5 = \frac{D_5}{L} = \frac{2.84}{2.29} \qquad = 1.24$$

$$X_6 = \frac{D_6}{L} = \frac{2.65}{2.29} \qquad = 1.16$$

$$X_7 = \frac{D_7}{L} = \frac{2.29}{2.29} \qquad = 1.00$$

Using these values

$$S'' = \frac{S}{12} \quad (13.38)$$

$$= \frac{10}{12} \quad (13.38) = \underline{11.14 \text{ ft.}}$$

CROSS-SECTION OF MODEL TRACKS

Rectangular Cross-section

Circular Cross-section

Center of Rotation

Point 3
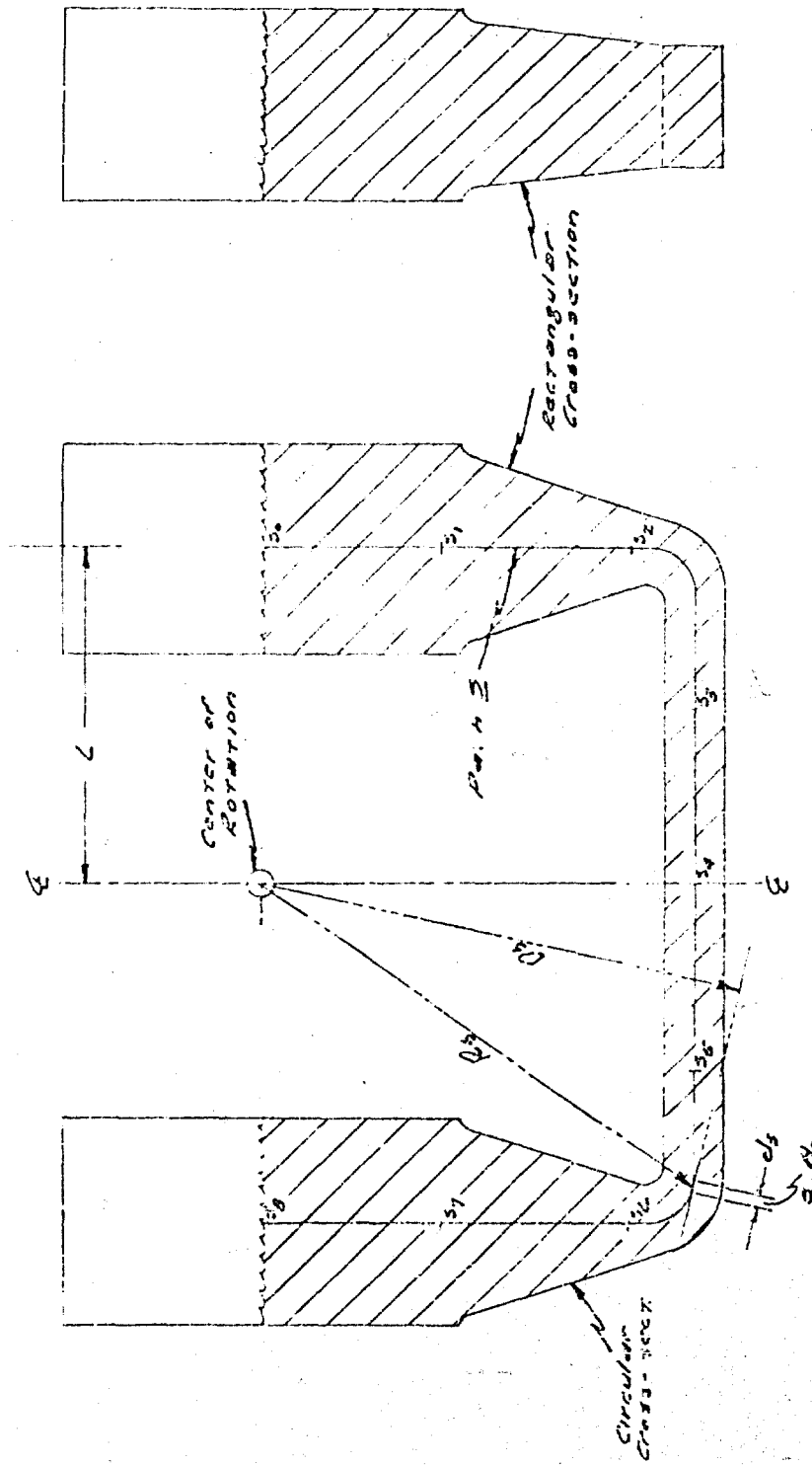
S — Distance along trajectory.

r_3 — Cross-section at S.

ℓ_3 — Distance from center of rotation to S.

q_3 — Perpendicular distance from center of rotation to tangent at S.

Scale in feet

FIG. 12

BIBLIOGRAPHY

(1) Minorsky, N. "Report of Investigation of Stabilization
of Ships by Means of Activated Tanks" (5 parts),
Materials Laboratory, New York Naval Shipyard Test
Series #4040-1 to 5 dated 17 March 1939. (Not pub-
lished)

(2) --------. "Experiments with Activated Tanks", _Trans-
actions of ASME_, October 1947.

(3) --------. "Self-Excited Oscillations in Systems
Possessing Retarded Actions", Paper.

(4) --------. "On Non-Linear Phenomenon of Self-Rolling",
Proc. Nat. Academy of Sciences, Vol. 31, No. 11,
November 1945.

(5) --------. "On Mechanical Self-Excited Oscillations",
Proc. of Nat. Academy of Sciences, Vol. 30, No. 10,
October 1944.

(6) --------. "Self-Excited Mechanical Oscillations", _Journal
of Applied Physics_, Vol. 19, No. 4, April 1948.

(7) Morris, A. J. "The Anti-Roll Stabilization of Ships by
Means of Activated Tanks", Engineers Thesis at Stan-
ford University, June 1950.

(8) Miller, S. E. "Sensitive DC Amplifier with AC Operation",
Electronics, November 1941.

(9) Morris, A. J. and Chadwick, J. H. "An Electromagnetic
Induction Method of Measuring Oscillating Fluid Flow",
Paper presented at A.I.E.E. Pacific General Meeting
in Pasadena, California, in June 1950.

(10) Ramo and Whinnery. _Fields and Waves in Modern Radio._
New York: John Wiley.

(11) Ahrendt and Taplin. _Automatic Regulation._ Ahrendt and
Taplin publ.

1. Model Pendulum
2. Main Shaft
3. Driving Springs
4. Stevenson Mechanism Component
5. Stevenson Mechanism Component
6. Stevenson Mechanism Component
7. Driving Motor
8. Driving Motor
9. Driving Motor
10. Tank
11. Tank
12. Transfer Duct
13. Pump
14. Control Valve
15. Servo Motor
16. Accelerometer
17. Pump Drive Motor
18. Bilge Keel Damping Paddle
19. Bilge Keel Damping Oil Tank
20. Accumulator Tank
21. Oil Pump Motor
22. Wave Slope Arm

SCHEMATIC DIAGRAM
5 TON MODEL STABILIZER

Date MAY 23, 1950 Dr.by I.A.Fron FIG. 1.

SLIDE 1 - EVACUATOR MILL STABILIZER AREA   FIGURE 8

MODEL STABILIZER - TOP VIEW   FIGURE 3
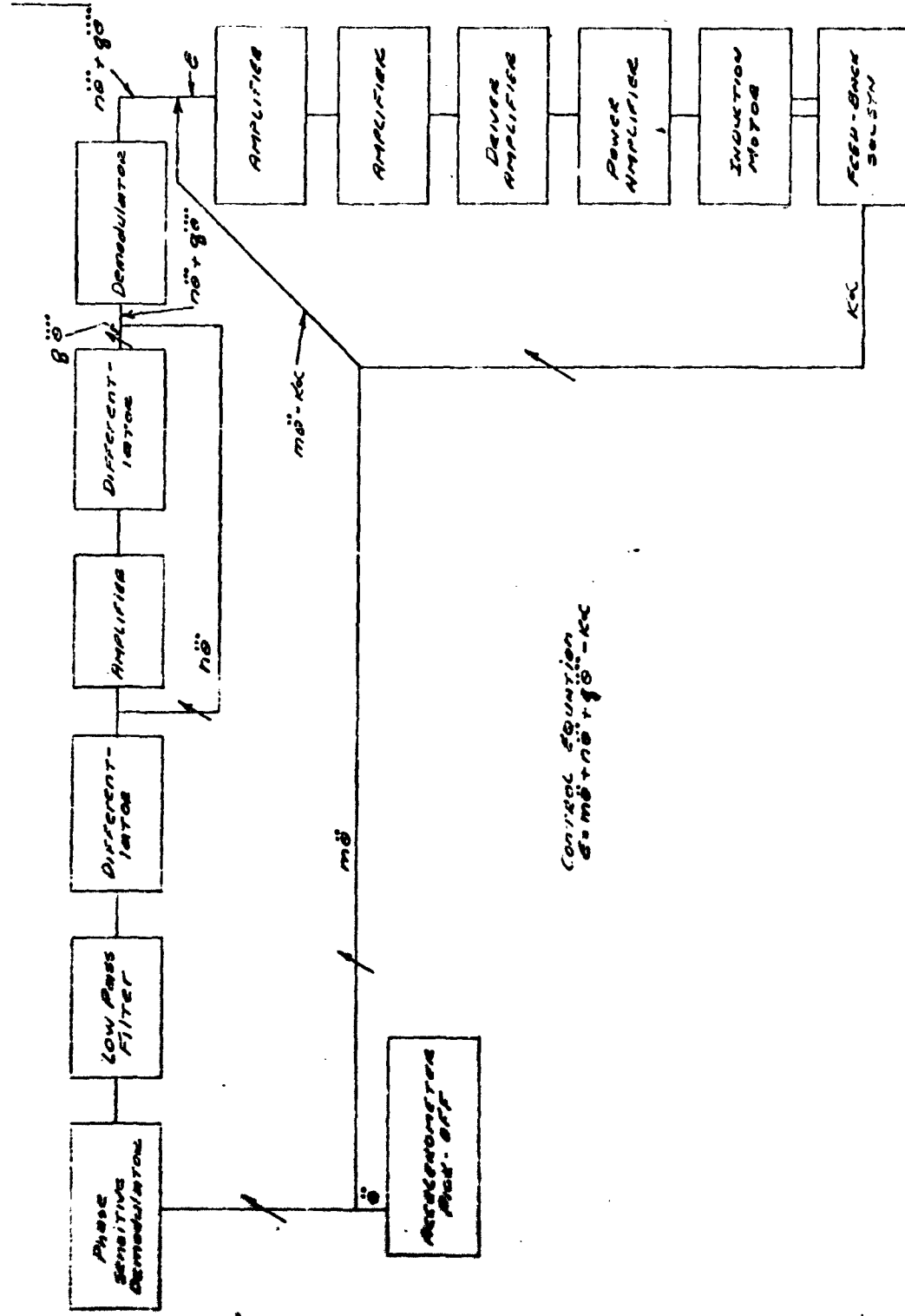
BLOCK DIAGRAM OF
SERVO - AMPLIFIER

CONTROL EQUATION
$\varepsilon = m\ddot{\theta} + n\dot{\theta} + g\dot{\theta} - kc$

Fig 4

Note: May 24, 1960 Grey Barton

HYDRAULIC PISTON
MECHANISM

Fig. 5

DRAIN

PRESSURE
SIDE

DRAIN

HYDRAULIC
CYLINDER

ACCUMULATOR
TANK

BILGE KEEL
DAMPING TANK

GEAR TYPE
PUMP

PRESSURE RELIEF
VALVE
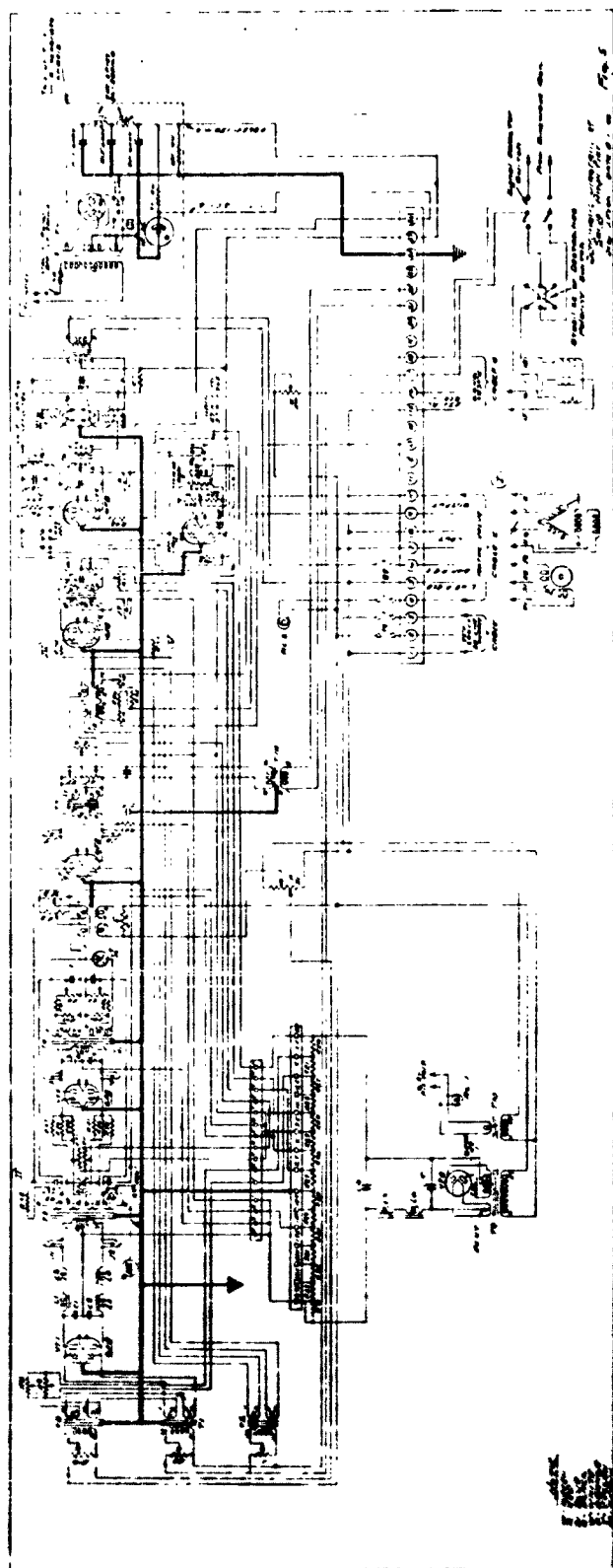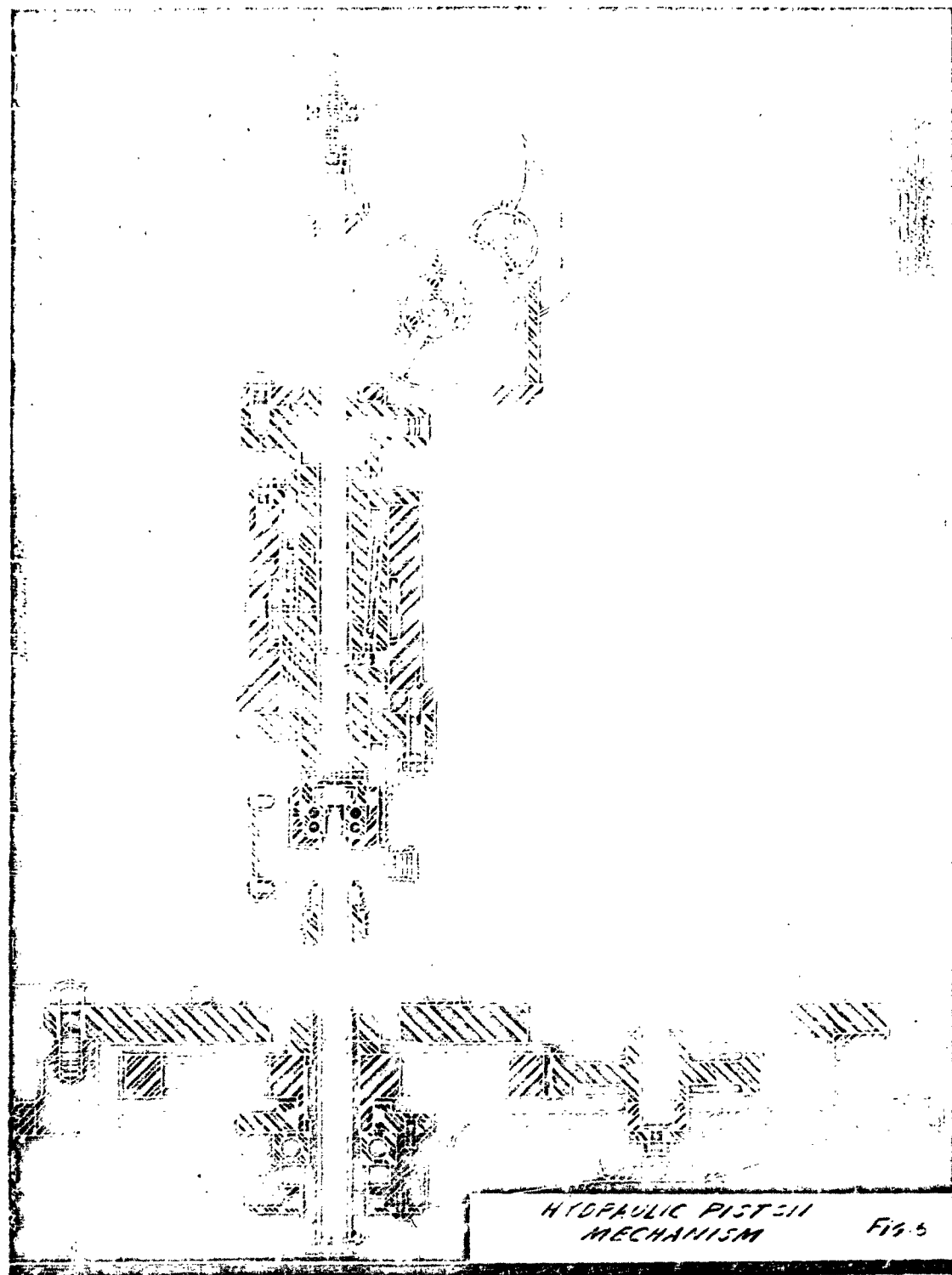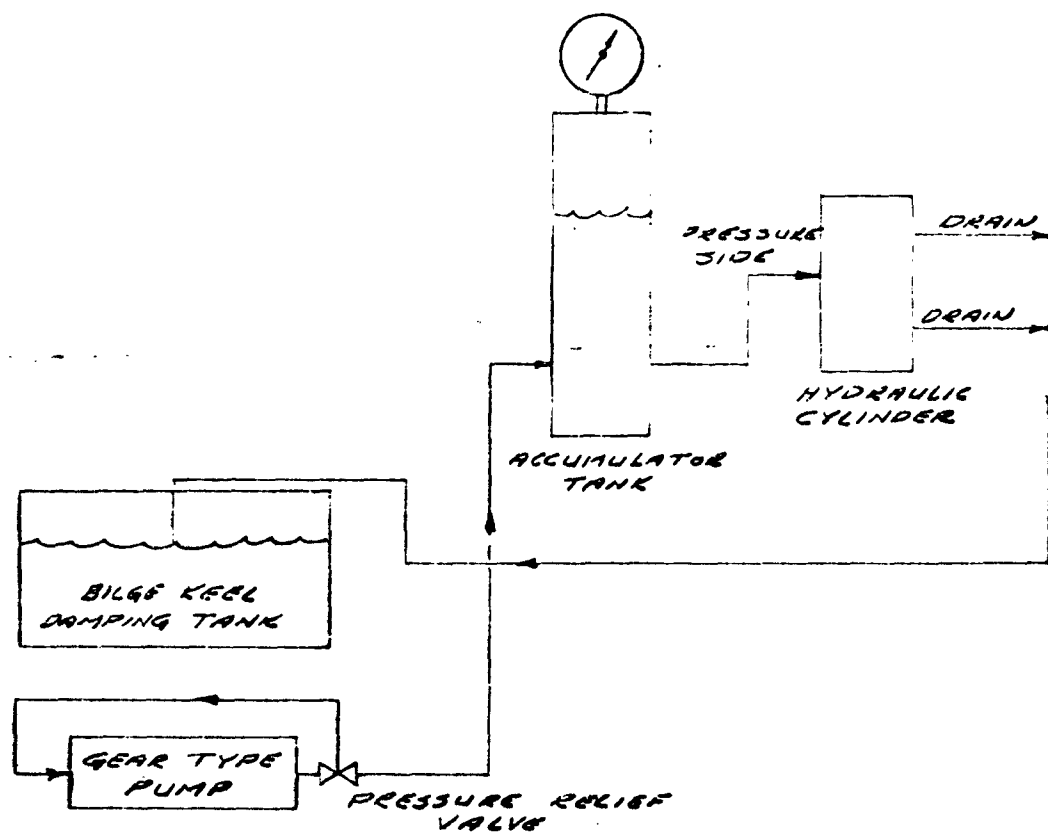
LINE DIAGRAM OF
CONTROL OIL SYSTEM

FIG. 7

DATE MAY 20, 1950   Dr. by J.A. FTON

TRANSFER FUNCTION BLOCK DIAGRAM OF SERVO-CONTROL LOOP

Fig 8

REGULATED POWER SUPPLY
+300v - 440 ma

SINE WAVE GENERATOR
DEC. 28 1949

Fig. 11

115V D.C.

55V 800~ A.C.
HALF TO FIRE

MODULATED 200~
SINE WAVE OUTPUT

FIELD SERIES

MOTOR

FIELD SHUNT

HIGH SPEED GROUND

MOTOR DATA
115V DC - COMPOUND WOUND - 1.4 AMPS - 1140 RPM.
SPEED REDUCER DATA
1140/115 RPM - 1/10 INPUT HP - 477 LBS TORQUE - GEAR RATIO 120/1380/1 -
SELSYN DATA
115V/800 900 CYCLE SELSYN MOTORS
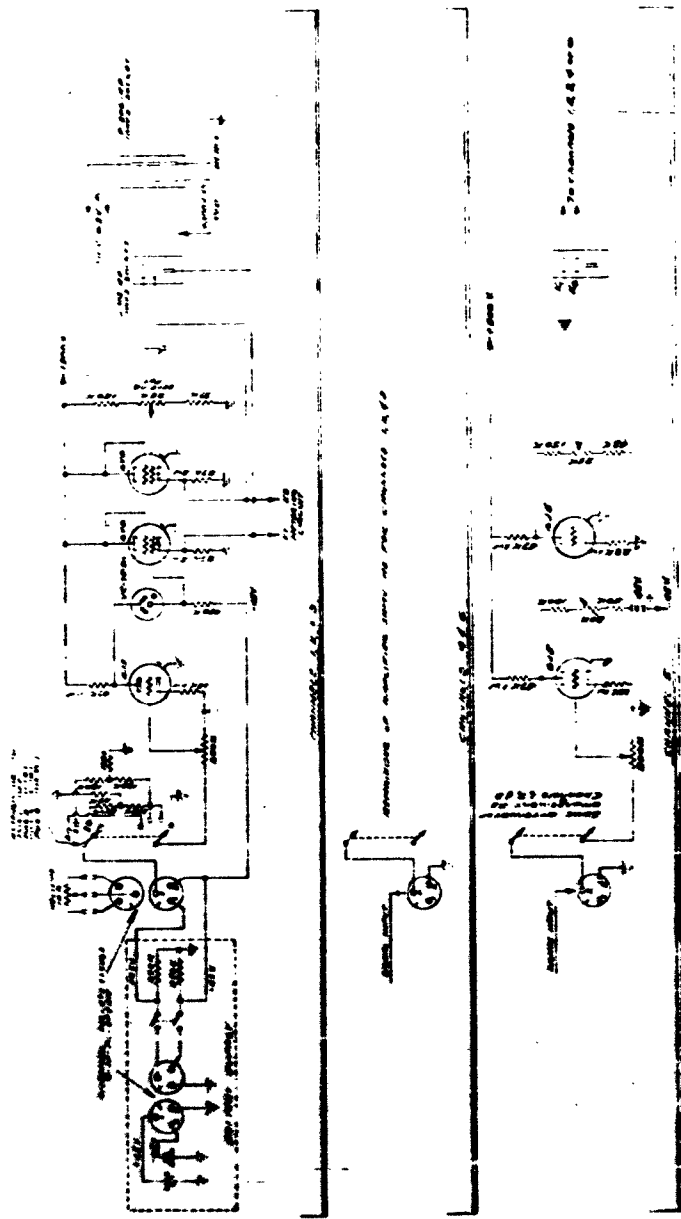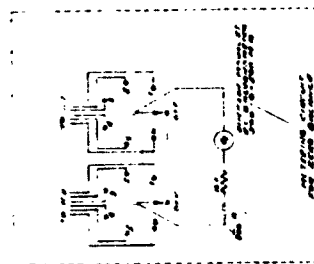
TWO STAGE DEMODULATOR
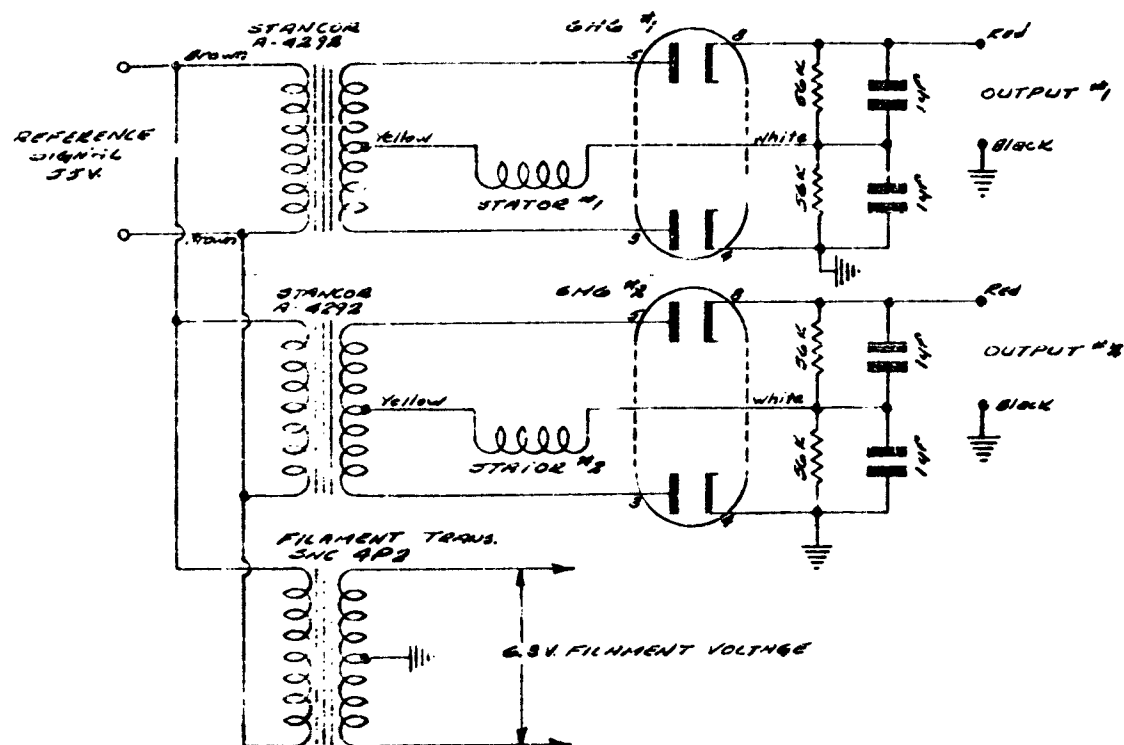
TIME CONSTANT = $56 \times 10^3 \times 1 \times 10^{-6}$ = .056 SECS

Signal Test Panel
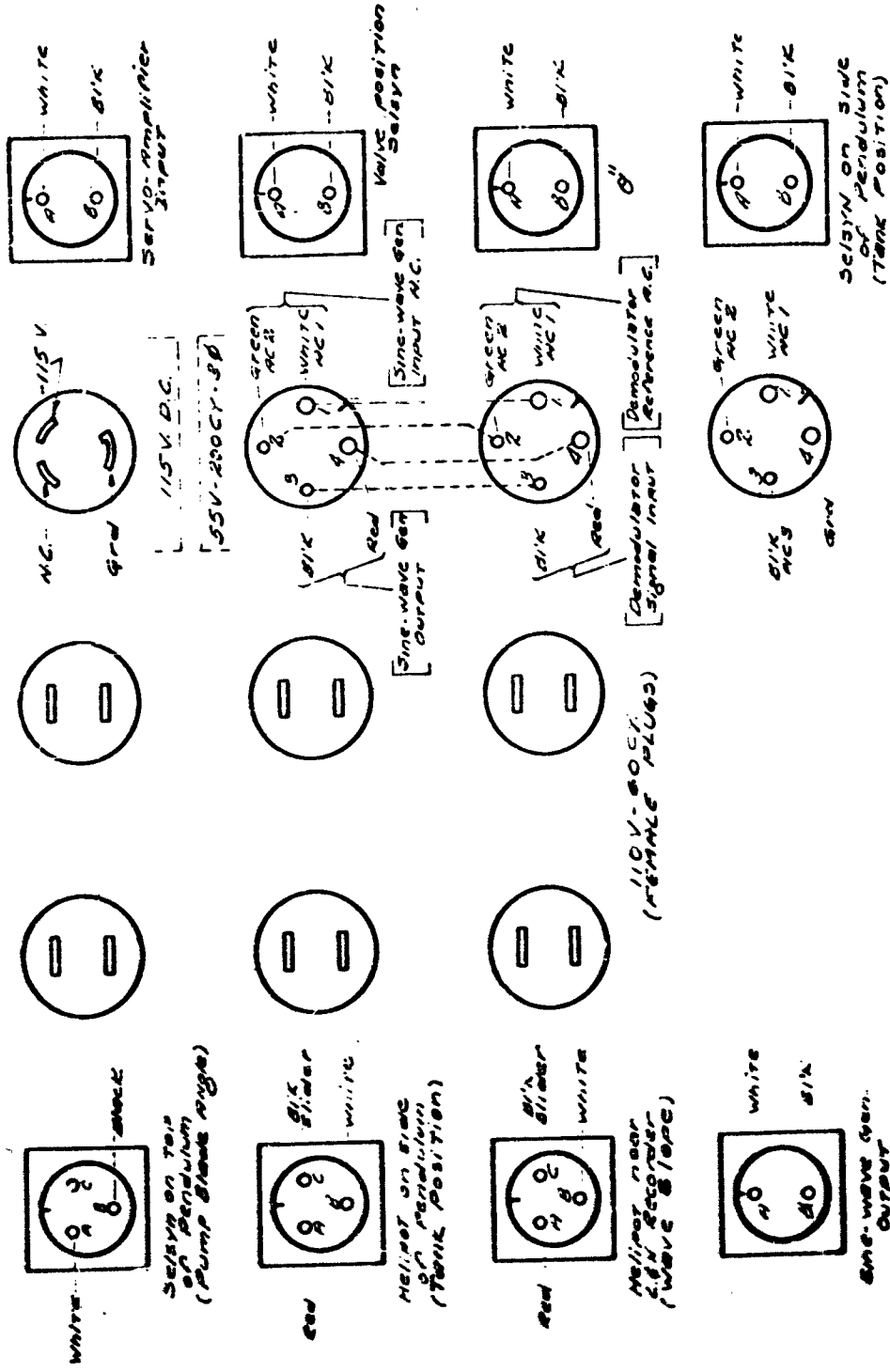
Fig. 13

Notes: All colors represent cable covers,
not panel wiring

SCHEMATIC DIAGRAM OF
ASSOCIATED FLOWMETER INSTRUMENTATION

Fig. 15

Date: May 5, 1960   Dr by J.a. From
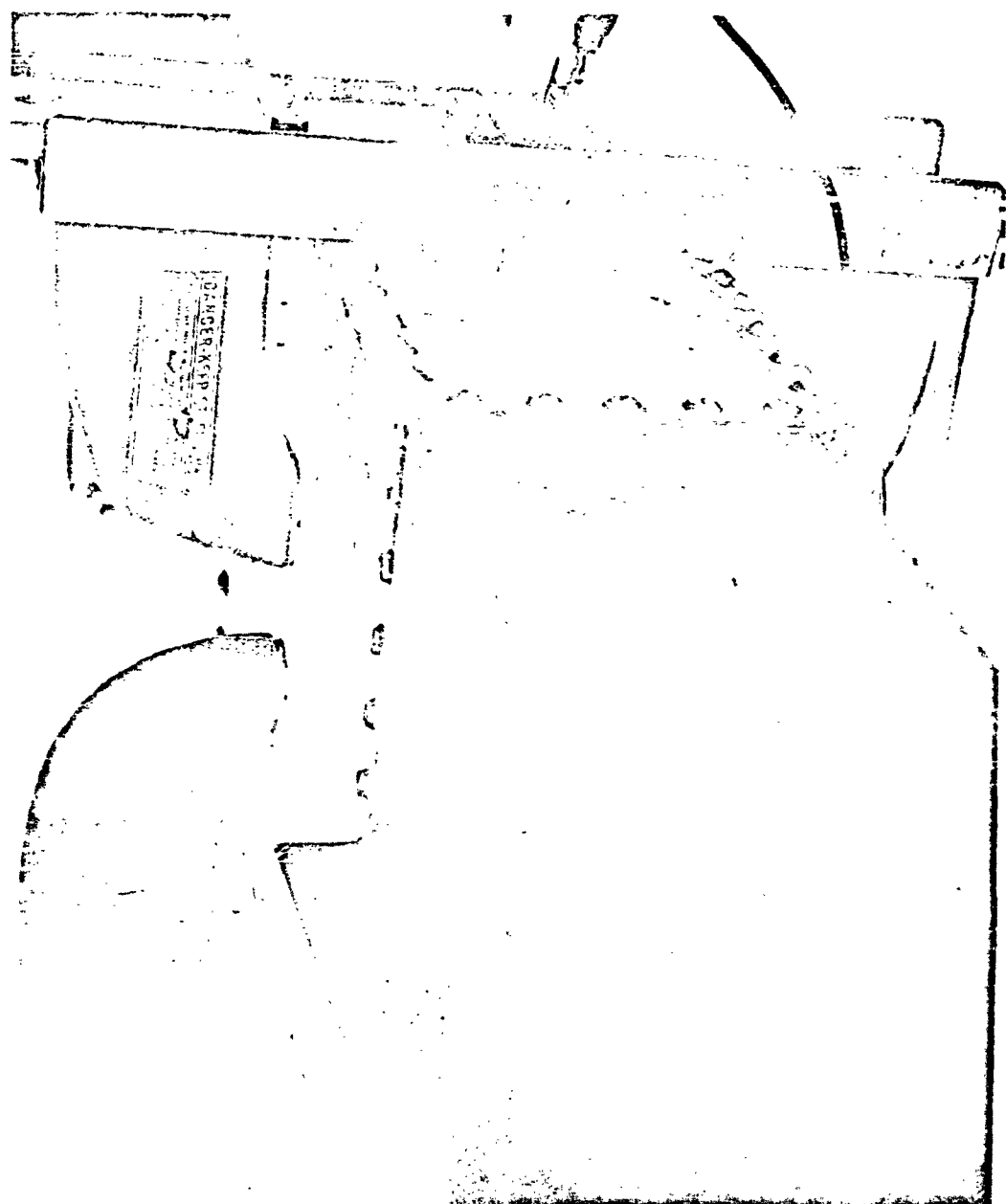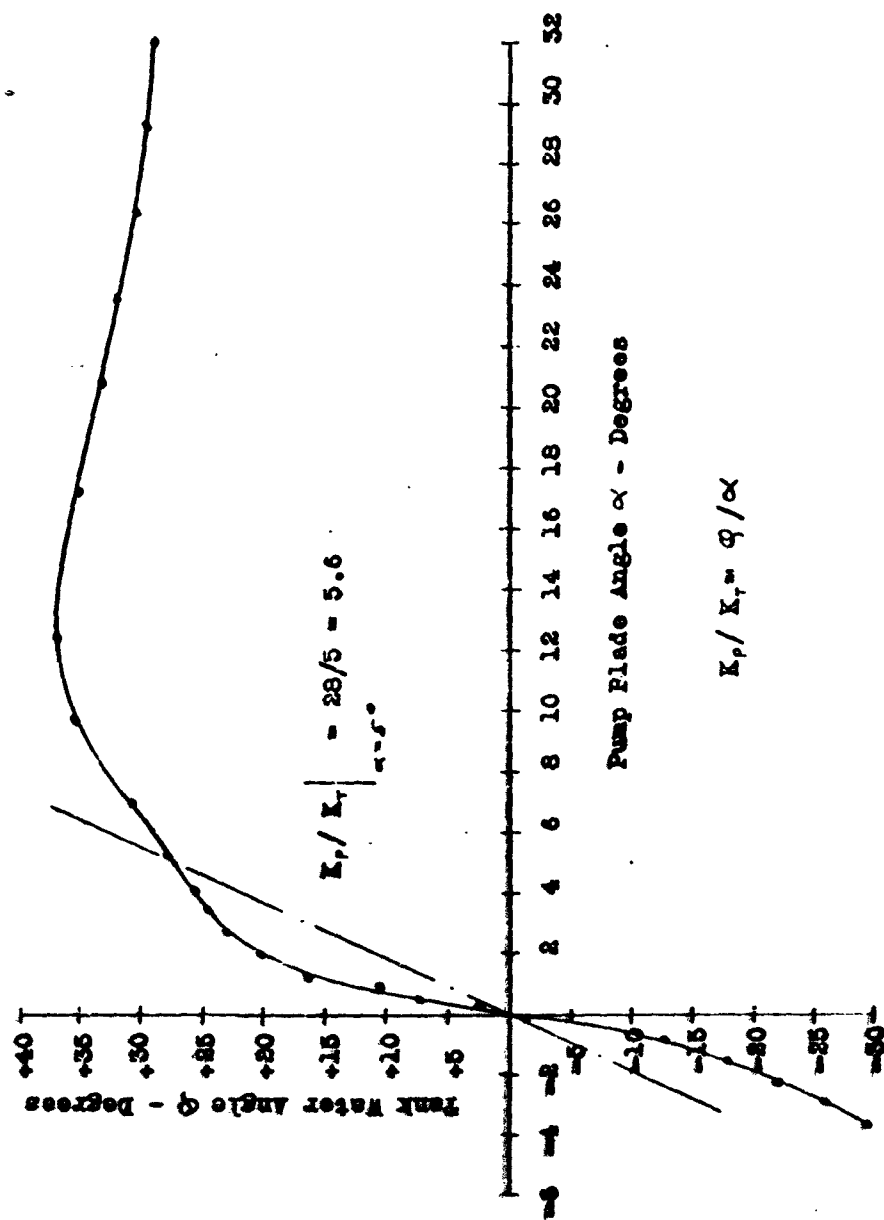
Figure 16   Static Pump Charateristic
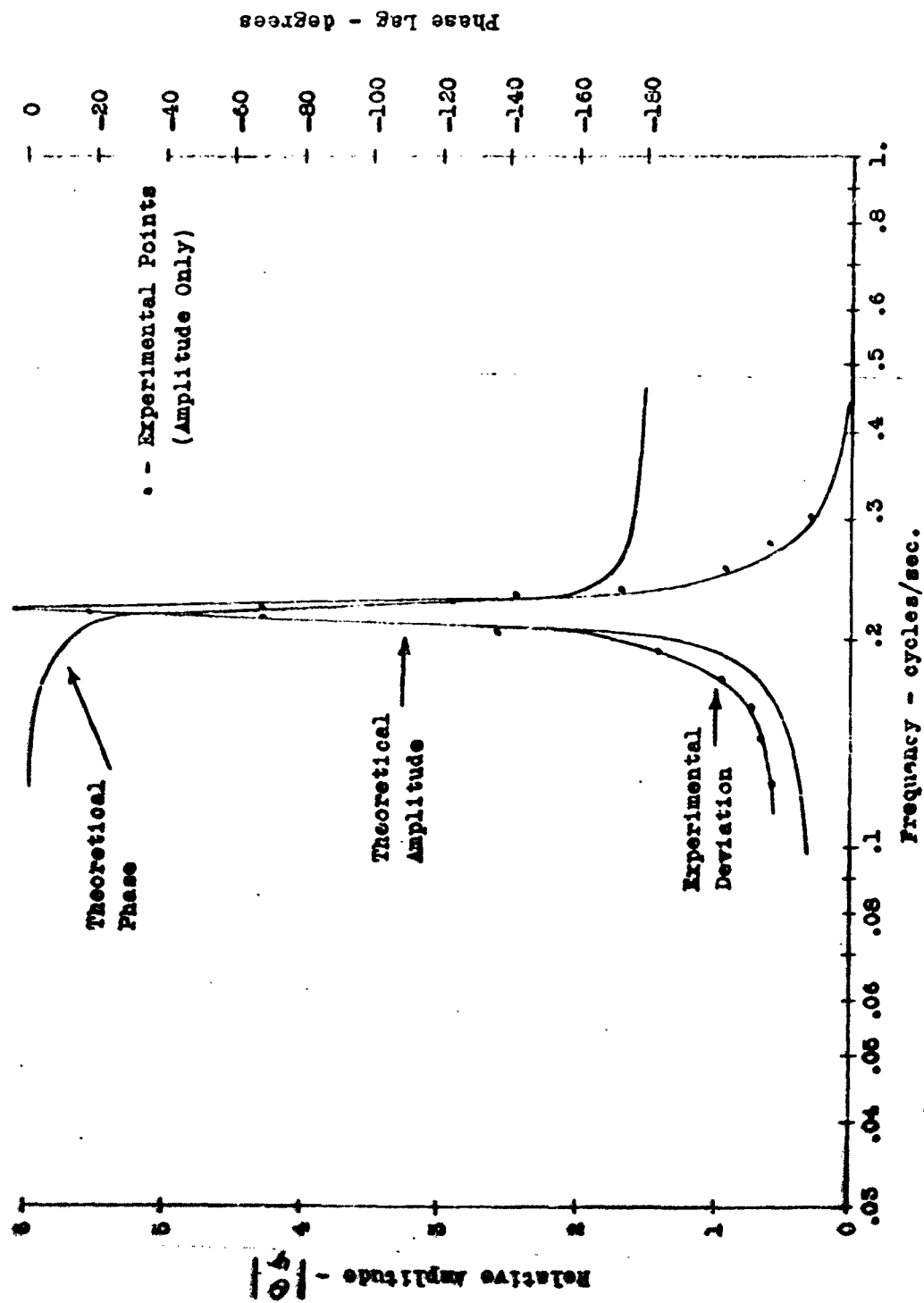
Figure 17 $\dfrac{\theta}{\phi}$ – ship response – single degree of freedom (duct blocked).

CALIBRATION .522°/mm DIVISION NAT PERIOD 8.55" SEC.
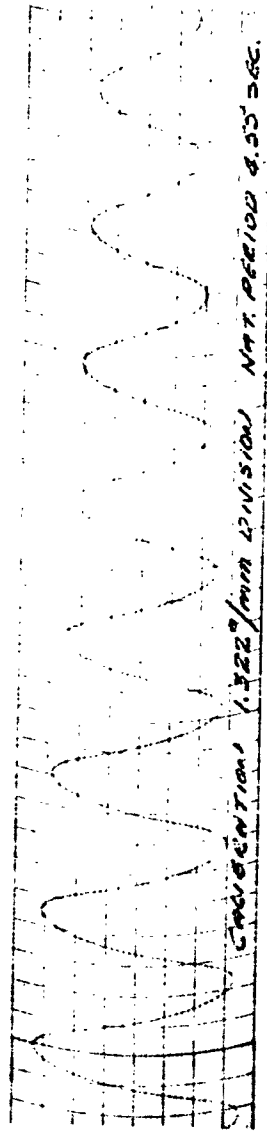
TANK ROLL DAMPING WITH DUCT BLOCKED

CALIBRATION .726°/mm DIVISION
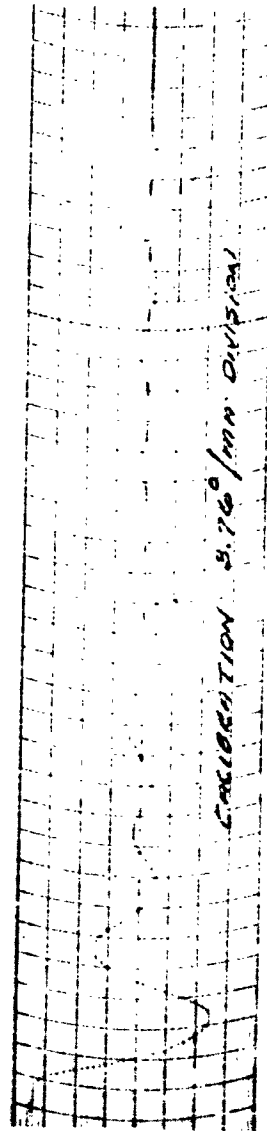
TANK ROLL DAMPING WITH PUMP BLADE
WIDE OPEN — DUCT UNBLOCKED
(NOTE LARGE FRANK ACTION)

Fig. 18

Relative Phase of $\frac{\dot{\theta}}{\dot{y}}$ Lead ← | degrees | Lag →

+100 +80 +60 +40 +20 0 -20 -40 -60 -80 -100

Frequency - cycles/sec.

• - Relative Amplitude
× - Relative Phase
$\gamma = 0.194$

Theoretical Phase

Theoretical Amplitude

Relative Amplitude of $\frac{\dot{\theta}}{\dot{y}}$
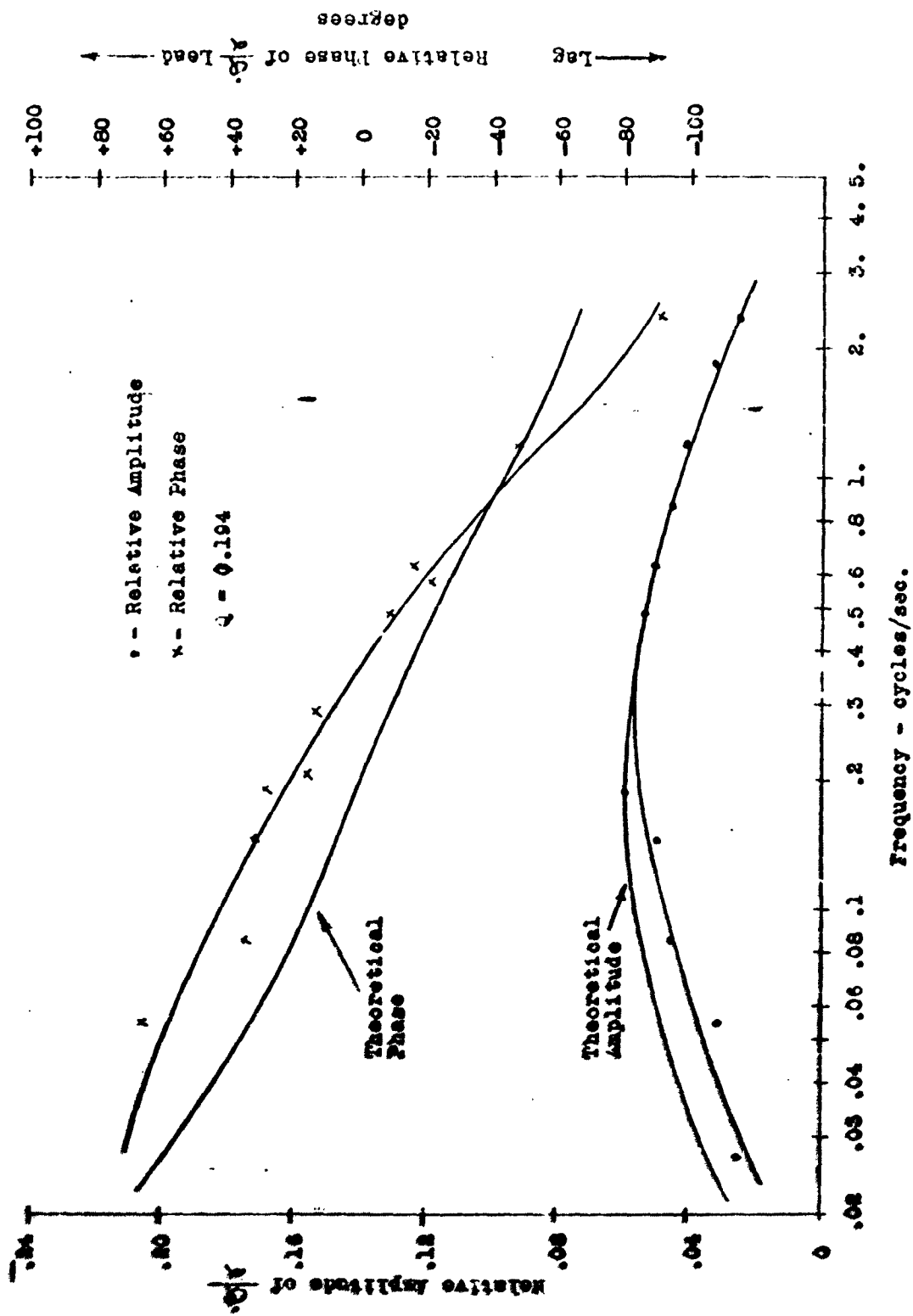
Figure 19 $\frac{\dot{\theta}}{\dot{y}}$ Tank water response - single degree of freedom (ship blocked).

Lag ← Relative Phase of $\frac{\theta}{\phi}$ degrees Lead →

+100 +80 +60 +40 +20 0 20 40 60 80 100

130° Phase Reversal at Secondary Resonance

• = Experimental Amplitude
× = Experimental Phase

Theoretical Phase

Theoretical Amplitude

Frequency – cycles/sec.

.5 .4 .3 .2 .1 .08 .06 .05 .04 .03 .02 .01

Relative Amplitude $\left|\frac{\theta}{\phi}\right|$
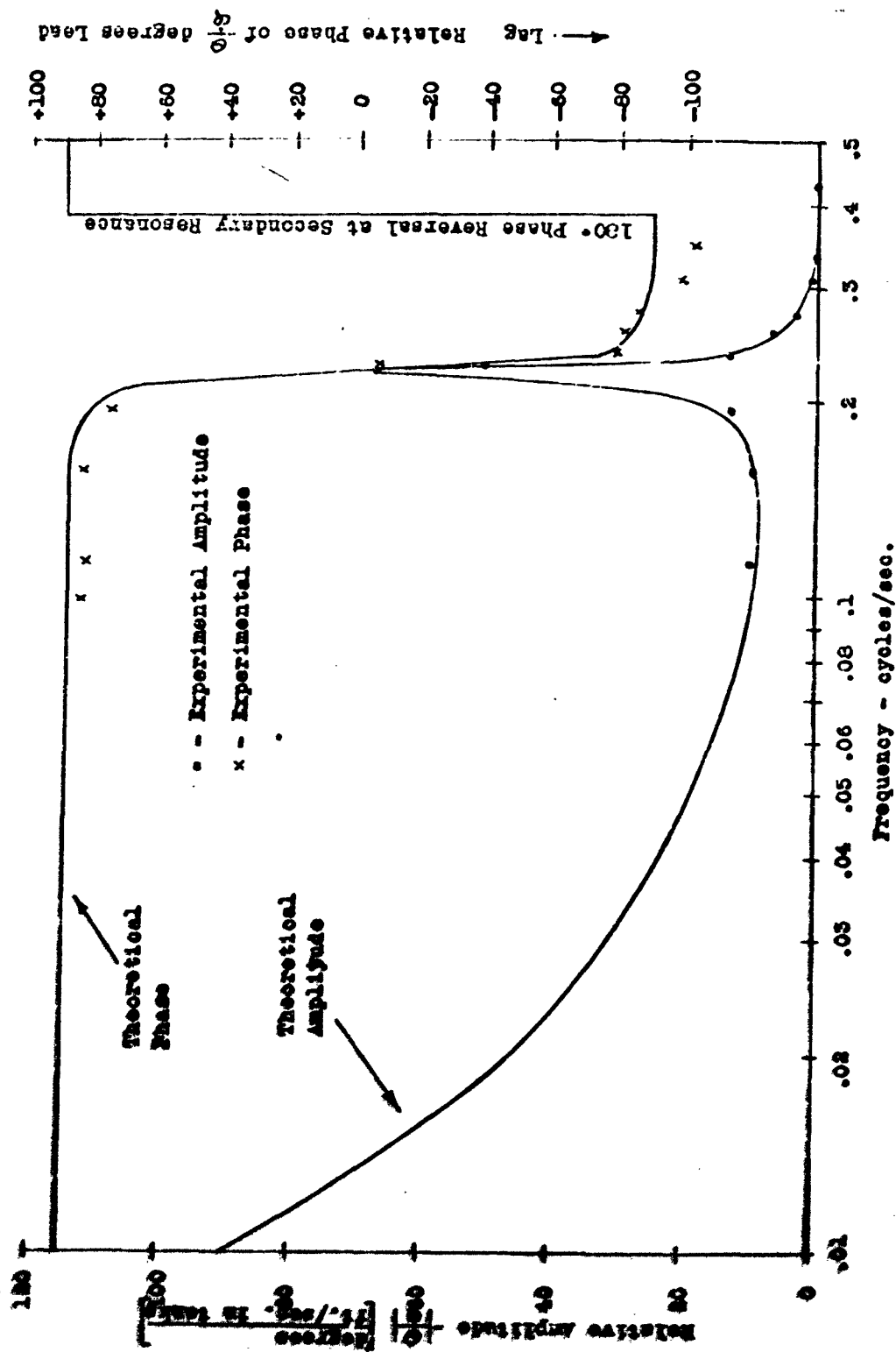
Figure 20 $\frac{\theta}{\phi}$-response, phase and amplitude.
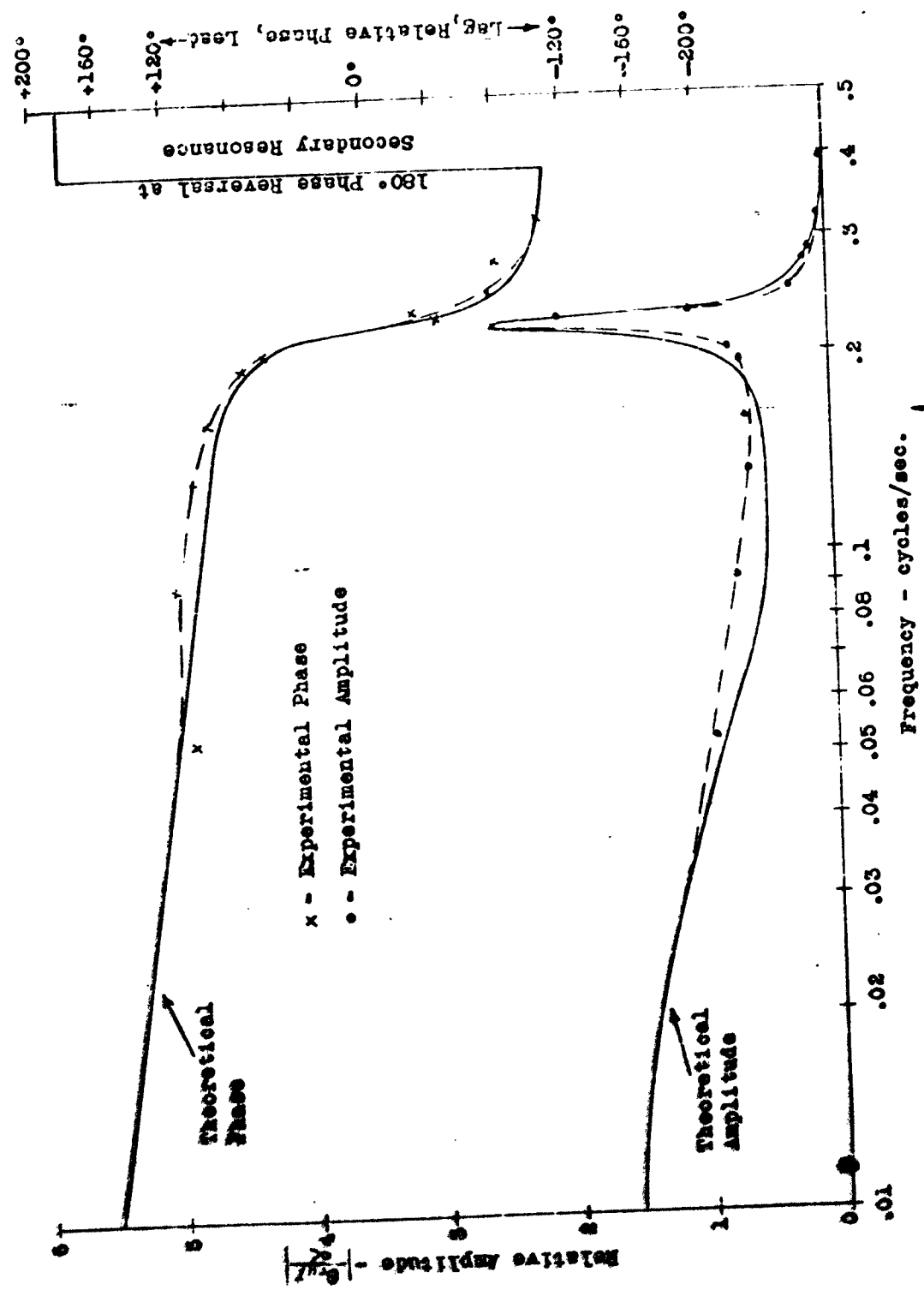
Figure 21. $\dfrac{\theta_{out}}{\alpha}$ Phase and Amplitude Response.
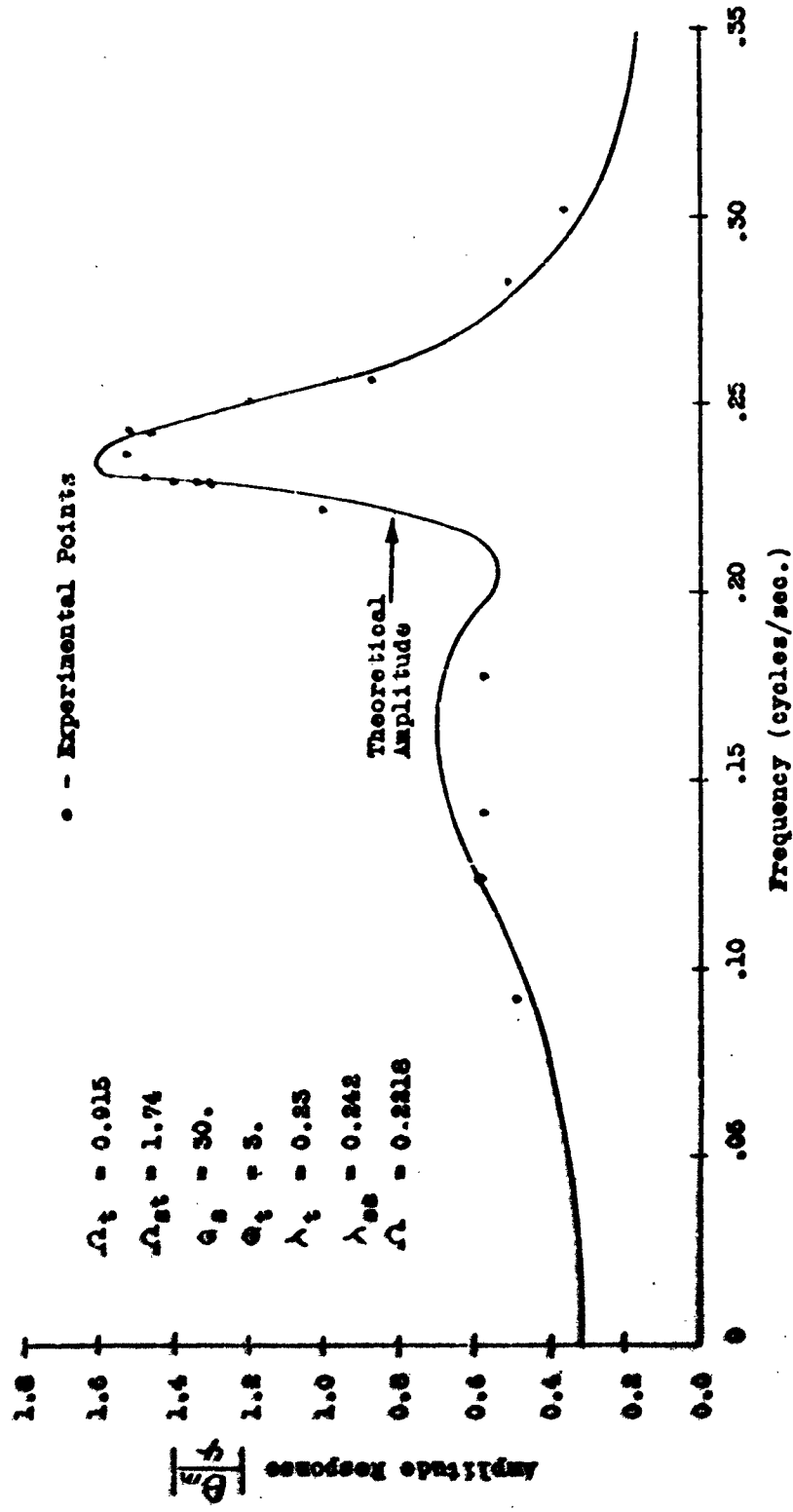
Figure 22 Fraim-damped Response vs. Frequency.

• - Experimental Points

Theoretical Amplitude

$\Omega_t = 0.015$
$\Omega_{st} = 1.74$
$a_s = 50.$
$a_t = 5.$
$\lambda_t = 0.85$
$\lambda_{ss} = 0.848$
$\Omega = 0.2216$

Frequency (cycles/sec.)

Amplitude Response $\left|\dfrac{\theta}{m}\right|$

.05 .10 .15 .20 .25 .30 .35

0.0 0.2 0.4 0.6 0.8 1.0 1.2 1.4 1.6 1.8

CHART NO. BL 909   THE BRUSH DEVEL

TAPE SPEED - 5mm/sec

R-3
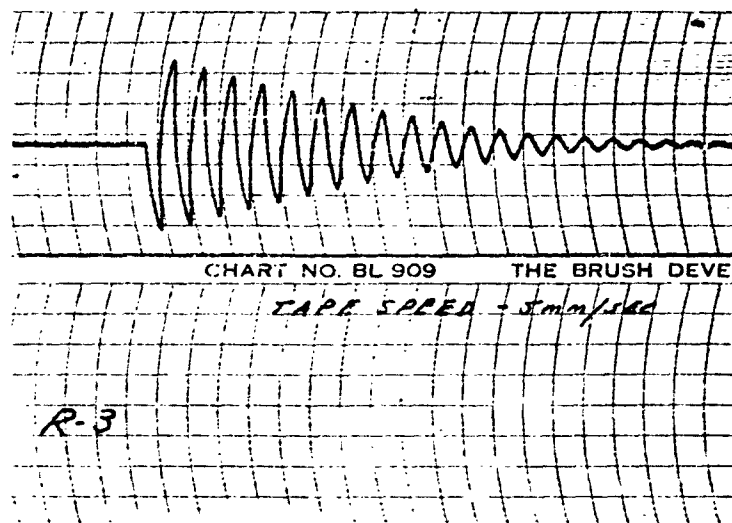
FREE OSCILLATION OF ACCELEROMETER
WITHOUT OIL DAMPING

SAE 50
PORTS CLOSED

R-4

(5mm/sec)

MENT CO.   PRINTED IN U.S.A.

SAE 50
PORTS OPEN

R-5

(5mm/sec)

OPMENT CO.   PRINTED IN U.S.A.

SAE 50
PORTS HALF CLOSED

(5mm/sec) R-6

CHART
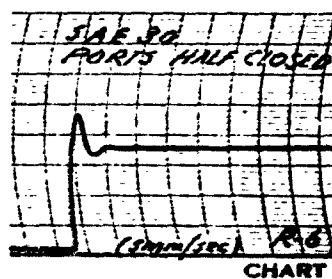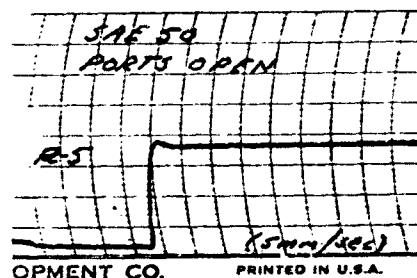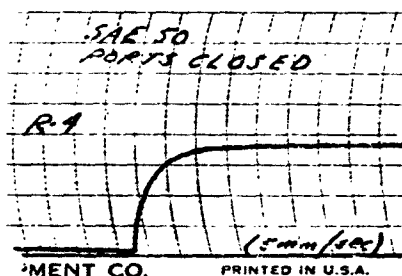
ACCELEROMETER DAMPING TESTS
RESPONSE TO STEP FUNCTION

Fig. 23
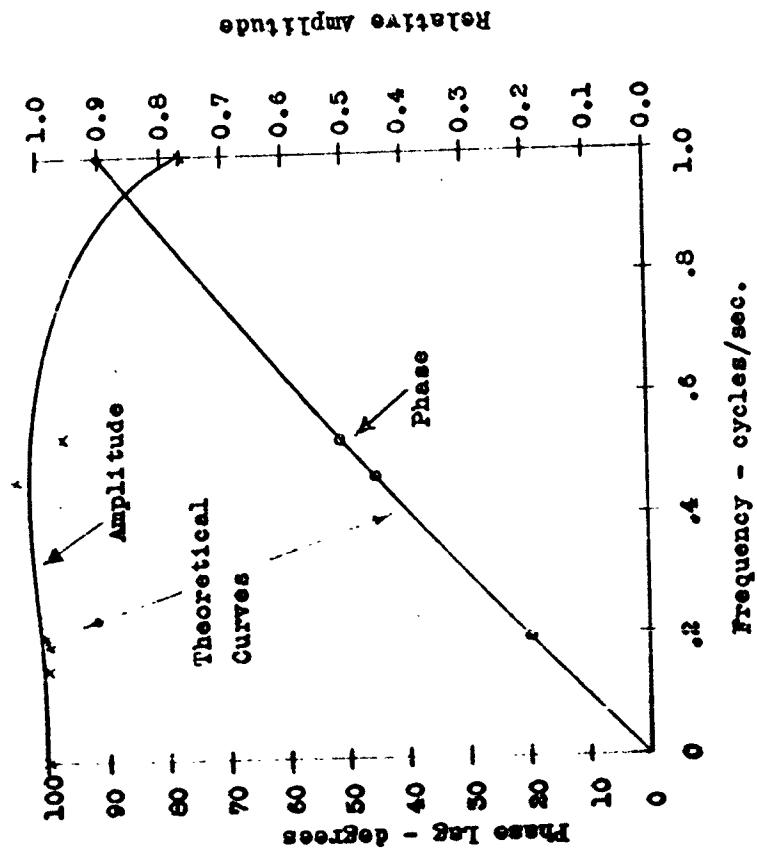
Figure 34 Accelerometer Response $\dfrac{e}{\theta'_{in}}$; Phase and Amplitude vs. Frequency.
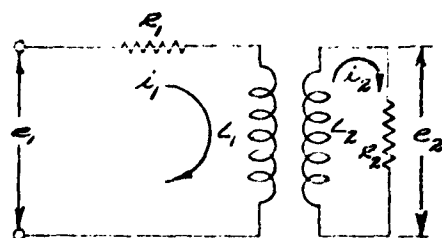
SCHEMATIC DIAGRAM
of TRANSFORMER
DIFFERENTIATING CIRCUIT
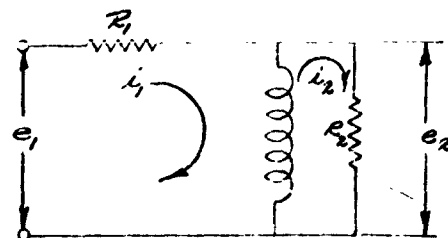
EQUIVALENT CIRCUIT
of TRANSFORMER
at LOW FREQUENCIES
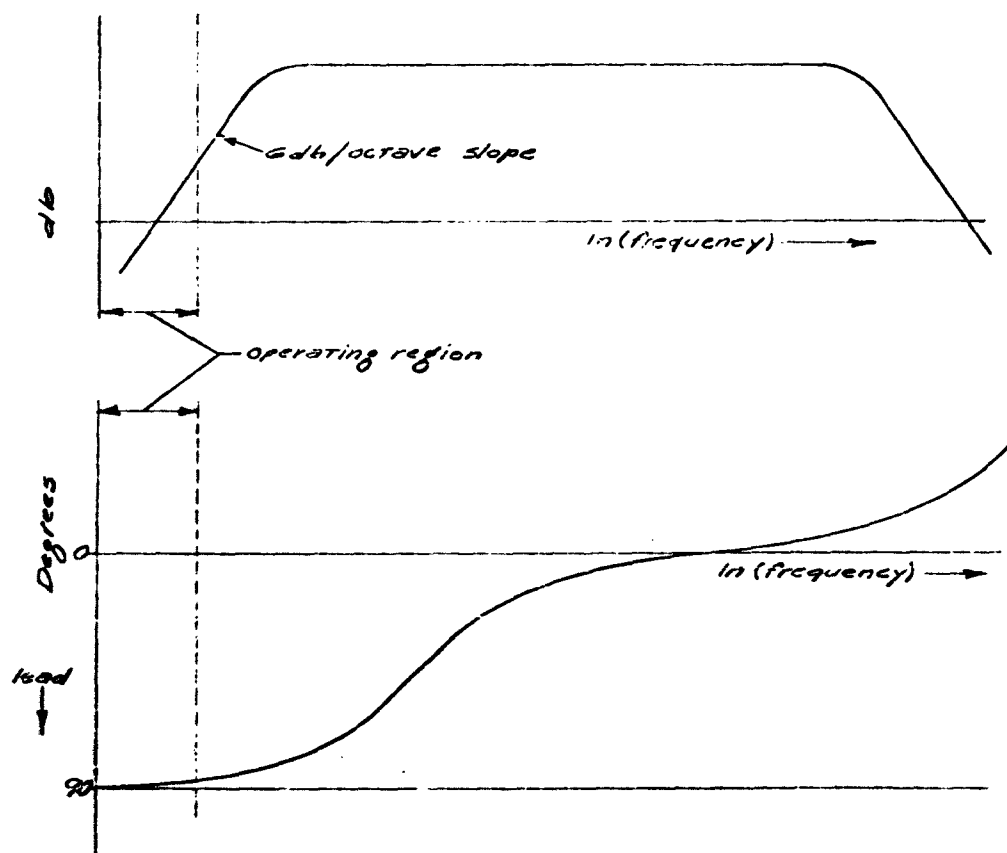
EQUIVALENT CIRCUIT
AND
RESPONSE OF DIFFERENTIATOR.

Fig. 25

DATE JAN 20, 1950   DR. by J. FTen
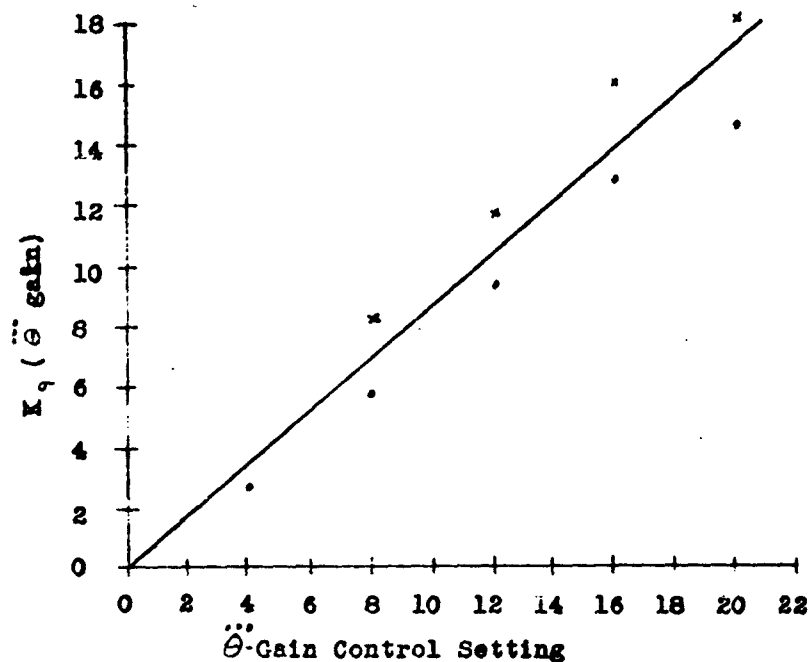
Figure 27   Calibration curve of $\ddot{\theta}$, gain control K_1.
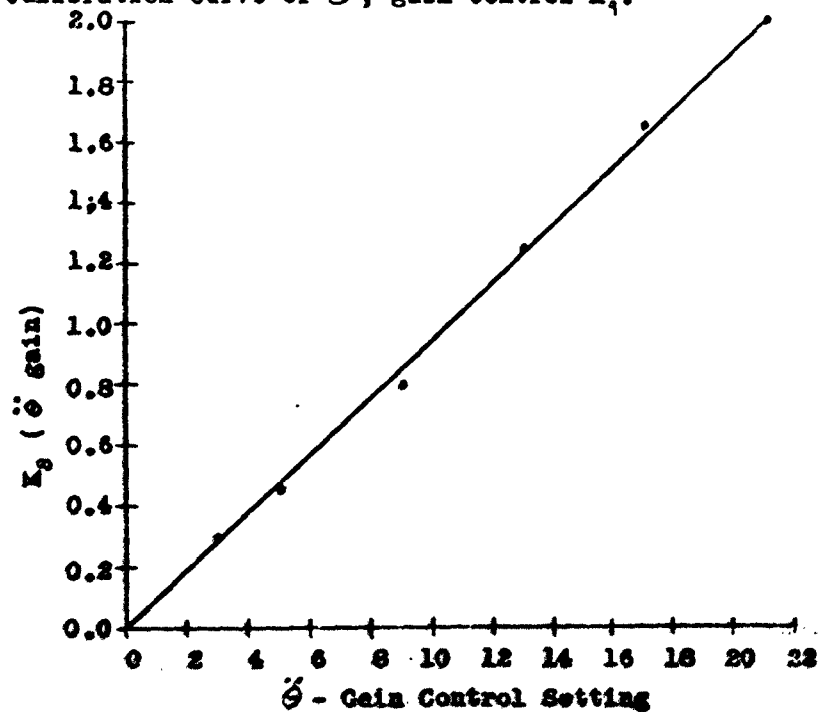
Figure 26   Calibration curve of $\ddot{\theta}$, gain control K_2.
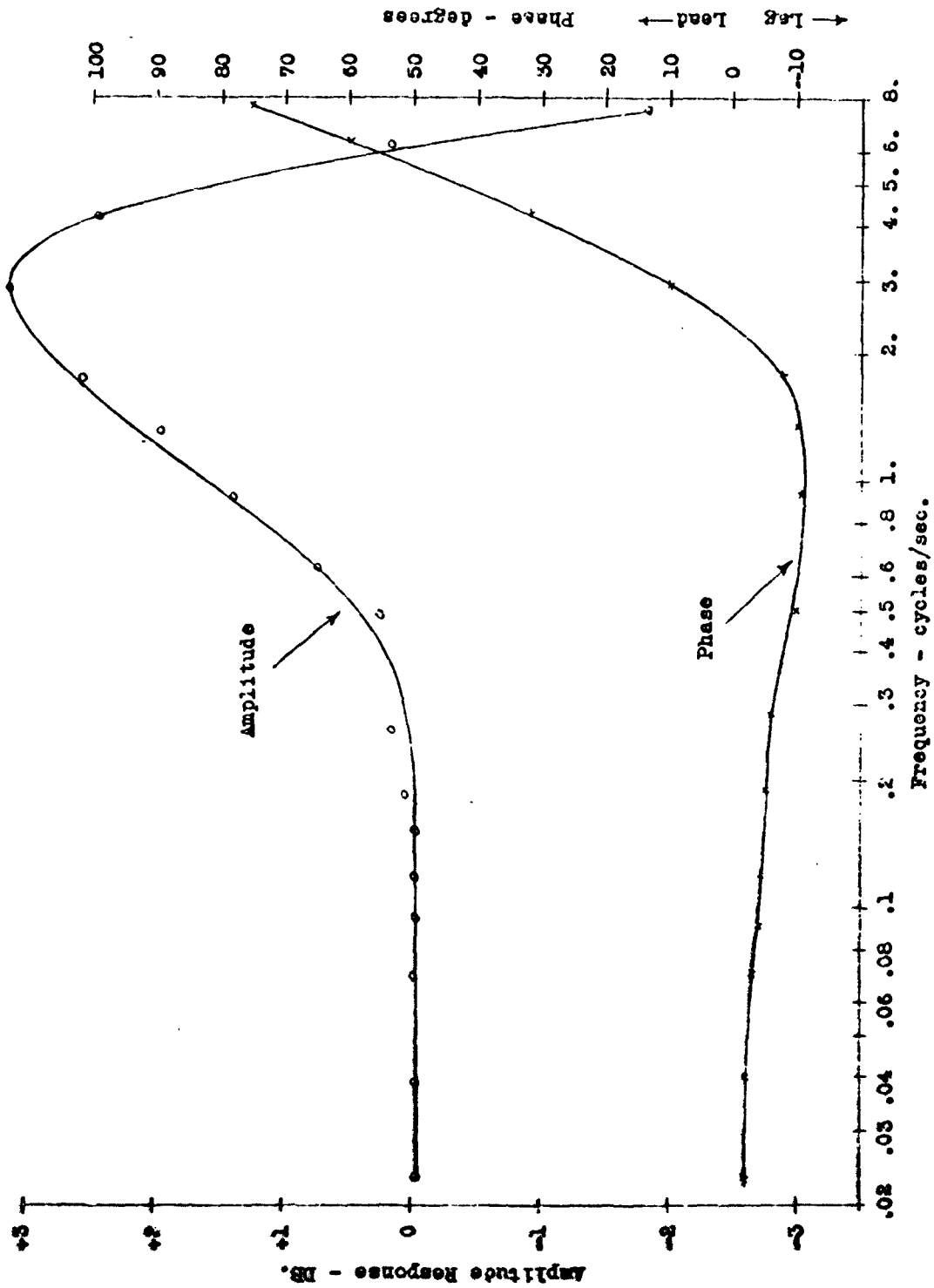
Figure 28 Response of Servo - Amplifier Input Demodulator - Filter
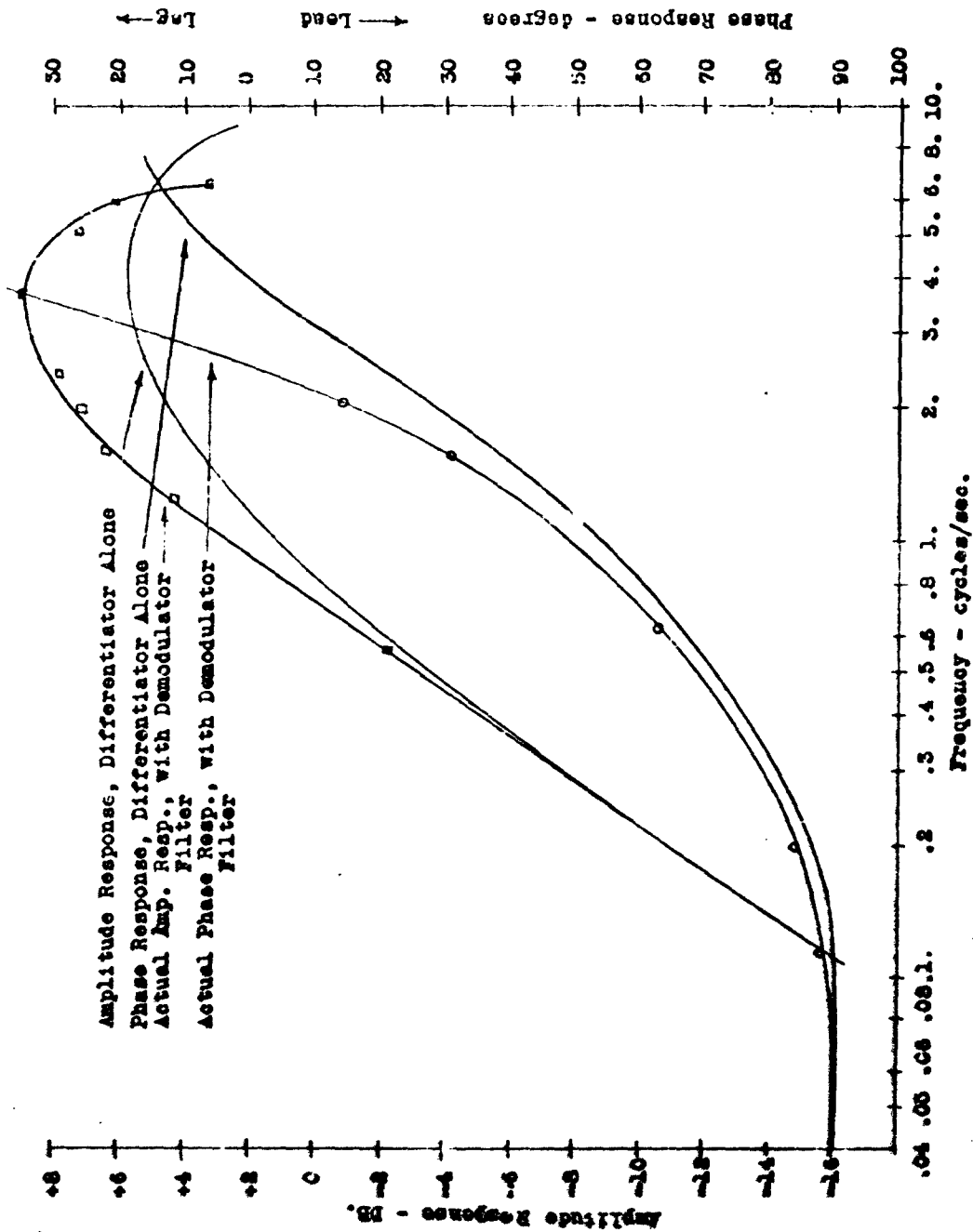
Figure 20 Transfer Response of Servo - Amplifier, Amplitude and Phase.
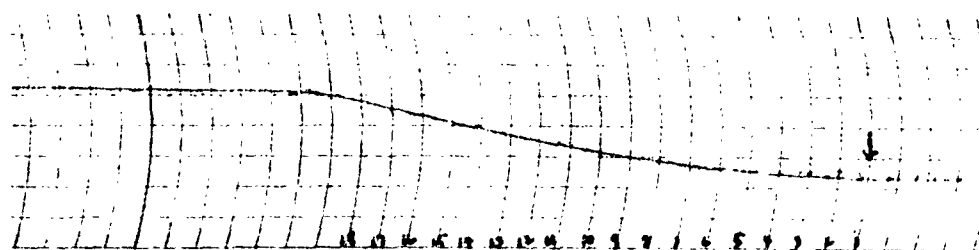
BEFORE ANY MODIFICATION
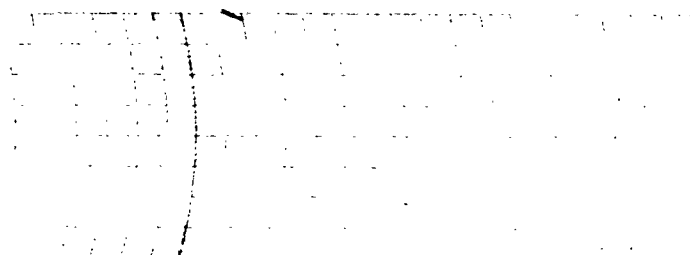
AFTER ADDING EDDY CURRENT DAMPER

TIME CONSTANT TEST OF SERVO-MOTOR
    POSITION VS TIME
    STEP VOLTAGE INPUT - OPEN LOOP
    PAPER SPEED 125 mm/sec

FIG. 30
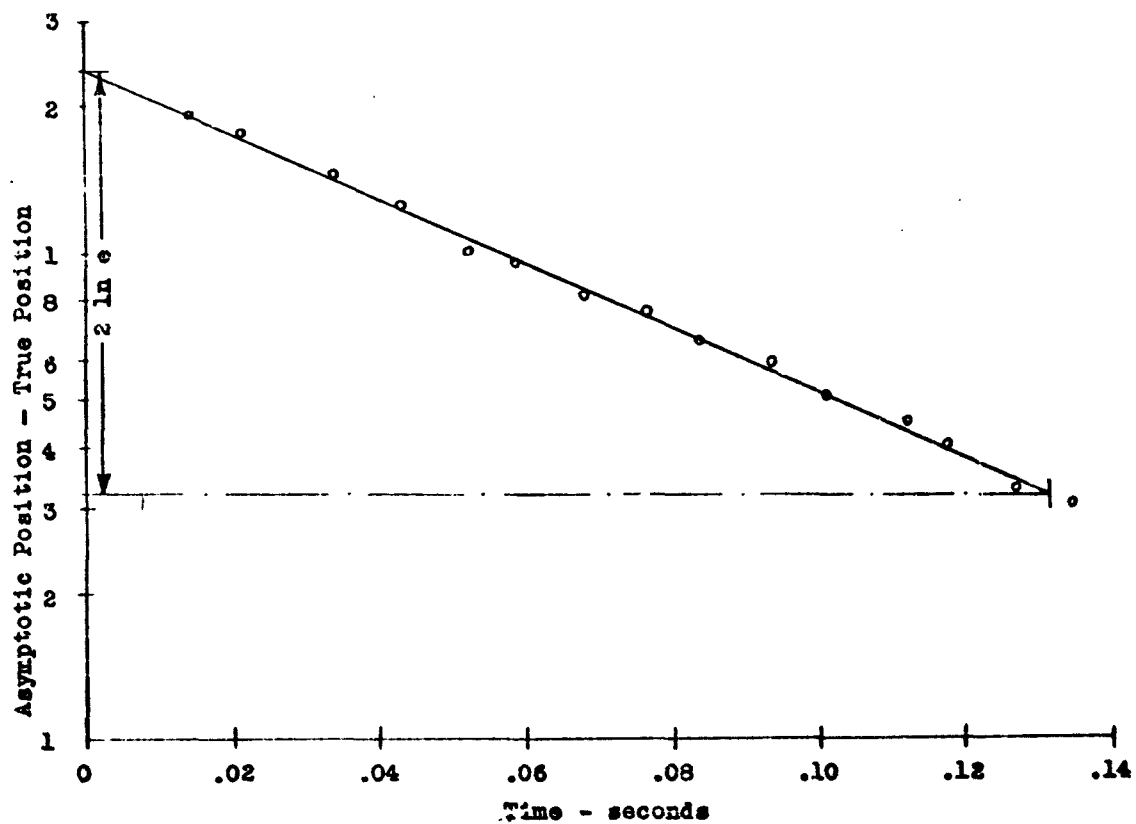
Figure 31 Determination of time constant for modified servo-motor (loop open, no pressure).

TYPICAL CLOSED LOOP SERVO-MOTOR TESTS
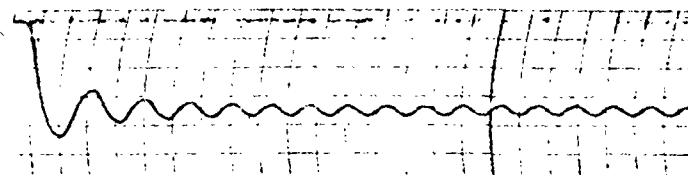
TYPICAL CLOSED LOOP UNDAMPED SERVO-MOTOR RESPONSE
TO STEP FUNCTION OF VOLTAGE (TAPE SPEED 25mm/sec).
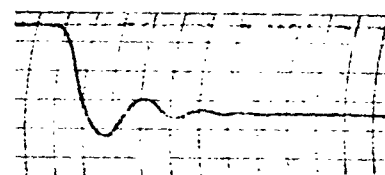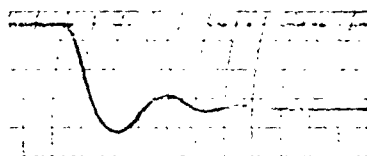
(EXTRA AMPLIFIER OUT)   (EXTRA AMPLIFIER IN)
SAME TEST EXCEPT RATE DAMPING NETWORK SHOWN
ON FIG.8 ADDED INTO LOOP WITH AND WITHOUT EXTRA
AMPLIFICATION (TAPE SPEED 25mm/sec).
(CIRCUIT CONSTANTS $R_1 = 77K$ $R_2 = 6.2K$ $C = .078\mu f$)
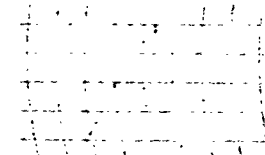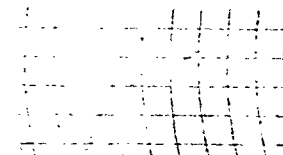
VALVE MOTION=.77"   VALVE MOTION=.63"   VALVE MOTION=.84"
T=.175   T=.148   T=.145
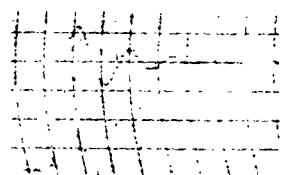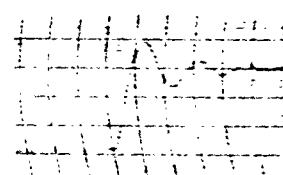
VALVE MOTION=.12"   VALVE MOTION=.09"
T=.137   T=.104
WITH EDDY CURRENT DAMPING
(TAPE SPEED 25mm/sec)

FIG. 32
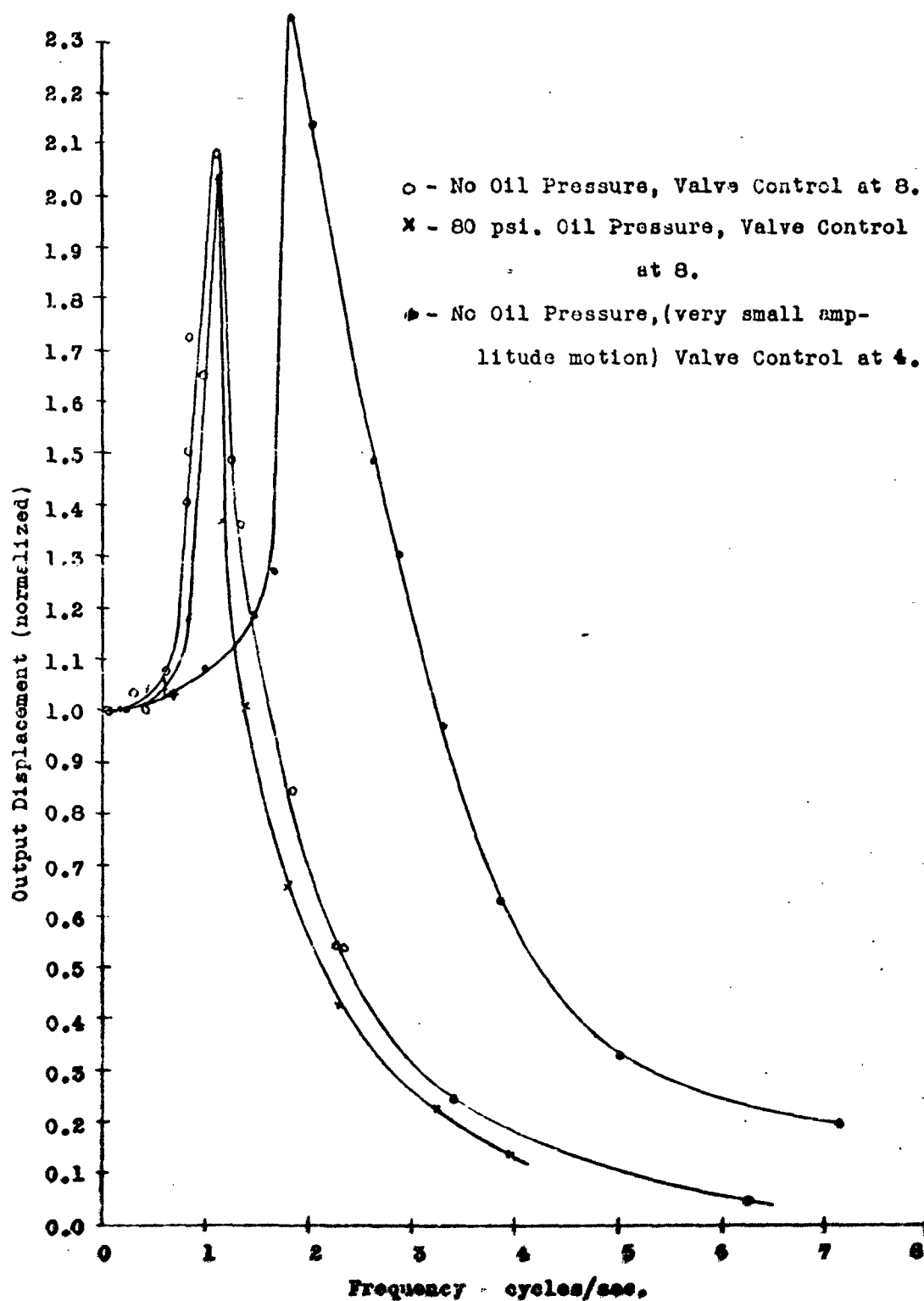
Figure 33 Closed loop response of servo-motor with eddy current damping (sinusoidal excitation).
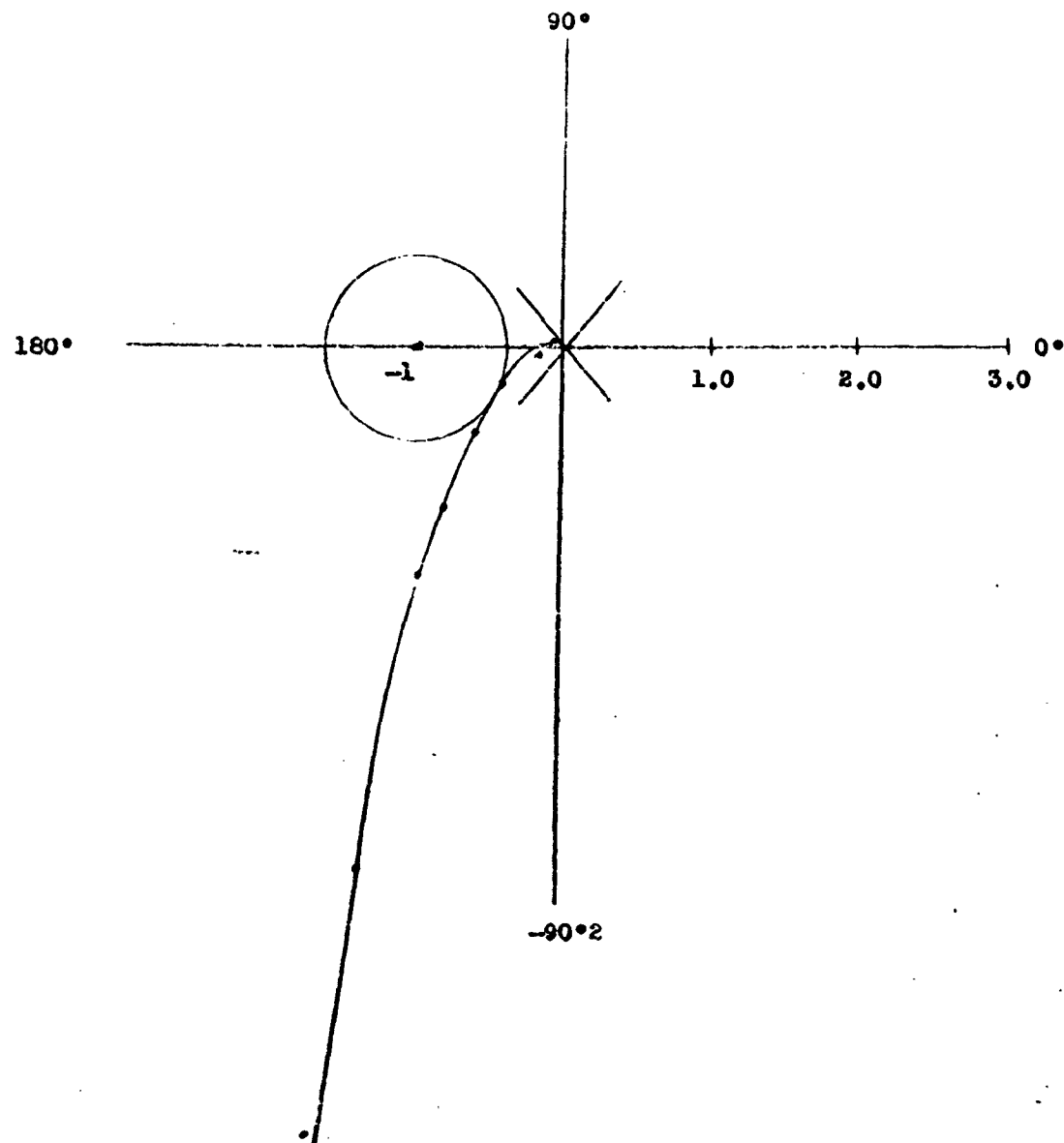
Figure 34 Open Loop Response of Servomotor (with eddy current damper, no pressure).

$T_2 \cong 1 + 0.69 \times (\text{Valve Control Setting})$
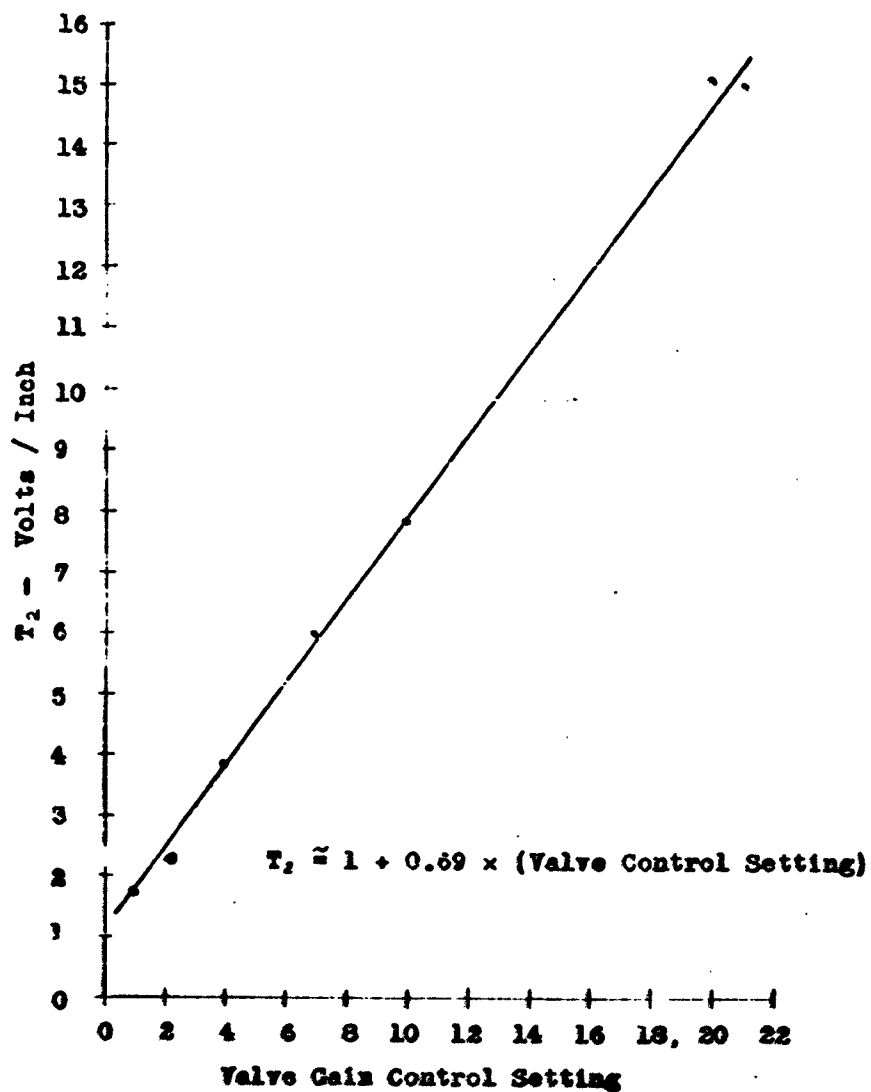
Figure 35 - Valve Gain Control Calibration Curve

T_2 vs. Control Setting

Oil Pressure = 110 – 115 psi.

• – Experimental points

Relative Response – DB.

Frequency – (cycles/sec.)
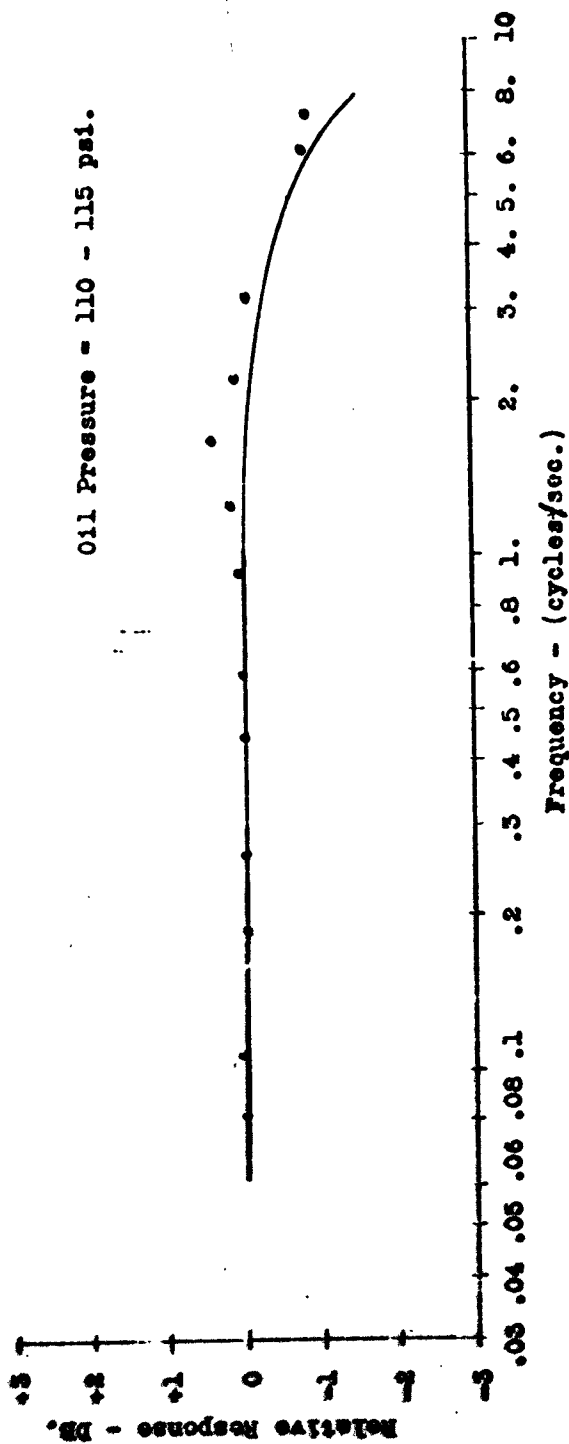
Figure 36 Amplitude Response of hydraulic amplifier – $\frac{X_2}{X_1}$.
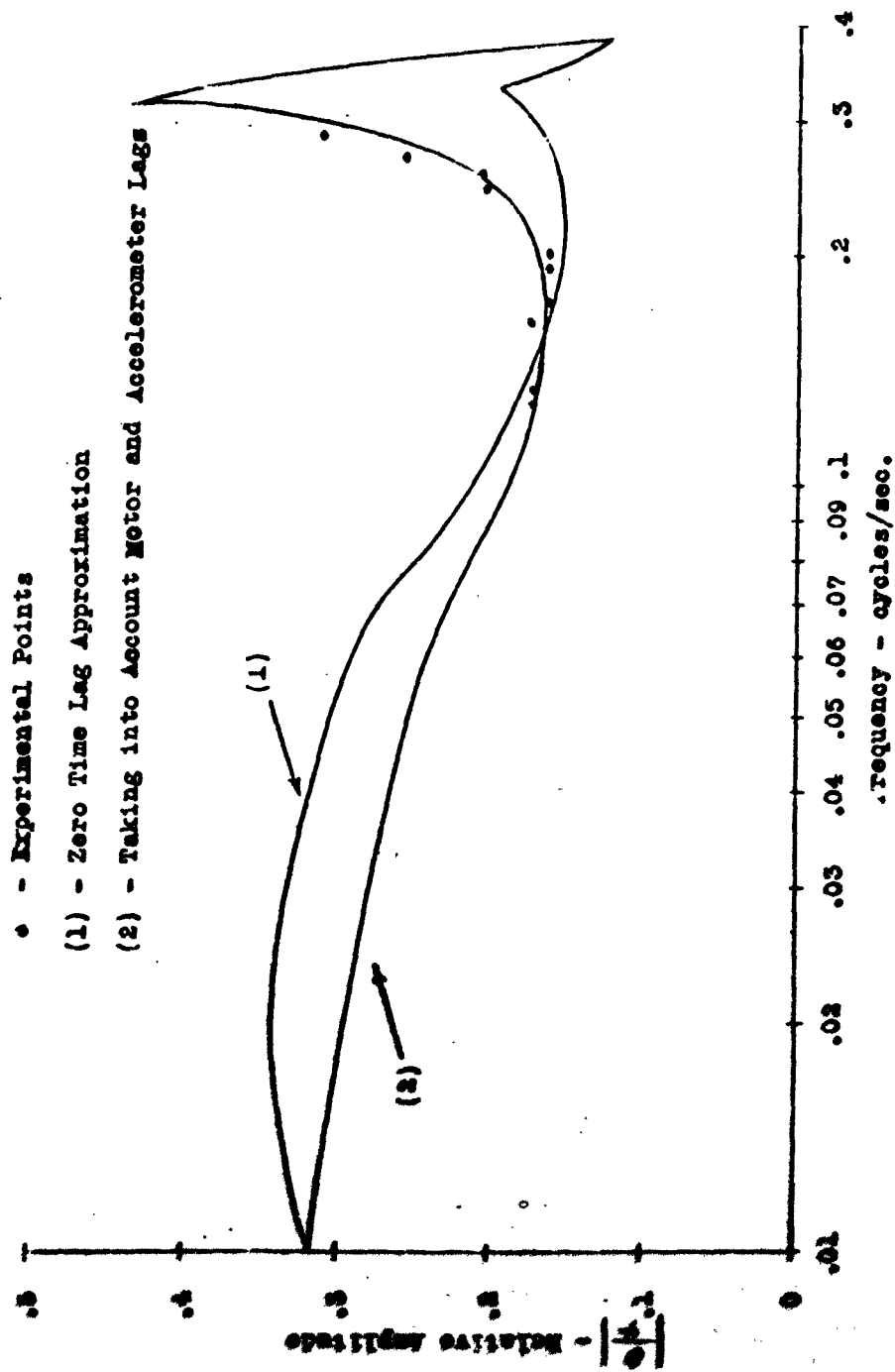
Figure 37 Stabilized Ship Response, $\left|\frac{\theta}{\psi}\right|$ vs Frequency for Minorsky Model.
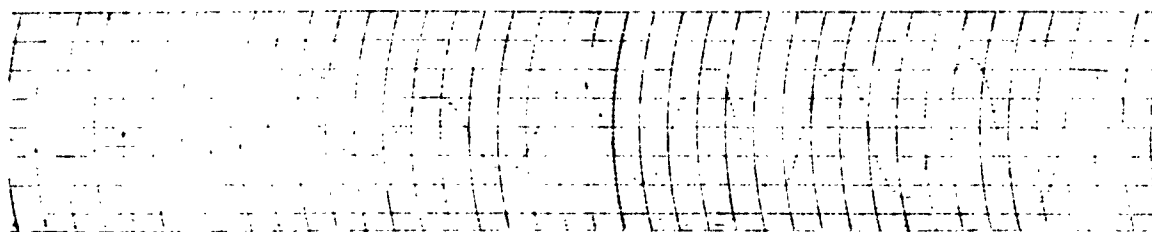
SLOW DESTABILIZE $\ddot{\theta}=7$ $\ddot{\theta}=6$
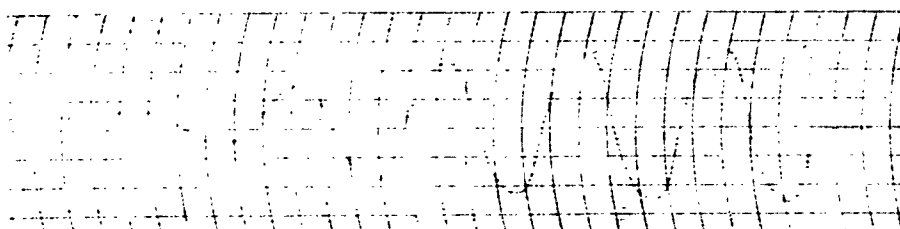
FAST DESTABILIZE $\ddot{\theta}=16$ $\ddot{\theta}=8$
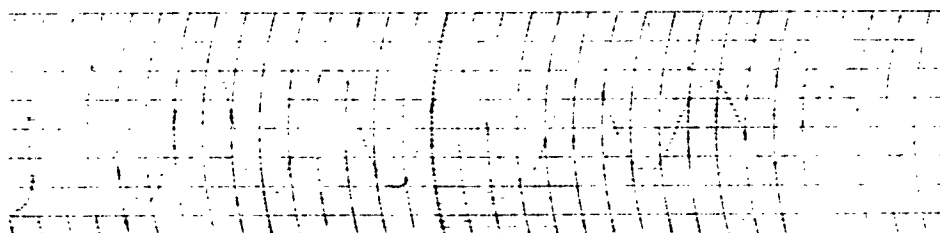
DAMPING DECREMENT — UNSTABILIZED
DATA FOR CURVES (TAPE SPEED 5mm/sec) (0.285 DEGREES/DIV.)
(VALVE GAIN CONTROL AT 4) (EXTRA AMPLIFIER OUT)

$\ddot{\theta}=16$ $\ddot{\theta}=8$ $\ddot{\theta}=21$ $\ddot{\theta}=10$
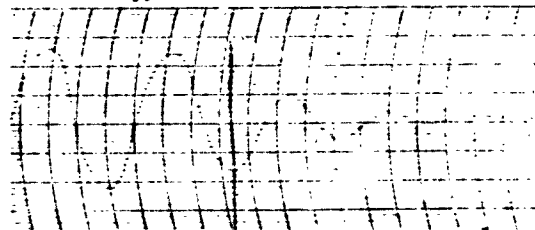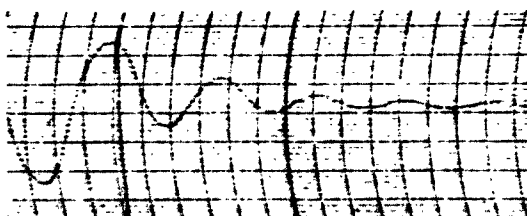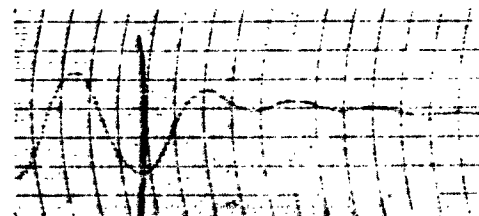
$\ddot{\theta}=21$ $\ddot{\theta}=25$ $\ddot{\theta}=21$ $\ddot{\theta}=10$

DAMPING DECREMENT - STABILIZED
(STABILIZATION TURNED ON AT END)

TRANSIENT ROLLING CURVES   Fig. 30
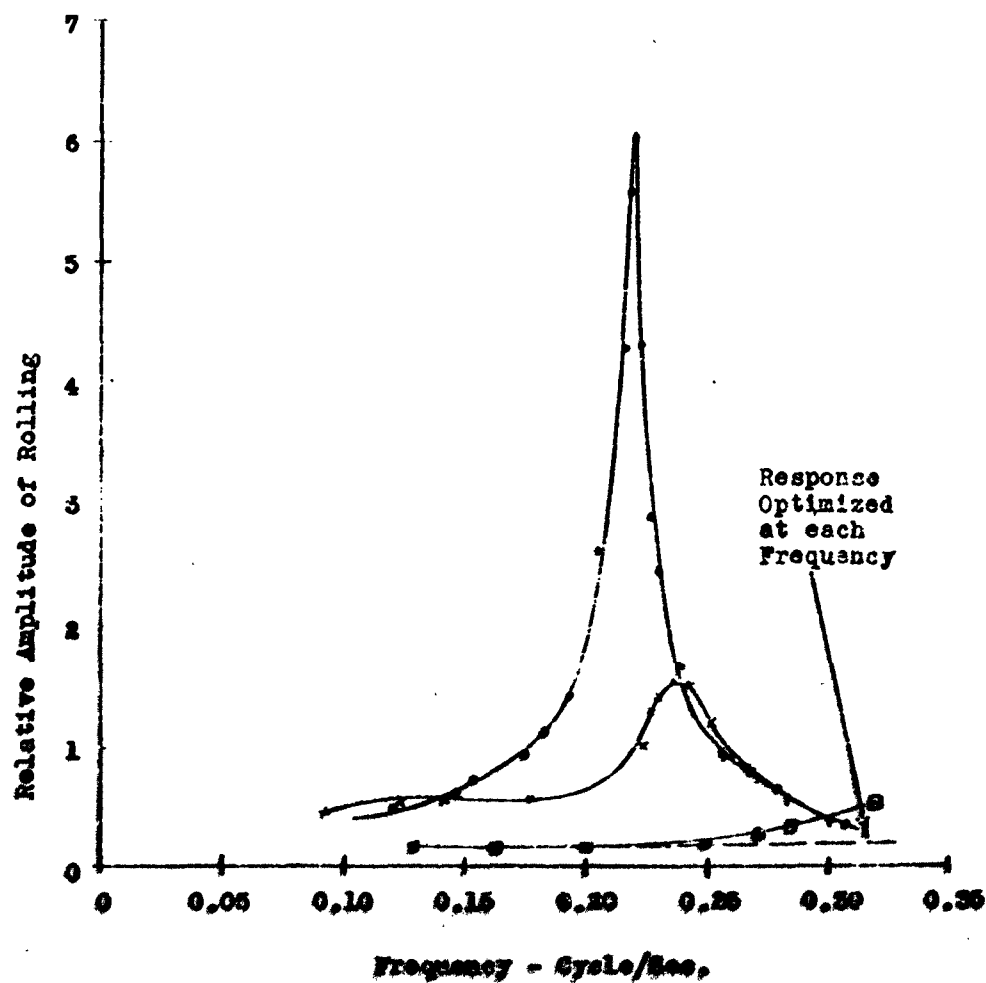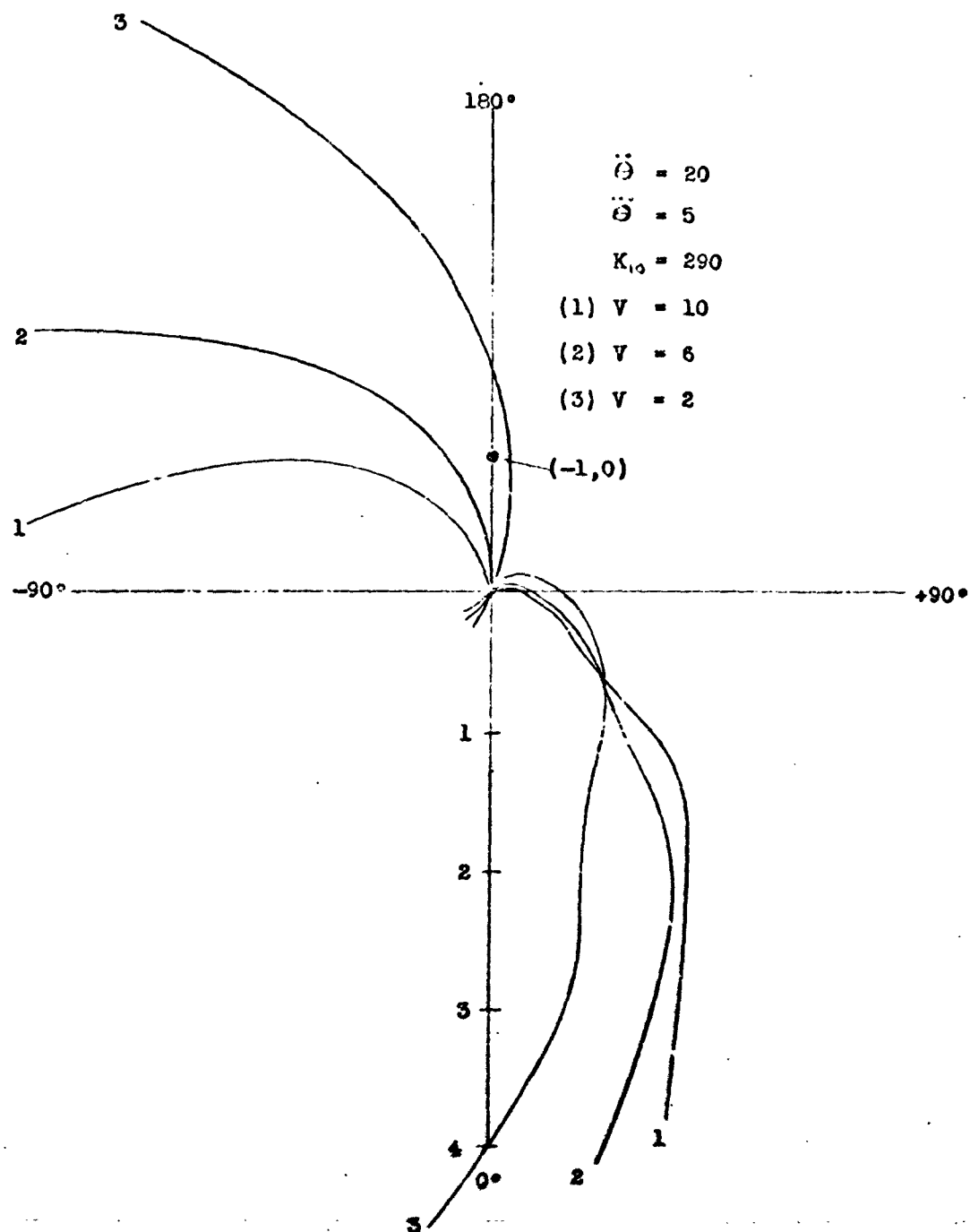
Figure 39 Amplitude Response of Tanks.

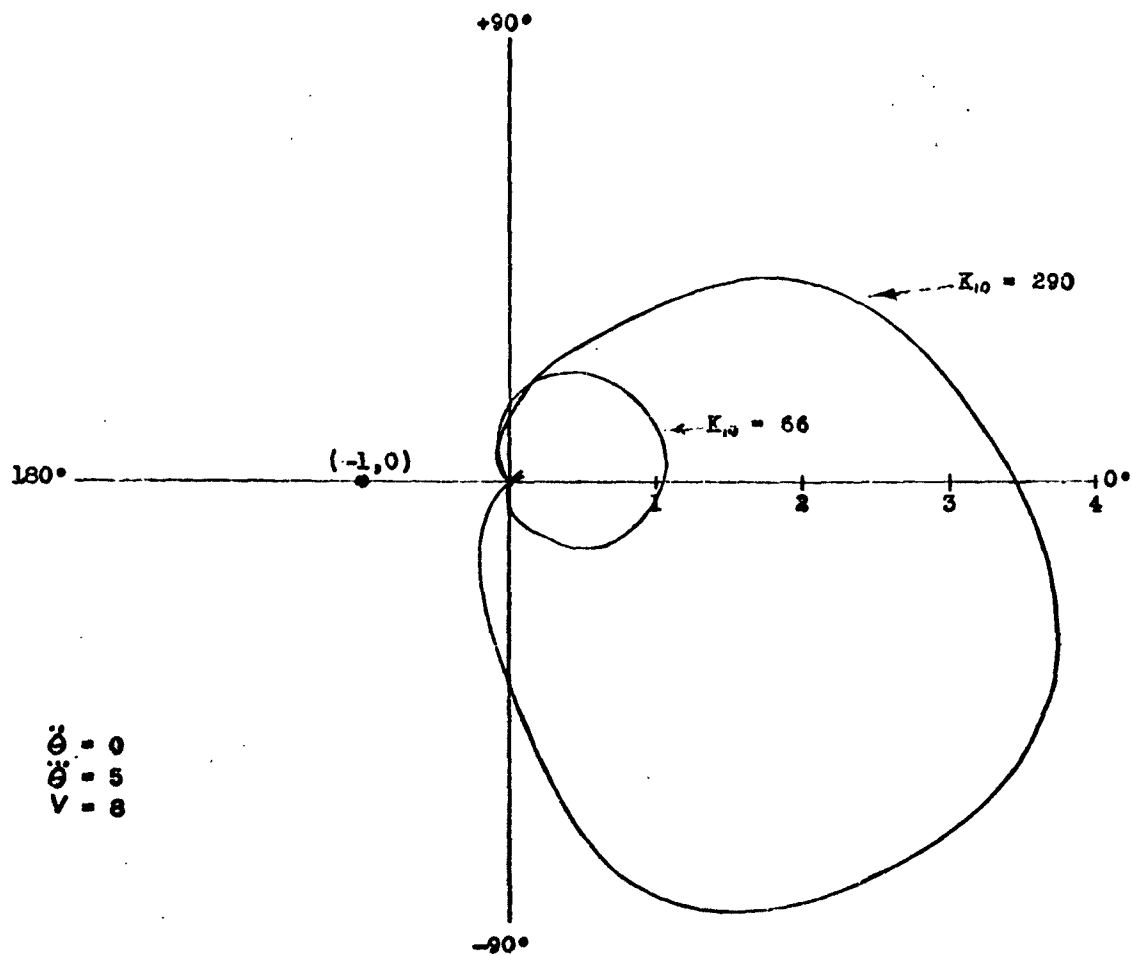**Figure 40** Nyquist Diagram- showing effect of varying valve gain control.

Figure 41 Nyquist Diagram showing effect of varying gain parameter K_{io} in the servo-loop.
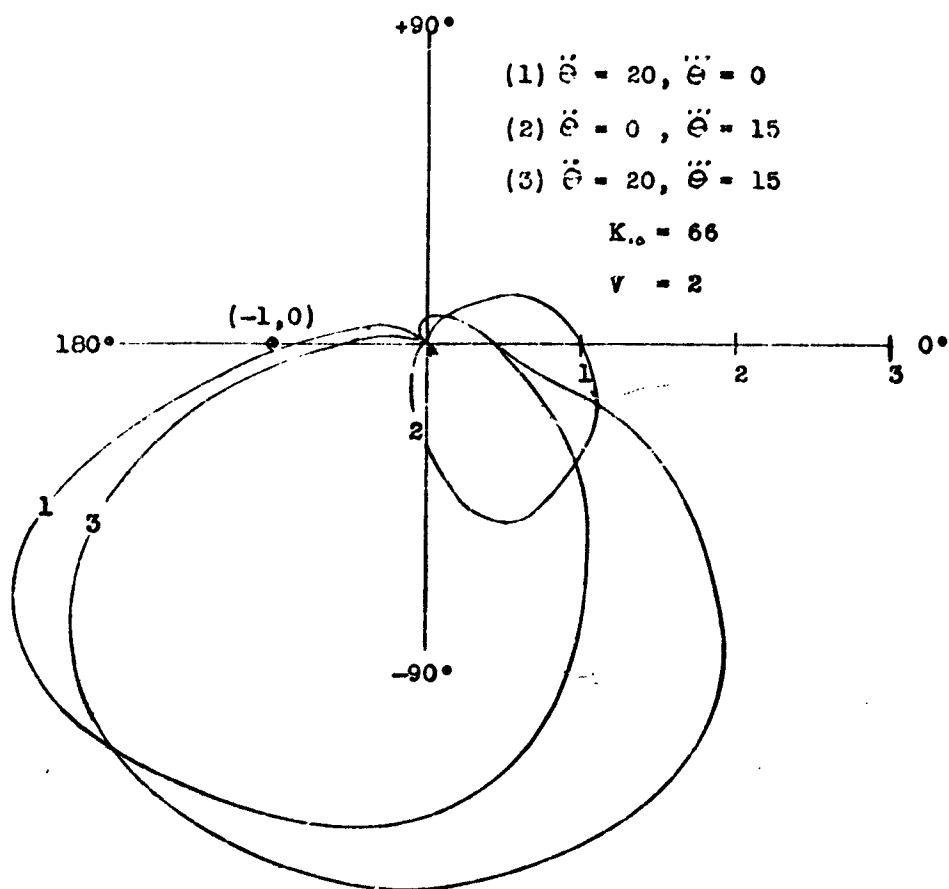
Figure 42   Nyquist Diagram- showing effect of different combinations
of $\ddot{\Theta}$ and $\dddot{\Theta}$ controls.